PNL-6746
UC-95f

18J

Inert Electrodes Program

Fiscal Year 1987 Annual Report

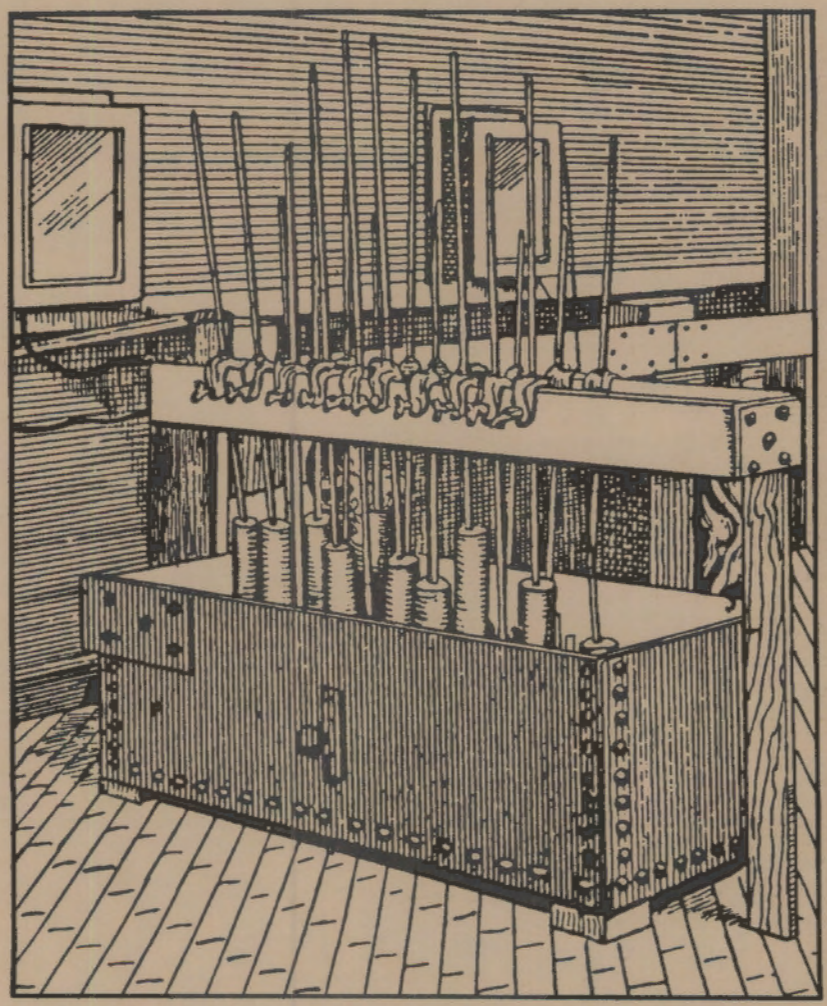

December 1988

Prepared for the U.S. Department of Energy
under Contract DE-AC06-76RLO 1830

Pacific Northwest Laboratory
Operated for the U.S. Department of Energy
by Battelle Memorial Institute

Battelle

PNL-6746

On the cover:

Aluminum reduction pots at the Pittsburgh Reduction Company's (Alcoa's) plant in 1889. Adapted from a photograph, courtesy of Alcoa.

PACIFIC NORTHWEST LABORATORY
operated by
BATTELLE MEMORIAL INSTITUTE
for the
UNITED STATES DEPARTMENT OF ENERGY
under Contract DE-AC06-76RLO 1830

Printed in the United States of America
Available from
National Technical Information Service
United States Department of Commerce
5285 Port Royal Road
Springfield, Virginia 22161

NTIS Price Codes
Microfiche A01

Printed Copy

Pages	Price Codes
001-025	A02
026-050	A03
051-075	A04
076-100	A05
101-125	A06
126-150	A07
151-175	A08
176-200	A09
201-225	A10
226-250	A11
251-275	A12
276-300	A13

PNL-6746
UC-95f

Inert Electrodes Program

FISCAL YEAR 1987 ANNUAL REPORT

Compiler:
C. M. Strachan

Principal Authors:
O. H. Koski
S. C. Marschman
C. H. Schilling
C. F. Windisch

Contributing Authors:
B. B. Brenden
N. C. Davis
P. E. Hart

December 1988

Prepared for
the U.S. Department of Energy
under Contract DE-AC06-76RLO 1830

Pacific Northwest Laboratory
Richland, Washington 99352

SUMMARY

In the Inert Electrodes Program, work during FY 1987 centered on three main areas of concern -- Materials Development and Testing, Materials Evaluation, and Stable Cathode Studies. Although the development of process sensors was carried out under separate funding, that work is reported here since it was related to the development of inert anodes.

In the Materials Development and Testing Task, new anode materials were developed. These materials have higher metal content than the anode material currently being studied, between 17% and 25% metal phase. One of the materials contains about 1% aluminum metal. It is speculated that the addition of this small amount of aluminum is responsible for the increase in electrical conductivity to about four times that of carbon. These new anode materials have not been adequately tested.

Results also suggested that an inert anode should be operated at low current density, where a passivating film forms on the surface of the anode. This film protects the anode from attack by the molten salt.

Research results obtained in the Materials Evaluation Task suggest that a series of reactions takes place on the surface of a copper anode. These reactions result in the conversion of Cu metal to Cu(I) and then to Cu(II). The first step, conversion of Cu to Cu(I) as CuF, occurs in the absence of Al_2O_3. Copper(I) flouride is then converted to Cu_2O in the presence of Al_2O_3. Anodic polarization at 2.1 V converts Cu(I) to Cu(II), probably as CuF_2 or CuO. Some of these reaction products are found in the Na_3AlF_6 and some are suggested by ac impedance and cyclic voltammetry experiments.

A combination of soak and electrolysis tests was used to identify the most probable corrosion mechanism for TiB_2-graphite materials and to evaluate the various materials that have been suggested for use as dimensionally stable cathodes. Acceptable materials appear to be TiB_2-based, i.e. TiB_2, TiB_2-graphite, and TiB_2-AlN. Experiments with replaceable anode/cathode fixtures suggest that the spacer material is the weak point; a materials development effort is needed. The likely corrosion mechanism for TiB_2-graphite under static conditions appears to be one in which Al_3C_4 forms in the composite. The

nearly 3:1 volume expansion between Al_3C_4 and graphite causes the composite to fracture and spall. This mechanism does not appear to take place under electrolysis conditions.

Under the Sensors Development Program, digital signal analyses of the cell process signals were used to prove the existence of a passivating film on the surface of the anode while in use. A method based on the thermal arrest of a cooling molten salt was used to determine the liquidus temperature of Na_3AlF_6-based molten salts. This technique was successfully demonstrated at the Kaiser Aluminum plant in Mead, Washington. Other methods for determining bath properties were rejected.

CONTENTS

FIGURES

TABLES

INTRODUCTION

The Inert Electrodes Program is being conducted at the Pacific Northwest Laboratory (PNL) for the U.S. Department of Energy (DOE), Office of Industrial Programs (OIP). The purpose of the program is to develop long-lasting, energy-efficient anodes, cathodes, and ancillary equipment for Hall-Heroult cells used by the aluminum industry. The program is divided into three tasks with the following objectives:

- Inert Anode Development - to improve the energy efficiency of Hall-Heroult cells by development of inert anodes.
- Stable Cathode Studies - to develop methods for retrofitting Hall-Heroult cells with TiB_2-based cathode materials.
- Sensor Development - to devise sensors to control the chemistry of Hall-Heroult cells using stable anodes and cathodes.

This Inert Electrodes Program annual report highlights the major technical accomplishments of FY 1987. The accomplishments are presented in the following sections: Management, Materials Development and Testing, Materials Evaluation, Stable Cathode Studies, and Sensor Development.

1.0 MANAGEMENT

D. M. Strachan and P. E. Hart

During FY 1987, substantial progress was made at PNL on the development and use of inert anodes for the production of aluminum by the Hall-Heroult process. It now appears promising that commercial aluminum production facilities using an inert anode/cathode combination could save between $0.05 and $0.10 per pound of aluminum produced. Several patent applications and disclosures were written on the materials and processes developed this year to protect the technology and provide a vehicle to make the U.S. aluminum industry more competitive.

Promising TiB_2 cathode materials and attachment techniques were also evaluated during FY 1987. Several materials (TiB_2-graphite, TiB_2-AlN, and pure TiB_2) were selected for further evaluation. It was found that TiB_2 was corroded by molten Na_3AlF_6 when not protected with aluminum and not under polarized conditions.

Several contact and noncontact methods were evaluated for sensing the bath liquidus temperature and chemistry. Some of these methods were evaluated in scouting tests; the thermal arrest method was demonstrated at the Kaiser Aluminum Plant in Mead, Washington. No further development of these methods is planned. A reference anode was used as a sensor to monitor the corrosion state of the working anode. A patent report was filed on the methodology of using the reference anode as a control for the operation of the working anode.

During FY 1987 the following reports were issued:

- Windisch, C. F., Jr. and S. C. Marschman. 1986. Electrochemical Polarization Studies on Cu and Cu-Containing Cermet Anodes for the Aluminum Industry. PNL-SA-14299.
- Pool, K. H., J. L. Brimhall, P. J. Raney, and P. E. Hart. 1987. Evaluation of Wear Rates and Mechanisms of Titanium Diboride-Graphite Composite Materials Proposed for Use as Cathodes in Hall-Heroult Cells. PNL-6069.

- Schilling, C. H., D. I. Hagen, and P. E. Hart. 1987. Stable Attachment of TiB_2-Based Cathodes for the Aluminum Industry: Review and Recommendation. PNL-6144.
- Marschman, S. C., and N. C. Davis. 1987. Materials Development for Inert Anodes: Progress Report for the Period from November 1985 to February 1987. Limited Distribution.
- Marschman, S. C., N. C. Davis, and R. W. Stephens. 1987. Nonconsumable Anode Electrical Contacts and Support Mechanisms. Limited Distribution.
- Hart, P. E., B. B. Brenden, N. C. Davis, O. H. Koski, S. C. Marschman, K. H. Pool, C. H. Schilling, C. F. Windisch, and B. J. Wrona. 1987. Inert Anode/Cathode Program Fiscal Year 1986 Annual Report, PNL-6247.
- Schilling, C. H., and N. C. Davis. 1987. Inert Anode/Cathode Program Supplement to the Fiscal Year 1986 Annual Report, Limited Distribution.

During FY 1987, the following papers were submitted for publication:

- Windisch, C. F., and S. C. Marschman. 1987. "Electrochemical Polarization Studies on Cu and Cu-Containing Cermet Anodes for the Aluminum Industry." Light Metals 1987, ed. R. D. Zabreznik, pp. 351-356. The Metallurgical Society of the AIME, Warrendale, Pennsylvania.
- Schilling, C. H., and S. C. Marschman. 1987. "Stable TiB_2-Based Cathodes for the Aluminum Industry: Laboratory Testing Methods at Battelle." In Proceedings of the Light Metals Production Research Group Aluminum Electrolysis Workshop. February 28. Carnegie Mellon University, Pittsburgh, Pennsylvania.
- Schilling, C. H., N. T. Saenz, H. E. Kjarmo, G. L. Graff, and S. C. Marschman. 1987. Elemental Segregation in TiB_2-Graphite Cathode During Aluminum Smelting, Poster presented at Annual Meeting of the American Ceramic Society, April 26-30, Pittsburg, Pennsylvania.

Several meetings were attended by program staff during FY 1987. These included program review meetings held on January 6, April 8 and 9, and November 3, 1987. In addition, details of the program were presented to representatives of the Bonneville Power Administration, the Northwest aluminum industry, the Northwest Power Planning Council, and the Washington and Oregon Power Planning Offices in Portland, Oregon on April 6. A technology transfer meeting was held September 15 and 16 with representatives of the major aluminum companies in the U.S. to inform them of the progress and scope of the program. A two-day workshop was held by the program consultants in April. On February 28, C. H. Schilling presented the work on the stable cathode studies at the Light Metals Production Research Group Cathode Workshop at Carnegie Mellon University. In a related activity, S. C. Marschman attended a workshop held by EMEC Consultants on the production of aluminum and other products from lunar ores using the inert anodes developed in this program.

Through attendance at these meetings and publication of topical and annual reports, the program is gaining acceptance by the industry. Comments received at the meetings and conversations with technical staff at the aluminum plants also indicate a general acceptance that the program is making progress in ways that will enhance the competitiveness of the U.S. aluminum industry. Large-scale tests need to be performed along with the supporting laboratory tests to demonstrate the technology. These tests will require participation by the industry, which will be sought during FY 1988.

2.0 MATERIALS DEVELOPMENT AND TESTING

S. C. Marschman, O. H. Koski, and N. C. Davis

The objectives of the Materials Development and Testing Task include the selection, fabrication, and evaluation of candidate non-consumable anode materials.

SUMMARY

Research performed in FY 1987 focused primarily on the development and evaluation of cermets based on the two-phase oxide system, NiO-$NiFe_2O_4$, containing a third, electrically conductive metal phase composed primarily of Cu and Ni.

The efforts of this task were focused into three areas: materials fabrication, small-scale materials testing, and laboratory-scale testing. Materials fabrication efforts included development of fabrication procedures for NiO-$NiFe_2O_4$-Cu-Ni-Al cermets, production of standard NiO-$NiFe_2O_4$-Cu-based cermets for materials testing, and development of brazing techniques for attaching cermet non-consumable anodes to metal rods for electrical connection and support. The small-scale testing effort was directed toward evaluation of materials in small electrolysis cells. The laboratory-scale testing effort centered on the evaluation of electrolyte chemistry effects on the performance of the anode materials.

The materials fabrication efforts performed in FY 1987 resulted in the development of improved NiO-$NiFe_2O_4$-Cu-Ni-Al cermet microstructures and alternate processing parameters. The NiO-$NiFe_2O_4$-Cu-Ni-Al cermets first developed in FY 1986 were improved through careful control of the processing parameters, particularly the powder blending step. Cermets were fabricated with densities at approximately 95% of theoretical density. High-density NiO-$NiFe_2O_4$-Cu-Ni-Al cermets were successfully produced using dry-blending techniques where previously Freon[(a)]-based solvents were necessary in the powder-blending step.

(a) Freon is a registered trademark of Dupont de Nemours Corp., Wilmington, Delaware.

The small-scale electrolysis testing effort was completed near the end of FY 1987. Testing results indicated that the NiO-$NiFe_2O_4$-Cu-Ni-Al cermets were the best candidate non-consumable anode materials developed by PNL. The results were based on the high electrical conductivity values obtained for these materials and their performance in the small-scale electrolysis tests.

The laboratory-scale electrolysis testing effort was instrumental in determining electrolysis cell operating parameters. Although not optimized, NiO-$NiFe_2O_4$-Cu-based cermets were successfully operated in Na_3AlF_6-based electrolytes ranging in bath ratios from 1.1 to 1.35, in electrolytes containing 1.5 wt% LiF, and at conditions other than Al_2O_3 saturation. Operating conditions which lead to anode degradation have been identified, and control methods have been developed to ensure proper operation of small electrolysis cells using non-consumable anode technology.

TECHNICAL PROGRESS

Research conducted during FY 1986 resulted in the recommendation of four candidate NiO-$NiFe_2O_4$-Cu-based cermet materials for further study. During FY 1987 these candidates were evaluated, resulting in the NiO-$NiFe_2O_4$-Cu-Ni-Al cermets being selected as the most promising anode material. New technical developments and discoveries made by PNL staff during FY 1987 indicate that the cermets can be operated under a wide range of conditions. These efforts are described in detail below.

Materials Fabrication

Most of the materials fabrication effort was devoted to production of standard anode materials for testing. These anode materials were composed of two oxide phases (NiO and $NiFe_2O_4$) and a Cu-based metal phase. Other efforts centered on the improvement of the fabrication procedures used to produce the NiO-$NiFe_2O_4$-Cu-Ni-Al cermets, and efforts to produce NiO-$NiFe_2O_4$-Cu cermets directly from the raw oxides, NiO and Fe_2O_3, and Cu metal powder were initiated. Development of electrical contacts and support mechanisms for non-consumable anode cermets was also accomplished.

$NiO-NiFe_2O_4$-Cu Cermets

This material was developed initially by Alcoa (Weyand et al. 1986) and improved at PNL. The cermet is composed with 17 wt% Cu prior to sintering, and has repeatedly been shown to withstand the corrosive attack of molten Na_3AlF_6 electrolytes. The process for fabricating this cermet is basically the same as reported in a previous document (Marschman and Davis 1987), and is briefly summarized here:

- Weigh and combine $NiO-NiFe_2O_4$ and Cu metal powders.
- Blend powders.
- Pre-press samples at low pressure to consolidate the powders.
- Isostatically press at 172 MPa (25 ksi) in thin rubber containers.
- Machine green bodies to shape (if required).
- Sinter samples.

The fabrication flowsheet detailed here should not be considered as the only method by which these cermets can be fabricated. The methods developed at PNL, and presented here, are those which were found to work. Variations in the fabrication procedure of $NiO-NiFe_2O_4$-Cu-based cermets will undoubtedly be developed as fabrication procedures evolve.

Care was taken to ensure that processing parameters and cermet composition would not change while batches of anodes were being produced for a particular series of tests. A typical anode is shown in Figure 1. The sample on the left is an as-pressed green body, while the sample on the right is a densified sintered body. These cermets exhibit approximately 16% linear reduction in size upon sintering. Variations in process parameters have been shown to produce changes in the final microstructure and density of these cermets. However, these variations have not, as yet, been shown to significantly effect the performance of these materials when used as non-consumable anodes.

Variations in the $NiO-NiFe_2O_4$ powder were also shown to influence the final cermet product. During FY 1987, the lot of spray-dried $NiO-NiFe_2O_4$ powder which was furnished by Alcoa was totally consumed. The next lot of powder was obtained directly from the Stackpole Corporation, which had produced the original lot furnished by Alcoa, and was somewhat different than the original powder. The original powder could be blended with Cu powder to

FIGURE 1. $NiO-NiFe_2O_4$-Cu (17 wt% Cu) Anode Before (on left) and After (on right) Sintering

produce a cermet of near theoretical density (95%) at sintering temperatures as low as 1150°C. Cermets blended from the same Cu powder source and the new $NiO-NiFe_2O_4$ powder lot required sintering at 1300 to 1350°C to produce similar densities, although both powder lots were supplied "press ready." Apparently, the process control used during powder preparation can have a direct effect on the powder attributes.

The phrase "press ready" is often used to describe a powder which, as produced, is ready for processing. The spray-dried $NiO-NiFe_2O_4$ powder obtained from Stackpole had excellent flowability and tap density to obtain the needed die-fill to as-pressed ratio. The spray drying operation is the final step in the powder preparation operation that fixes the highly sinterable particles with binder in agglomerates ready for processing.

PNL-Developed $NiO-NiFe_2O_4$ Oxides

A minor effort was made during FY 1987 to develop the $NiO-NiFe_2O_4$-Cu (17 wt% Cu) cermet material from basic oxides, Fe_2O_3 and NiO, and Cu powder. The weight percentages of NiO and Fe_2O_3 for the $NiO-NiFe_2O_4$ powder mixture were determined by Alcoa (Weyand et al. 1986) to be 51.7 wt% NiO and 48.3 wt% Fe_2O_3.

These powders were wet milled with water in a conventional ball mill using steel mixing balls for 16 h. After drying, the powder was recovered and divided into samples, which were then calcined for 2 h at 700°C, 750°C, 800°C, or 900°C. The powder mixtures reacted to form the NiO-$NiFe_2O_4$ duplex oxide mixture at each of these temperatures. Since the lower calcining temperatures were adequate, subsequent milling was minimal and a highly sinterable powder was maintained. After calcining at 750°C, the NiO-$NiFe_2O_4$ powder was vibratory milled with 17 wt% Cu and 1 wt% poly-vinyl alcohol (PVA) for 1 h with steel balls in water. The PVA was added as a binding agent to aid in subsequent shape pressing.

This process does not produce a powder with the same flowing attributes of the spray-dried NiO-$NiFe_2O_4$ powder purchased from Stackpole and, subsequently, the powder is more difficult to form into green shapes. However, once sintered, the resulting cermet has an excellent dispersion of Cu throughout a homogenous NiO-$NiFe_2O_4$ oxide matrix. The microstructure of this cermet is shown in Figure 2. Although this was a cursory effort, the results indicate that this is a feasible method for producing the NiO-$NiFe_2O_4$-Cu-based cermets.

NiO-$NiFe_2O_4$-Cu-Ni-Al Cermets

Researchers at Alcoa postulated that a copper aluminate ($CuAl_2O_4$) phase may form on the surface of NiO-$NiFe_2O_4$-Cu cermet non-consumable anodes during electrolysis. This "passivating" layer provided the anode with protection from the corrosive attack of the electrolyte. It was proposed at PNL that this phase might be produced in-situ during cermet production by introducing Al metal into the cermet before sintering. Although subsequent SEM analysis has shown that the formation of a $CuAl_2O_4$ phase did not occur, the resulting microstructures unexpectedly possessed high electrical conductivities (at least four times higher than other NiO-$NiFe_2O_4$-Cu-based cermets), and have performed well in electrolysis testing. The final microstructures of Al-containing cermets have been shown to be dependent on composition, powder particle size, and fabrication procedure.

Two primary types of microstructures have been developed: one that is porous (90% of full density), and one which is much closer to full density (96% dense). Both of these microstructures were unexpectedly produced, and were

FIGURE 2. PNL-Developed NiO-$NiFe_2O_4$ Powder Vibratory Milled with 17 wt% Cu (2 µm)

found only when Al metal was added to the cermet prior to sintering. A representative microstructure of the porous material is shown in Figure 3; the sample shown contained 71 wt% NiO-$NiFe_2O_4$ powder, 25 wt% Cu, 3 wt% Ni, and 1 wt% Al prior to sintering. The porosity of the sample has been linked directly to the presence of Al metal, which is added to the cermet, and the processing procedure. Porous Al-containing cermets typically had densities in the vicinity of 5.7 g/cm^3. The higher density Al-containing cermets had densities in the vicinity of 6.35 g/cm^3. A representative microstructure of the dense material is shown in Figure 4. This sample also contained 71 wt% NiO-$NiFe_2O_4$ powder, 25 wt% Cu, 3 wt% Ni, and 1 wt% Al. Electrical conductivity measurements of both materials yielded values of about 410 $ohm^{-1}cm^{-1}$ at 950°C. This is a significant increase over the NiO-$NiFe_2O_4$-Cu and NiO-$NiFe_2O_4$-Cu-Ni cermets.

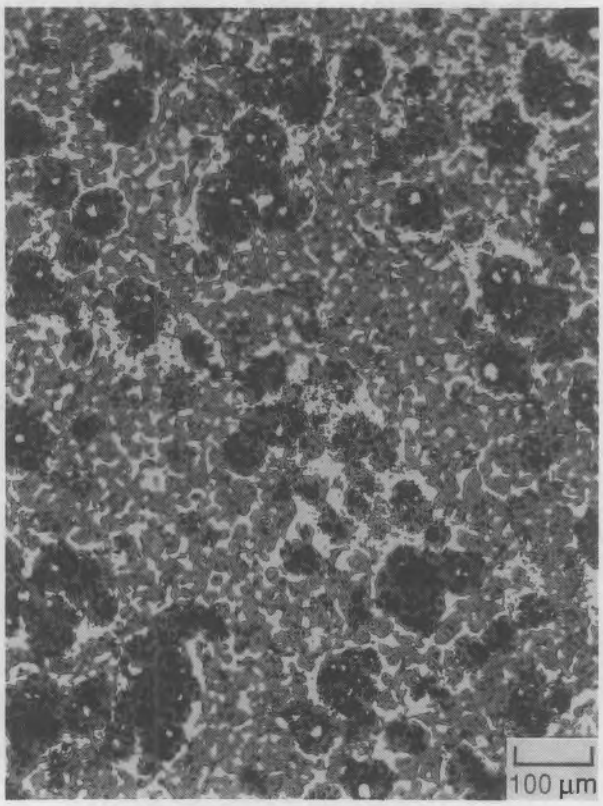

FIGURE 3. Porous NiO-$NiFe_2O_4$-Cu-Based Material

(Marschman and Davis 1987). The porous microstructure Al-containing cermet can be produced using Cu powder sources with particle size distributions ranging from 1 to 50 µm. It has also been determined that a porous microstructure will be formed when the Cu, Ni, and Al powders are blended with the NiO-$NiFe_2O_4$ powders using simple shaker-mixer blending techniques prior to pressing and sintering.

The more dense Al-containing microstructure could not be produced using coarse (5- to 15-µm) Cu powder. Through experimentation, it was determined that a smaller Cu particle size was necessary to produce the more dense microstructure, and a suitable Cu powder source was identified (Cerac 2-µm Cu powder). A more intimate mixing of the powders was also required to produce the more dense microstructures. This was accomplished using vibratory milling in a Freon solution with stainless steel milling balls for 1.5 h. The Freon was

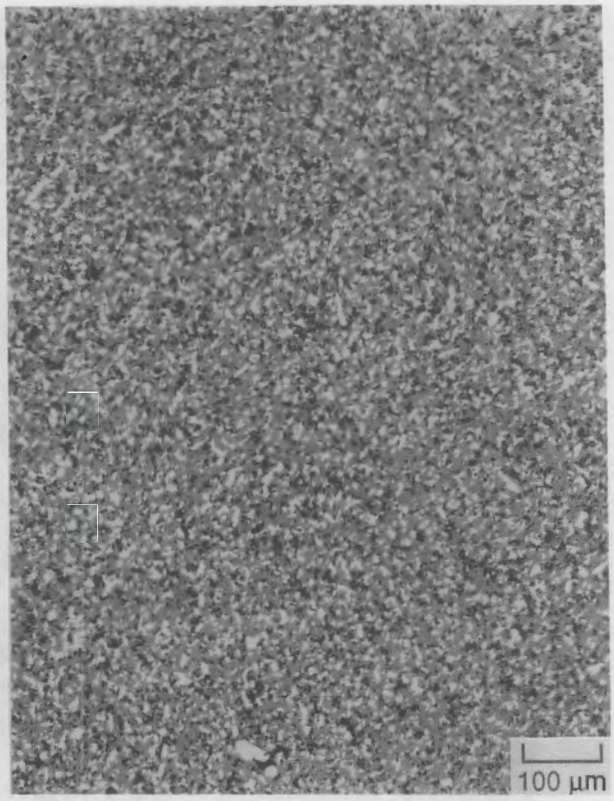

FIGURE 4. Sintered $NiO-NiFe_2O_4$-Cu-Based Material

removed from the mixture by evaporation. At this point, the powder mixture was pressed and sintered according to a schedule similar to that used to produce the $NiO-NiFe_2O_4$-Cu cermets.

Neither the porous microstructure shown in Figure 3, nor the dense, highly refined, homogeneous microstructure shown in Figure 4 has been reproduced without the presence of the Al metal in the composition. It is postulated that the Al reacts with the NiO and NiFe2O4 by the following reactions:

$$2Al + 3NiO = Al_2O_3 + 3Ni \quad (1)$$

$$8Al + 3NiFe_2O_4 = 4Al_2O_3 + 3Ni + 6Fe \quad (2)$$

Free Al_2O_3 is probably not formed but goes into solid solution with the spinel. Additional reduced metal is created if these reactions occur, and from observation of the microstructures in Figures 3 and 4, the metal phase appears

to be interconnected. Interconnection of the metal phase could account for the increase in the electrical conductivity of these cermets. However, the increasing electrical conductivity with increasing temperature suggests that electrical conduction occurs through the semiconductors in the solid. No other mechanisms are currently known that would account for the high electrical conductivity.

Brazing Techniques

Attachment methods that provide anode support and electrical contact must be developed for successful implementation of non-consumable anode technology. A small effort at PNL is focused on this problem and an attachment method resulted which was used to successfully join metal Ni rods to NiO-$NiFe_2O_4$-Cu-based cermet anodes. The method is a brazing technique that has been discussed in detail elsewhere (Marschman, Davis, and Stephens 1987). The technique can be briefly summarized as follows:

- Machine a hole in the cermet anode prior to or after sintering.
- Reduce the surface of the hole in the cermet to a metal using a reducing Ar/4% H_2 atmosphere for 20 min at 800°C.
- Prepare the reduced surface with a wire brush or sandpaper.
- Insert a small amount of powdered brazing alloy into the hole; the amount of powder depends upon the size of the braze joint.
- Insert a metal rod into the hole; Ni rods were used in this study.
- Furnace braze in an inert Ar atmosphere at 1250°C, for approximately 10 min.
- Furnace cool under the inert Ar atmosphere.

This procedure was used successfully to make connections to cylindrical cermet bodies as large as 3 cm in diameter and 5 cm in height. The Ni rods used in this study provided adequate strength for support of the anode as well as the electrical contact. An example of the resultant braze joint is shown in Figure 5. Some porosity exists in the braze joint; this porosity may be due to dissolved gases which evolve from the braze alloy and are trapped during cooling and solidification shrinkage. Although the reduced surface layer appears

FIGURE 5. Photomicrograph of Brazed Connection Between Ni Rod and $NiO-NiFe_2O_4$-Cu-Based Cermet Anode Material

metallic to the naked eye, the photomicrograph shows that the layer retains a significant number of oxide particles, indicating that the reduction process is not 100% efficient. However, the exposed metal surface area of the reduced metallic layer is sufficient to allow wetting by the braze alloy. A small crack appears between the reduced metallic layer and the bulk $NiO-NiFe_2O_4$-Cu-based cermet material. This crack may be due to a thermal expansion mismatch of the two materials augmented by radial stresses induced by thermal expansion during heating and cooling of the anode.

Materials Analysis

Analyses of non-consumable anode materials involve small-scale and laboratory-scale electrolysis testing. Analytical support including optical microscopy and chemical analyses was provided by technical support groups at PNL.

Small-Scale Electrolysis Testing

A small-scale electrolysis cell was developed at PNL during FY 1986 for the purpose of providing a versatile test bed for use in evaluating candidate non-consumable anode materials. This cell has been described in detail in a previous report (Marschman and Davis 1987). Use of this small-scale electrolysis cell ended midway through FY 1987 when the goals of the effort were accomplished, and the useful limits of the cell had been exceeded. However, the most significant results obtained in FY 1987 using this cell are described below.

Short-Term Testing. Small-scale electrochemical tests were performed on NiO-$NiFe_2O_4$-Cu-Ni-Al cermet materials. Samples were polarized at 1 A/cm^2 for up to 7 h. After 2 h of polarization, cyclic dc polarization experiments were performed. The resulting voltammogram obtained from one cycle performed at a scan rate of 10 mV/s is shown in Figure 6. The significance of this curve is that no major perturbations were detected on it that can be attributed to active corrosion processes, other than a small amount of hysteresis which is due to the disturbance of the passivation layer present on the cermet from the testing procedure. This test represented the first time a NiO-$NiFe_2O_4$-Cu-based cermet behaved similarly to an ideal inert electrode. Previously, all cermet anode materials developed at PNL had exhibited some type of perturbation in the voltammograms which could be attributed to corrosion of the Cu metal phase. A photomicrograph of the anode after electrolysis testing is shown in Figure 7. The sample shows very little corrosion, the chip missing from the end occurred during sectioning.

Long-Term Testing. A long-term electrolysis experiment was performed with the goal of obtaining 200 h of continuous operation. This test was performed jointly with the Stable Cathode Studies Task and was designed to test a

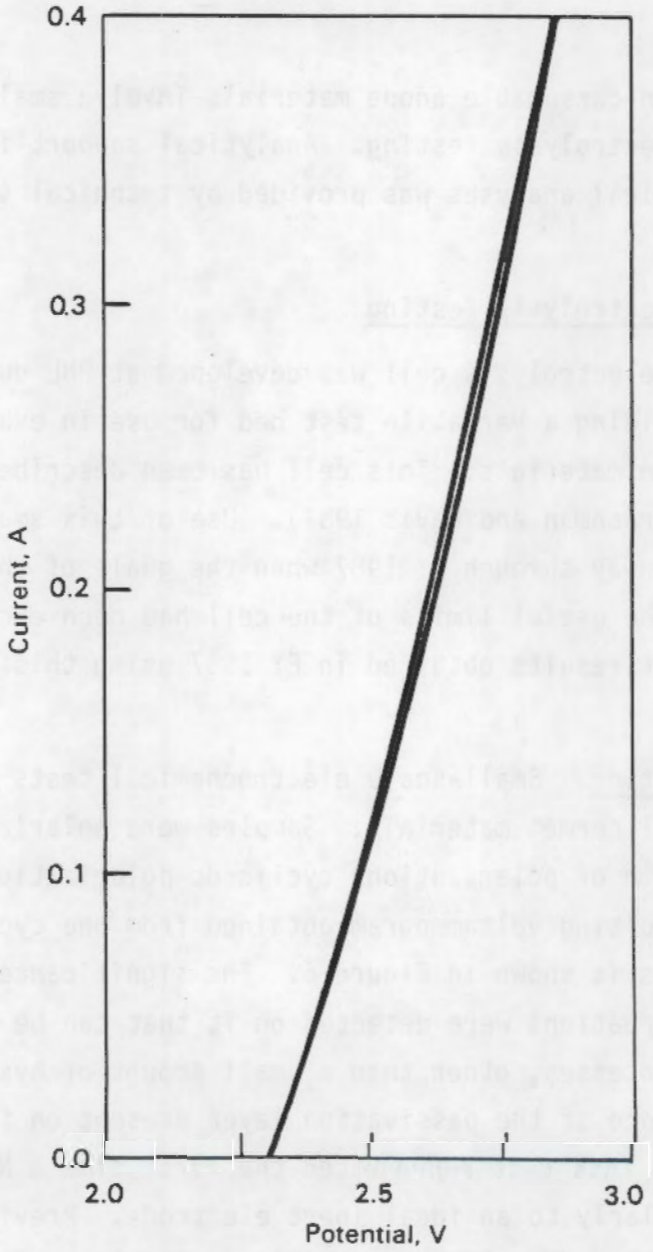

FIGURE 6. Voltammogram Obtained from NiO-$NiFe_2O_4$-Cu-Ni-Al Cermet Anode Galvanostatically Polarized for 2 h at A/cm^2 Prior to Cyclic dc Polarization Sweep

TiB_2-based cathode material as well as cermet anode materials. The anodes used in the test were NiO-$NiFe_2O_4$-Cu-Ni-Al cermets brazed to Ni support rods. The cell was operated between 950°C and 960°C using a 1.08 bath ratio electrolyte. The cell was operated at 5.1 A at a current density of 1.0 A/cm^2.

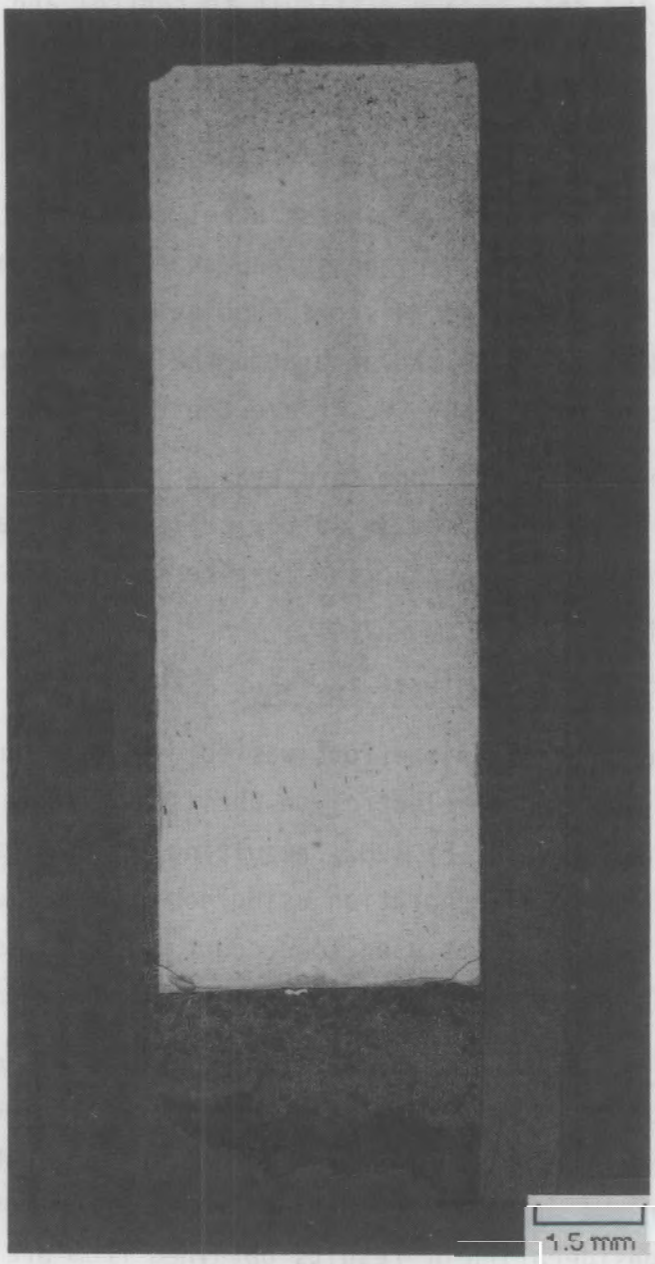

FIGURE 7. NiO-$NiFe_2O_4$-Cu-Ni-Al Cermet Anode After 7 h of Polarization at 1 A/cm^2 in an Electrolyte of 1.08 Bath Ratio. Corner was chipped during sectioning and is not due to the electrolysis testing.

The cell operated without problems for approximately 60 h. At this point, the Al_2O_3 sidewall failed (as determined by post-failure analysis) and current began passing through the cell sidewalls to the graphite crucible beneath the

Al_2O_3 crucible. The cell became difficult to control and anode wear rates increased; the first anode had to be replaced at 66 h.

Post-failure analysis of the cell indicated that the graphite crucible was also penetrated at the air/electrolyte interface. Thus, current would pass directly from the anode to the stainless steel containment crucible. The bath became contaminated with Fe, and the second anode failed at 116 h. The third anode lasted until the test was discontinued at 141.5 h. The experiment was halted when the dissolving Fe had saturated the electrolyte and raised the liquidus temperature high enough to freeze the top of the cell.

This test indicated that long-term evaluation of anode and cathode materials would have to be performed in larger cells. The small-scale electrolysis cells would not be useful in gathering long-term test data due to the problems uncovered by this one test.

Laboratory-Scale Electrolysis Testing

The principal goal of this effort was to evaluate non-consumable anode performance as a function of electrolyte chemistry. Many experiments were performed over the course of FY 1987, resulting in at least one major discovery regarding electrolysis cell operation using non-consumable anode technology. The electrolysis cell that was used to conduct these tests was described in a previous report (Hart et al. 1987), and for brevity will not be discussed here.

Electrolyte Variation Tests. A series of tests was designed to evaluate the performance of NiO-$NiFe_2O_4$-Cu-based anodes in a variety of electrolyte compositions. The electrolyte mixtures were selected statistically after careful review of the operating conditions found at commercial reduction facilities and consideration of results obtained from preliminary experiments. The concentrations of components of the electrolytes ranged as follows:

Bath ratio = 1.0 to 1.5
Al_2O_3 = 2 to 10 wt%
CaF_2 = 0 to 10 wt%
MgF_2 = 0 to 6 wt%
LiF = 0 to 5 wt%

TABLE 1. Experiments Performed Through FY 1987

EXP. NUMBER	ANODE NUMBER	DURATION (HOURS)	CURRENT (AMPS)	ANODE CURRENT DENSITY (A/cm2)	ALUMINUM PRODUCED (GMS)	COULOMBIC EFFICIENCY	BATH RATIO	AlF3	Al2O3	CaF2	MgF2	LiF	wt% Fe in Al metal	wt% Ni in Al metal	wt% Cu in Al metal	wt% Fe in bath	wt% Ni in bath	wt% Cu in bath	SUCCESS OR FAILURE	COMMENTS
58	102-1 & 101-2	20.0	20.1	0.5	0	0%	1.15	9.5	8.0	4.0	0	0	-----	-----	-----	-----	-----	-----	SUCCESS	2 Al-anodes, very slight edge wear
57	106-2	17.0	10.5	0.5	80.2	95%	1.35	3.7	8.0	5.0	0	0	-----	-----	-----	-----	-----	-----	SUCCESS	Cerox test; slight edge wear beneath coating
56	106-1	20.0	11.5	0.5	44.6	58%	1.15	9.5	8.0	4.0	0	0	-----	-----	-----	-----	-----	-----	SUCCESS	No wear
55	104-1	19.0	10.55	0.5	61.1	91.5%	1.15	9.5	8.0	4.0	0	0	-----	-----	-----	-----	-----	-----	SUCCESS	Al-anode, only very slight edge wear
54	105-2	20.0	11.0	0.5	68.7	93%	1.15	9.5	8.0	4.0	0	0	0.112	0.022	0.112	-----	-----	-----	SUCCESS	No wear
53	105-1	15.0	11.2	0.5	47.2	85%	1.15	9.5	8.0	4.0	0	0	0.103	0.013	0.081	-----	-----	-----	SUCCESS	No wear
52	103-2	20.0	10.8	0.5	64.3	88%	1.15	9.5	8.0	4.0	0	0	0.121	0.002	0.015	-----	-----	-----	SUCCESS	No wear
51	103-1	10.0	21.45	1.0	63.1	88%	1.15	9.5	8.0	4.0	0	0	-----	-----	-----	-----	-----	-----	FAILURE	Cerox, catastrophic, medium
50	100-2	20.0	21.8	1.0	No weight taken	---	1.0	14.7	2.0	10.0	0	0	-----	-----	-----	-----	-----	-----	FAILURE	slight edge, bottom, side wear
49	92-1	11.5	21.0	1.0	No weight taken	---	1.0	13.4	4.5	10.0	5.0	0	-----	-----	-----	-----	-----	-----	FAILURE	slight edge, bottom, side wear
48	96-3	15.0	20.5	1.0	No weight taken	---	1.0	14.7	2.0	10.0	0	0	-----	-----	-----	-----	-----	-----	FAILURE	catastrophic, med-large
47	96-2	14.0	20.4	1.0	No weight taken	---	1.0	13.4	4.5	10.0	5.0	0	-----	-----	-----	-----	-----	-----	FAILURE	catastrophic, med-large
46	97-2	20.0	22.0	1.0	111.0	75%	1.3	5.3	5.0	4.0	0	0	0.181	0.014	0.045	0.050	0.147	0.269	SUCCESS	very slight to nil wear
45	97-1	20.0	21.9	1.0	100.0	68%	1.1	10.0	5.0	10.0	0	0	0.235	0.105	0.245	-----	-----	-----	SUCCESS	very slight edge wear
44	82-2	20.0	21.9	1.0	No weight taken	---	1.07	11.7	11.6	4.0	0	0	ICP numbers not useable			0.032	0.022	0.020	SUCCESS	No wear
43	92-2	5.0	22.7	1.0	No weight taken	---	1.07	11.7	11.6	4.0	0	0	-----	-----	-----	-----	-----	-----	SUCCESS	very slight, even, edge, bottom, side wear
42	90-3	20.0	22.3	1.0	82.2	55%	1.07	11.7	11.6	4.0	0	0	-----	-----	-----	-----	-----	-----	FAILURE	catastrophic, med-large
41	90-2	20.0	20.7	1.0	120.0	87%	1.1	10.0	5.0	10.0	0	0	-----	-----	-----	-----	-----	-----	FAILURE	catastrophic, large
40	85-2	20.0	21.5	1.0	113.5	78%	1.0	14.7	2.0	10.0	0	0	ICP numbers not useable			0.168	0.168	0.413	FAILURE	cat. small-med
39	85-1	20.0	21.0	1.0	118.0	83%	1.1	10.0	5.0	10.0	0	0	ICP numbers not useable			0.093	0.300	1.070	FAILURE	cat. med.
38	86-4	30.0	14.95	1.0	123.0	82%	1.07	11.7	11.6	4.0	0	0	-----	-----	-----	-----	-----	-----	FAILURE	cat. small-med
37	86-2	30.0	23.4	1.0	114.7	49%	1.07	11.7	11.6	4.0	0	0	-----	-----	-----	-----	-----	-----	FAILURE	slope wear
36	86-3	20.0	18.9	1.0	102.4	80%	1.07	11.7	11.6	4.0	0	0	-----	-----	-----	-----	-----	-----	SUCCESS?	good? not identified
35	86-1	20.0	18.9	1.0	99.8	88%	1.07	11.7	11.6	4.0	0	0	-----	-----	-----	-----	-----	-----	PARTIAL SUCCESS	slight edge wear
34	63-3	20.0	17.8	1.0	22.9	19%	1.3	5.0	8.0	8.0	0	0	-----	-----	-----	-----	-----	-----	FAILURE	slope wear
33	63-2	20.0	16.9	1.0	72.4	64%	1.2	7.0	6.0	8.0	2.0	0	-----	-----	-----	-----	-----	-----	FAILURE	cat. med.
32	63-1	19.0	20.0	1.0	111.1	81%	1.0	14.1	5.0	4.0	8.0	0	-----	-----	-----	-----	-----	-----	FAILURE	cat. large
31	54-2	20.0	20.0	1.0	74.0	53%	1.0	13.4	4.5	10.0	5.0	0	-----	-----	-----	-----	-----	-----	FAILURE	cat. med-large
30	62-4	20.0	20.0	1.0	101.4	74%	1.3	7.1	8.0	3.0	4.0	2.0	-----	-----	-----	-----	-----	-----	FAILURE	cat. med.
29	62-2	20.0	19.0	1.0	82.2	62%	1.1	11.0	10.0	4.0	2.0	1.0	-----	-----	-----	-----	-----	-----	FAILURE	cat. med.
28	62-1	20.0	21.0	1.0	111.7	79%	1.25	9.1	5.0	7.0	3.0	2.5	-----	-----	-----	-----	-----	-----	FAILURE	cat. med.
27	54-1	7.0	20.1	1.0	No weight taken	---	1.1	10.0	11.0	4.0	0	5.0	-----	-----	-----	-----	-----	-----	FAILURE	cat. no pics taken
26	54-3	20.0	21.4	1.0	126.0	88%	1.1	10.0	5.0	10.0	0	0	-----	-----	-----	-----	-----	-----	FAILURE	severe edge wear
25	54-4	12.2	20.9	1.0	No weight taken	---	1.25	9.1	5.0	7.0	3.0	2.5	-----	-----	-----	-----	-----	-----	FAILURE	anode fell off, cat. large
24	55-4	20.0	19.9	1.0	119.4	89%	1.0	13.4	4.5	10.0	5.0	0	-----	-----	-----	-----	-----	-----	FAILURE	cat. edge and side, bottom was minimal
23	55-1	17.5	21.2 ave	1.0	No weight taken	---	1.1	10.3	10.3	4.0	6.0	5.0	-----	-----	-----	-----	-----	-----	FAILURE	anode fell off, no pics
22	55-3	20.0	21.0	1.0	107.9	77%	1.3	5.3	5.0	4.0	0	0	-----	-----	-----	-----	-----	-----	PARTIAL SUCCESS	slight edge wear only
21	55-2	20.0	21.0	1.0	119.9	85%	1.0	14.0	5.0	4.0	8.0	0	-----	-----	-----	-----	-----	-----	FAILURE	cat. edge only
20	52-2	20.0	21.0	1.0	73.0	52%	1.0	13.4	2.0	10.0	5.0	0	-----	-----	-----	-----	-----	-----	FAILURE	cat. large
19	52-1	20.0	21.0	1.0	87.1	48%	1.1	10.3	10.3	4.0	6.0	5.0	-----	-----	-----	-----	-----	-----	FAILURE	cat. med.-large
18	53-3	20.0	20.9 ave	1.0	130.2	88.5%	1.0	14.7	2.0	10.0	0	0	-----	-----	-----	-----	-----	-----	FAILURE	cat. small
17	53-2	17.5	20.2 ave	1.0	41.2	35%	1.0	13.4	4.5	10.0	5.0	0	-----	-----	-----	-----	-----	-----	FAILURE	anode fell off, cat. large
16	42-2	30.0	21.2 ave	1.0	52.2	24%	1.1	10.0	11.0	3.0	0	5.0	-----	-----	-----	-----	-----	-----	FAILURE	cat. med
15	40-1	30.0	20.7 ave	1.0	120.4	58%	1.1	10.3	10.3	3.9	6.0	5.0	-----	-----	-----	-----	-----	-----	FAILURE	cat. med-large
14	42-3	30.0	18.9 ave	1.0	134.3	71%	1.07	11.7	11.6	4.0	0	0	-----	-----	-----	-----	-----	-----	FAILURE	cat. small-med.
13	41-3	30.0	21.1 ave	1.0	114.9	54%	1.07	11.7	11.7	11.6	4.0	0	0.855	0.488	0.504	-----	-----	-----	FAILURE	slope wear
12	41-4	30.0	19.8	1.0	146.8	73%	1.07	11.7	11.6	4.0	0	0	0.611	0.414	0.282	-----	-----	-----	FAILURE	slope wear
11	52-3	30.0	19.5 ave	1.0	170.9	87%	1.1	11.0	10.0	4.0	2.0	1.0	0.265	0.185	0.714	-----	-----	-----	FAILURE	cat. edge & side, bottom ok
10	41-1	20.0	20.0	1.0	85.0	64%	1.1	12.7	10.0	4.0	4.0	2.0	0.700	0.587	0.568	-----	-----	-----	PARTIAL SUCCESS	bottom not flat
9	41-2	30.0	20.2	1.0	No weight taken	---	1.07	11.7	11.6	4.0	0	0	-----	-----	-----	-----	-----	-----	FAILURE	cat. med. no other data recorded

1 through 8 were scoping experiments and data not available.

The legend for the Comment column is shown on following page. Metal/bath analyses were not performed or reported on most experiments that failed or on many of the successful experiments for one of the following reasons: 1) experiments were performed to demonstrate anode stability only, 2) not all the aluminum produced could be recovered to allow back calculation of impurities due to the anode, 3) analysis failed, or 4) was limited.

No wear

Discoloration, slight wear

Edge wear

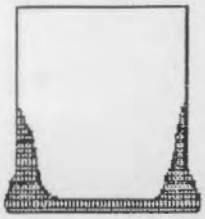

Catastrophic, small

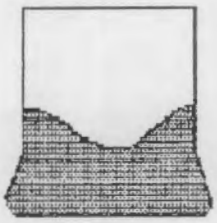

Catastrophic, medium

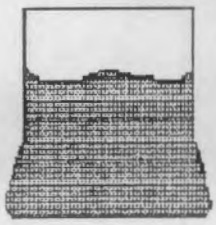

Catastrophic, large

Slope wear

Legend for Table 1, Comments column. Slight wear is meant to define wear of less than 0.5 mm, which is just visible to the eye. Edge wear is qualified the same as slight wear, however, only the edge of the anode is affected. Slope wear appeared on some anodes, and although the anode appeared sound, it did not maintain the original shape. Catastrophic failures were characterized by severe degradation of a portion of the anode cermet matrix.

Approximately 30 experiments designed to evaluate the effect of electrolyte chemistry on non-consumable anode performance were performed during FY 1987. These experiments are listed in Table 1, experiment numbers 9 through 38. Of those experiments, four were considered to be reasonably successful. The experimental failures were largely attributed to variations in the electrolyte chemistry. All of the anodes from the four partially successful tests exhibited some type of degradation. Although relatively high electrolysis cell current efficiencies (89% maximum) and Al purities (98.5%) were obtained, the degradation of the anodes was unsettling.

Anode degradation for the 30 tests ranged from severe, where the anodes were so badly corroded that they fell into the electrolyte (Figure 8), to only slight degradation of the anode edges (Figure 9). Four experiments (numbers

FIGURE 8. Anode That Failed Due to Severe Corrosion (from Experiment 25)

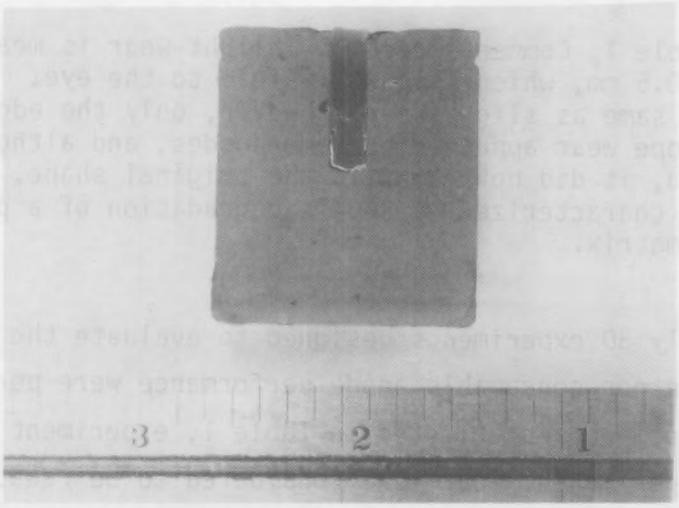

FIGURE 9. Anode That Has Only Slight Corrosion at the Edge (from Experiment 35)

39, 40, 41, and 42 in Table 1) were performed in an attempt to duplicate the partially successful experiments, but the anodes were severely corroded in each of these experiments (Figure 10).

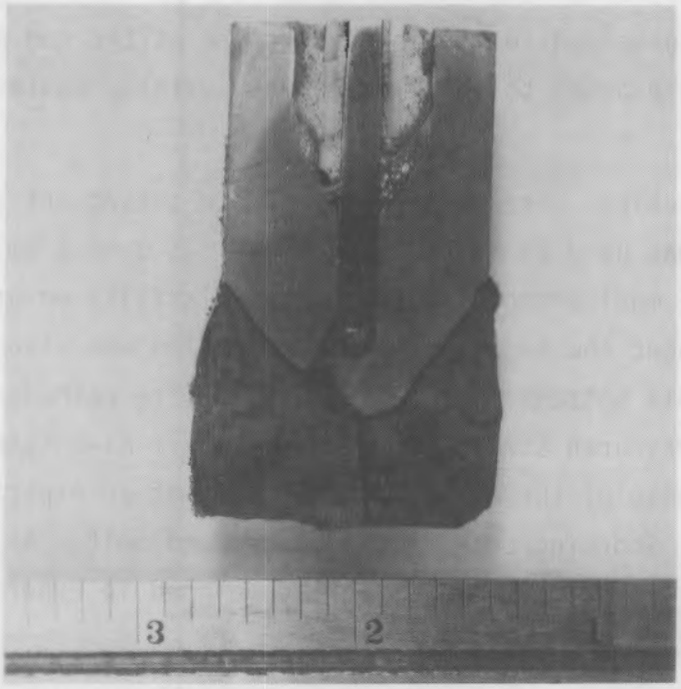

FIGURE 10. Anode from Experiment 41, Which Was an Attempt to Duplicate Previous, Partially Successful Experiments

These unsettling results led to a re-evaluation of the data obtained to that point, and a re-evaluation of the experimental procedures. After careful review of the electrolysis cell operating parameters, several problems were identified. It was determined that the amount of electrolyte used in the cells was insufficient to provide adequate volume for the duration of the test. Electrolyte volatility was found to contribute to large electrolyte losses during a 20-h test.

Initially it was believed that placing a large (250-g) high-purity Al pad into the electrolysis cells would aid in coalescing the Al that was produced. Although the molten Al could be consolidated into a large pad, the pad did not remain stable. Post-test analysis of several cells indicated that the Al pads were sufficiently large to extend to the electrolyte surface. This resulted in electrical shorting of the anodes to the molten Al cathodes, which was most likely responsible for anode failure. As a result of electrolyte volatility,

other cells contained so little electrolyte at the end of the tests that the Al metal pad was exposed to the electrolyte surface, again resulting in anode shorting.

These problems were easily solved. In subsequent experiments, sufficient electrolyte was used to maintain the level at 6 to 8 cm above the molten Al pad. Careful monitoring of electrolyte volatility ensured adequate electrolyte depth throughout the tests. The other problem was also effectively solved by lining the cell bottoms with a TiB_2-G composite cathode material obtained from Great Lakes Research Corporation. Use of this Al-wetting cathode material allowed the size of the Al pad at the start of an experiment to be reduced by a factor of 4. Shorting between the anodes and molten Al cathodes was eliminated. These improvements were developed in experiments 43 through 50 shown in Table 1.

Verification Tests. Additionally, experiments 45 through 50 (Table 1) were conducted in an attempt to reproduce the partly successful tests performed earlier using the improved cell operating procedures. Experiments 45 and 46 were successful, and little or no wear was apparent on the anodes (Figure 11). However, experiments 47, 48, 49, and 50 produced anodes that had amounts of degradation that could not be explained (Figure 12). These four

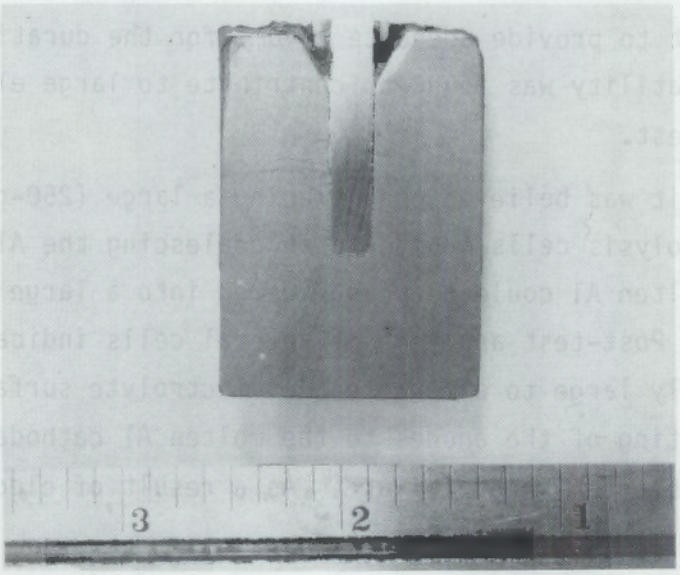

FIGURE 11. Anode from Experiment 46. Only slight wear is apparent.

FIGURE 12. Anode from Experiment 48. Note the large amount of degradation.

cells were difficult to operate, and all required constant attention to maintain stable operation. The cell operating procedures were again scrutinized.

The Al_2O_3 feed used in the experiments to that point was a highly calcined Al_2O_3 obtained from J. T. Baker Chemicals. Cell mucking (sludging) was a continual problem, which indicated the dissolution kinetics of the highly calcined Al_2O_3 were slow. After consultation with aluminum industry representatives, the type of Al_2O_3 fed to the cells was changed. "Metal grade" Al_2O_3 was obtained from Alcoa for the next tests. This Al_2O_3 was found to dissolve much more easily, and mucking problems were less severe. The equations used to calculate the saturation concentration of Al_2O_3 in the electrolyte were also reviewed. This resulted in lower quantities of Al_2O_3 being added to the electrolyte, which reduced the possibility of oversaturating the electrolyte.

Process Control Development. Almost simultaneously with the verification tests, O. H. Koski (Sensors Development) was conducting research designed to provide information about electrolysis cell operation that would aid in the development of process sensors. His experiments showed that Al electrolysis cells could be described as a series of resistive components. Examination of

the data showed that the total cell resistance measured during electrolysis was not equal to the sum of the known cell resistances. Evaluation of the electrolysis process determined that a resistive film was formed or plated onto the surface of the anode (see Section 5.0).

The research performed at PNL has shown that anodes can be protected by this electrically resistive, yet still electrically conductive, film which forms on the surface of the anode material during the electrolysis process. It is postulated that the film involves an anion of some O-Al-F species or metal oxide species present due to impurity contamination. The exact chemical composition of this film has not been determined; current analytical chemistry techniques appear to be inadequate. Post-test analyses cannot detect the film because the anodes are always coated with a thin layer of electrolyte, which interferes with analytical techniques. In-situ analyses (such as Raman spectroscopy) have not proven successful due to interference from the surrounding physical and chemical environment (electric furnace noise, overlapping spectra, etc.). However, the presence of the film can be confirmed by simple electrochemical techniques discussed below.

Maintenance of the conditions necessary to promote the formation of the protective film is essential to ensure proper anode performance. Research at PNL has shown that the integrity of the protective film is influenced by operating temperature, Al_2O_3 concentration in the electrolyte, and anode current density. The effects of temperature on the observed anode and electrolyte resistance are shown in Figure 13. Experiments were performed with Al_2O_3 concentrations ranging from 0 to 15 wt%. The observed resistance shows a marked increase at temperatures below 940°C over the Al_2O_3 concentration range of 0 to 10 wt%, and at temperatures below 965°C for an Al_2O_3 concentration of 15 wt%.

The observed increase in anode and electrolyte resistance can be attributed to the formation of a highly resistive film layer deposited on the surface of the anode. The formation of this film is suggested by the result that no major changes in the resistance of the anode material, lead wires, or electrolyte resistance occur during electrolysis. Precipitation of electrolyte or Al_2O_3 on the anode surface was not possible because of the high temperature

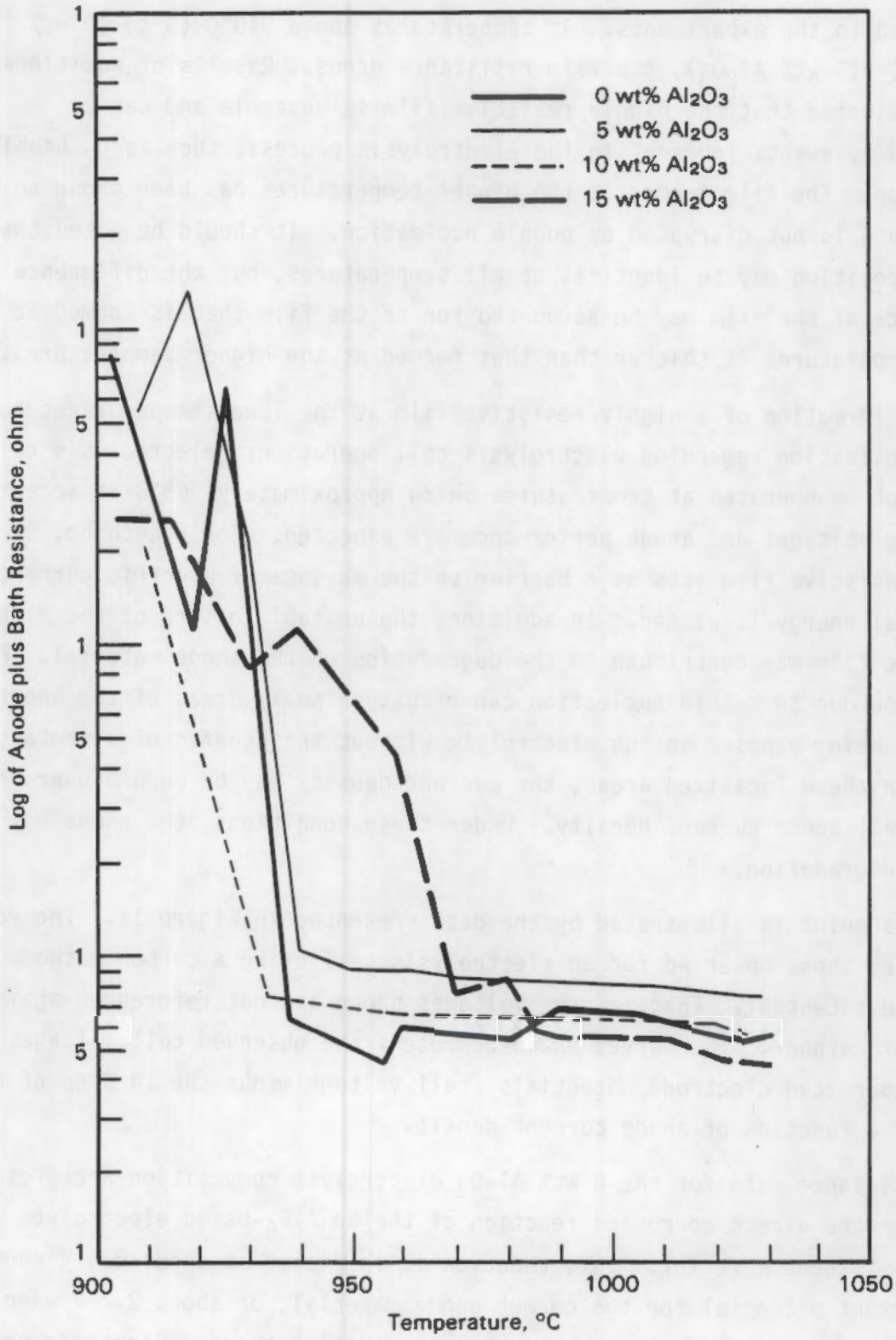

FIGURE 13. Anode and Electrolyte Resistance as a Function of Al_2O_3 Concentration Versus Cell Temperature

maintained in the experiments. At temperatures above 940°C (0 to 10 wt% Al_2O_3) and 965°C (15 wt% Al_2O_3), the film resistance drops. Results of additional tests indicated that the highly resistive film is unstable and can be disrupted by events inherent in the electrolysis process, such as O_2 bubble nucleation. The film formed at the higher temperatures has been shown to be stable, and is not disrupted by bubble nucleation. It should be noted that the film composition may be identical at all temperatures, but the difference in resistance of the film may be accounted for if the film that is formed at the lower temperatures is thicker than that formed at the higher temperatures.

The formation of a highly resistive film at the lower temperatures has one major implication regarding electrolysis cell operation: electrolysis cells should not be operated at temperatures below approximately 965°C if acceptable operating voltages and anode performance are expected. For one thing, the highly resistive film acts as a barrier to the passage of electric current, and electrical energy is wasted. In addition, the unstable nature of the highly resistive film may contribute to the degradation of the anode material. Film disruption due to bubble nucleation can result in small areas of the anode material being exposed to the electrolyte without the benefit of a protective film. In these localized areas, the current density may be much higher than the overall anode current density. Under these conditions, the anode may undergo degradation.

This point is illustrated by the data presented in Figure 14. The voltage values are those observed for an electrolysis cell using a carbon cathode of undefined potential. That is, the voltages shown are not referenced against a liquid-Al cathode. The curves shown represent the observed cell voltages and the IR-corrected electrode potentials (cell voltage minus the IR drop of the cell) as a function of anode current density.

Resistance data for the 0 wt% Al_2O_3 electrolyte composition are presumed to be for the direct corrosion reaction of the Na_3AlF_6-based electrolyte with the cermet anode material. This reaction is initiated at about 0.5 V above the zero current potential for the cermet anode material, or about 2.7 V when corrected to a cell referenced against a liquid Al cathode. Electrode potential decreases with increasing anode current density until a current density of

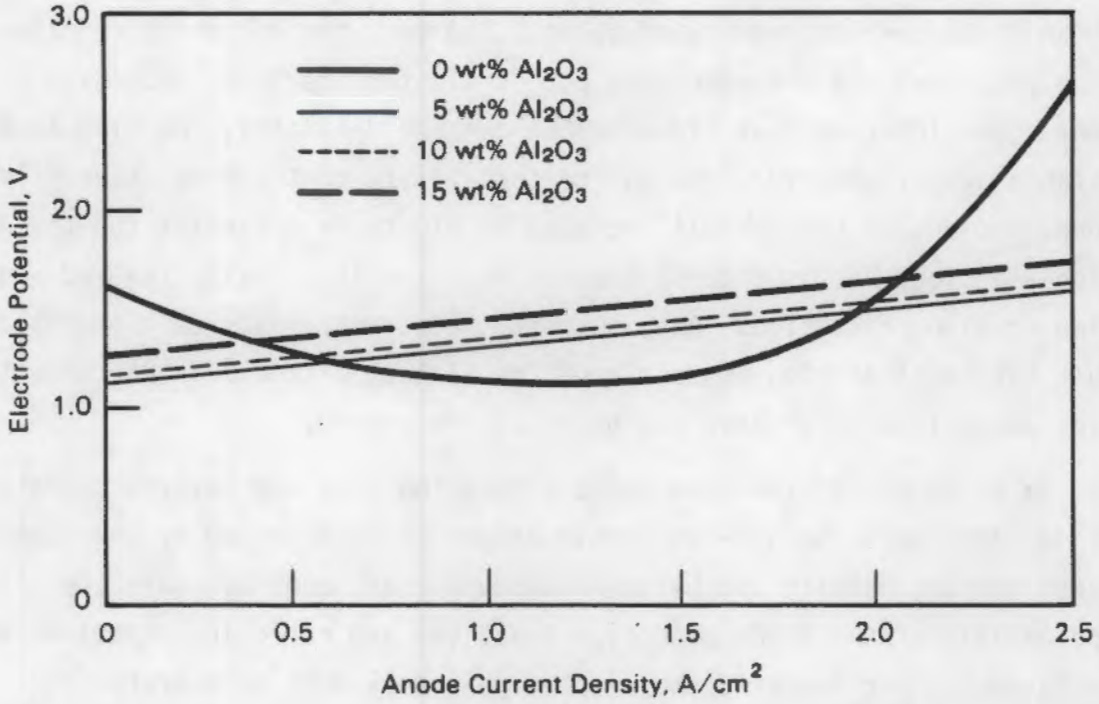

FIGURE 14. Electrode Potential Change with Variation of Anode Current Density

about 1.6 A/cm^2 is reached, at which point the electrode potential increases. This suggests that the corrosion reaction is self-catalyzing in the anode current density range from 0 to 1.6 A/cm^2.

The electrode potentials plotted for the three compositions of 5, 10, and 15 wt% Al_2O_3 illustrate the conditions under which Al metal is produced during electrolysis and a film is known to cover the anode. As is illustrated, the zero current potentials are approximately 0.5 V below those for the corrosion reaction. The electrode potentials remain below that observed for the corrosion reaction until an anode current density of about 0.5 A/cm^2 is reached. This implies that the corrosion reaction is not favored below 0.5 A/cm^2 anode current density and >5 wt% Al_2O_3. The film on the anodes is also known to be stable at these conditions. Above 0.5 A/cm^2 anode current density, the corrosion reaction is favored; the electrode potential for the corrosion reaction is lower than the electrode potential for the Al_2O_3 reduction reactions. The film on the anode has been shown to be generally unstable under these conditions.

At an anode current density of about 2.0 A/cm^2, the corrosion reaction electrode potential and the electrode potentials for the Al_2O_3 reduction reactions again intersect; at higher anode current densities, the film appears to be stable again. However, due to the instability of the protective film on the anode, and due to the overall increase in electrode potential for the Al_2O_3 reduction reactions, it is uncertain which reaction is actually favored--anode corrosion or Al_2O_3 reduction. Data suggest that electrolysis cell operation is difficult (at best) at high anode current densities, although anode current densities above 1.25 A/cm^2 have not been fully explored.

It can be concluded from the above discussion that the desired operating current density range for non-consumable anodes is represented by the region above zero current density and below an anode current density where the electrode potentials of the Al_2O_3 reduction reactions and corrosion reactions are equally favored. Furthermore, the electrolysis cell must be operated at a sufficiently high enough temperature so as to encourage the development of a stable, low-resistance film on the anode; the film is the primary corrosion protection mechanism for the anode material. These conditions cannot be expected to remain identical because electrolyte chemistry and other electrolysis cell parameters vary from one reduction facility to another.

A simple device has been developed for use in determining the stability of the protective film that forms on the anodes during operation. The device is basically a simple reference anode constructed from cermet material and fashioned into a small probe. The circuitry developed to use this device is illustrated in Figure 15. The probe is inserted into the molten electrolyte and fed a small dc current by means of a resistor connected to the main electrolysis dc current bus. The current fed to the probe provides a current density that is a small fraction of that found on the anode but ensures an electrochemical similarity between the anode and the probe. The dc voltage drop between the anode and probe is used as an analog of the anode-to-Na_3AlF_6 potential.

Stable electrolysis cell operation (stable anode film) is represented as a steady dc signal detected between the anode and probe. Any instability of the anode is easily detected as an unsteady dc signal between the anode and probe.

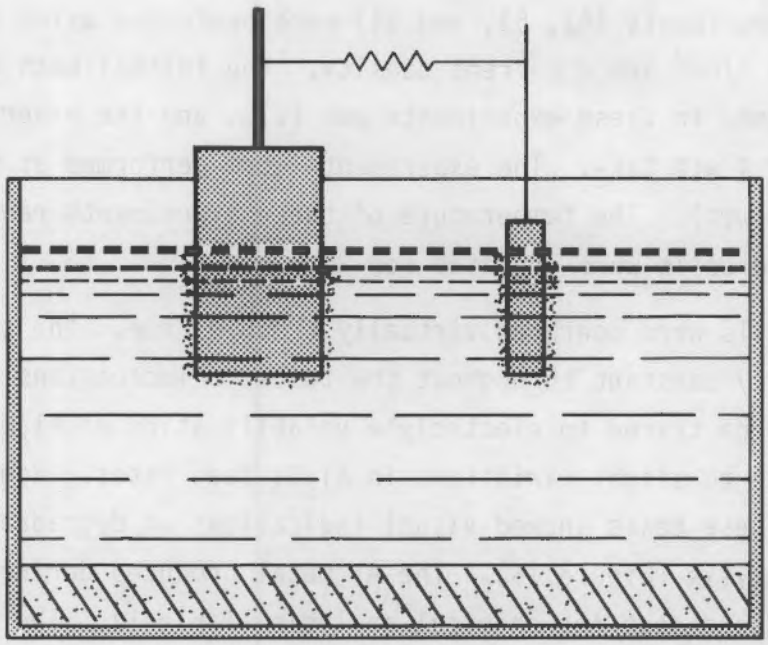

FIGURE 15. Schematic of Simple Process Control Sensor Used to Monitor Anode

Electrolysis cell control is deduced from this signal. Assuming constant Al_2O_3 concentration and anode current density, the temperature can be varied until instability sets in, thus identifying the lowest temperature at which stable operation can be maintained. By similar methods the optimum anode current density and Al_2O_3 concentration can be identified for any electrolyte composition.

This device has been employed in laboratory-scale electrolysis cells at PNL. The operation of electrolysis cells has been greatly improved since theimprovements discussed above were made in the operating conditions and the device has been used to monitor cell operating conditions.

Confirmation Testing. Experiments 52, 53, 54, 55, 56, and 58 were performed to study the behavior of $NiO-NiFe_2O_4$-Cu-based cermet anodes using the process control device described above. All of the experiments were performed at reduced anode current densities and actively monitored using the process control device. An immediate improvement in electrolysis cell operation and anode performance was realized.

Three experiments (52, 53, and 54) were performed using NiO-$NiFe_2O_4$-17%Cu anodes at 0.5 A/cm^2 anode current density. The initial bath ratio of the electrolyte used in these experiments was 1.15, and the experiments contained an additional 4 wt% CaF_2. The experiments were performed at or near Al_2O_3 saturation (8 wt%). The temperature of these experiments ranged from 960°C to 970°C, and the cells were operated for 20 h.

These cells were operated virtually trouble free. The cell voltages remained nearly constant throughout the tests. Fluctuations in the cell voltage could be traced to electrolyte volatilization or Al_2O_3 concentration variations due to slight variations in Al_2O_3 feed rates. None of the three anodes from these tests showed visual indications of degradation during the post-test analysis (Figure 16). The Al metal produced during these experiments was recovered and sent for chemical analysis (Table 1). The concentration data are corrected for the impurities introduced by the small Al pads placed in each cell prior to start-up.

In Experiment 54, a cell was operated for 20 h using an NiO-$NiFe_2O_4$-17%Cu cermet anode. The electrolyte and temperature of this experiment are shown in

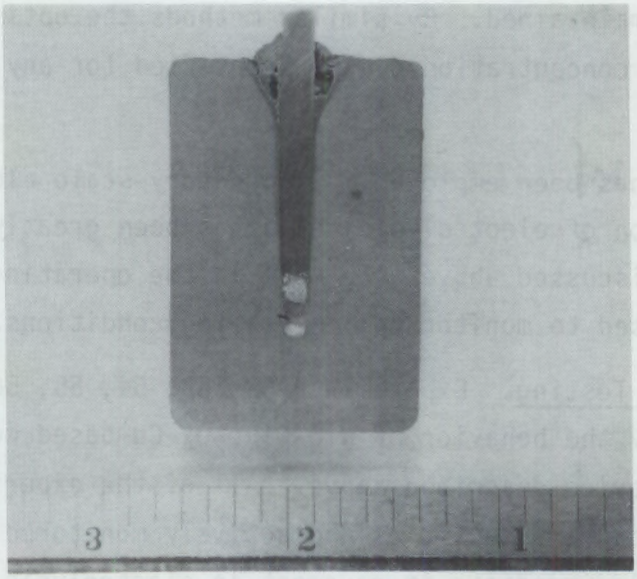

FIGURE 16. Anode from Experiment 52, Which Was Performed Using Process Control Device and Improved Operating Conditions. Crack in mode is a result of rapid air-cooling at end of experiment.

Table 1. The cell was started using an anode current density of 0.5 A/cm^2 and allowed to reach stable operation. After 6 h of operation, the cell current was increased from 11 A to 25 A (0.5 to 1.1 A/cm^2) in an attempt to "push" the anode protective film. The Al_2O_3 feed rate was adjusted to account for the increase in Al production expected. The cell operated smoothly for about 3 h, at which point the signal monitored between the process control device and anode became unstable. The instability increased rapidly (within 5 min), and the cell current was returned to 11 amps (0.5 A/cm^2) in an attempt to stabilize the cell. The instability continued, and the cell current was further reduced to 5 amps (0.23 A/cm^2). At this current density the cell instability ceased. The cell was allowed to stabilize under these conditions for about 10 min, and then the cell current was increased to 11 amps (0.5 A/cm^2). The cell remained stable for the remainder of the test.

Post-test analyses of the anode again showed no signs of degradation (Figure 17). Apparently the protective film that develops on the surface of the anodes during operation can be "pushed" to higher current densities for short periods. The technique used to eliminate the cell (anode) instability is

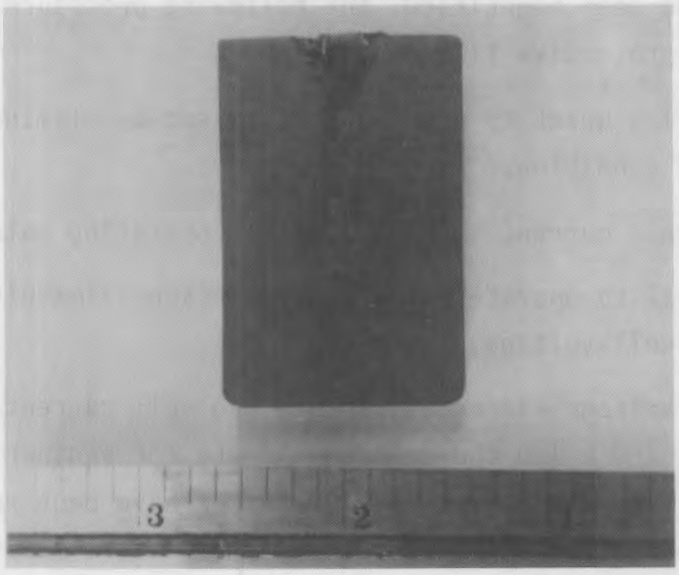

FIGURE 17. Anode That Underwent "Upset" Conditions During Experiment 54

reproducible and can be used not only to recover from conditions of excessive anode current density but also to recover from the non-consumable anode equivalent of an anode effect.

Alumina starvation was induced during the course of operating several cells by simply turning off the cell feeders. The cells were allowed to operate until insufficient Al_2O_3 was present in the electrolyte to permit steady operation. Once the Al_2O_3 content of the electrolyte was sufficiently depleted, the cell voltage rose sharply at a rate of approximately 0.2 V/min. Left uncorrected, the cell voltage would continue to climb and begin to oscillate sharply. Degradation of the anode would occur unless corrective measures were taken.

During conditions of depleted Al_2O_3, the protective film on the anode is either destroyed or redissolved into the electrolyte. This leaves the anode exposed to the electrolyte with no protection other than its inherent corrosion-resistant properties. Research at PNL has shown that the degradation process can be halted before damage results to the anode by following a corrective procedure similar to that described above. After a condition of depleted Al_2O_3 has been identified, the following procedure can be used to re-establish the protective film on the anode:

- Feed the cell a quantity of Al_2O_3 sufficient to eliminate the depleted condition.
- Reduce the cell current to about 1/2 the operating value.
- Allow the cell to operate for a period of approximately 5 min, and observe the cell voltage.
- If the cell voltage increases, reduce the cell current by 1/2 a second time, and allow the cell to operate for another 5 min. When the cell voltage decreases, the conditions have been reached that will promote reestablishment of the film.
- Hold the cell at the highest current that still results in a condition of decreasing cell voltage.

- Allow the cell to stabilize and maintain this operation for at least 10 min.
- Return the cell to the original anode current density.
- If the cell voltage begins to increase, repeat the procedure described above and lengthen the stabilization period.
- If the cell voltage remains stable, resume cell operation and Al_2O_3 feeding.

This procedure has been used successfully many times to recover from Al_2O_3-depleted conditions. It has failed only when the cell has been depleted in Al_2O_3 for extended periods and the cermet anode damaged beyond repair. The procedure is applicable to commercial cell operations, though refinement of the technique will be required. Since the process control device will provide the same information as the cell voltage, individual devices could be used to monitor each anode in a commercial cell and allow independent maintenance of each anode.

NiO-$NiFe_2O_4$-Cu-Ni-Al Cermet Experiments. Two experiments (numbers 55 and 58) were performed to test the NiO-$NiFe_2O_4$-Cu-Ni-Al cermet anode material. One experiment (number 55) used a single anode, the other experiment contained two anodes. The first experiment (number 55; single anode) was performed in an electrolyte with an initial bath ratio of 1.15, 4 wt% additional CaF_2, and Al_2O_3 saturation (8 wt%). The cell was operated for 20 h at 965°C, using the process control device. Post-test analyses of the anode showed no visual corrosion (Figure 18).

The second test (number 58) was performed in a larger, 15-cm-diameter electrolysis cell. Two anodes were placed in tandem to test the feasibility of using clustered anodes and one process control sensor for two anodes. The electrolyte was the same as in the first test. The cell was operated at 965°C for 20 h without incident. The process control device was effective in monitoring the performance of the two anodes, though it would not have been possible to distinguish between the two anodes if a problem had developed with one and not the other. Post-test optical microscopy of the anodes indicated

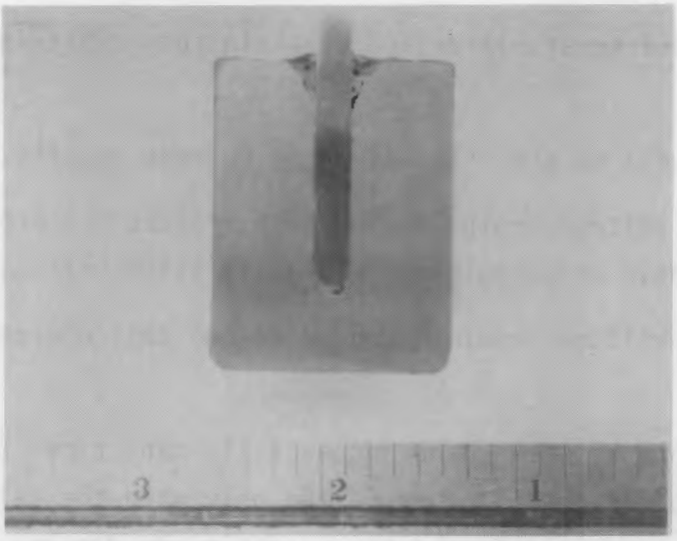

FIGURE 18. NiO-$NiFe_2O_4$-Cu-Ni-Al Anode Used in Experiment 55

virtually no corrosion; only one of the anodes showed evidence of a slight amount of corrosion at the edge. The effect of geometry on anode performance may need to be investigated further.

FUTURE DIRECTIONS

Research performed through the end of FY 1987 has lead to new discoveries about the use of non-consumable anodes for the electrolytic production of Al. The importance of cell control and anode monitoring has been realized, and these techniques must be made applicable to commercial electrolysis cells if this technology is to be implemented by commercial industry. Future research will focus on the verification and confirmation of the operation techniques discussed in the preceding section, and on expansion of the range of electrolytes that can be used with the cermet anodes. Although the NiO-$NiFe_2O_4$-Cu-Ni-Al cermet material appears to be the most promising non-consumable anode material developed (high electrical conductivity, good performance in cells), the standard NiO-$NiFe_2O_4$-17%Cu anode material may prove cheaper and easier to produce. This issue will also be addressed in FY 1988. The final goal of the future work is, of course, implementation of non-consumable anodes by the aluminum industry. Continued success and promising results should allow the realization of that goal.

REFERENCES

Hart, P. E., et al. 1987. Inert Anode/Cathode Program Fiscal Year 1986 Annual Report. PNL-6247, Pacific Northwest Laboratory, Richland, Washington.

Marschman, S. C. and N. C. Davis. 1987. Materials Development for Inert Anodes: Progress Report for the Period from November 1985 to February 1987. PNL-6343, limited distribution document, Pacific Northwest Laboratory, Richland, Washington.

Weyand, J. D., D. H. DeYoung, G. P. Tarcy, and F. W. Baker. 1986. Inert Anodes for Aluminum Smelting - Final Report for the Period 29 September 1980 to 30 September 1985. DOE/CS/40158-20, Alcoa Center, Pennsylvania.

3.0 MATERIALS EVALUATION

C. F. Windisch

The objectives of this subtask for FY 1987 were to identify the most corrosion-resistant candidate inert anode materials by determining their electrochemical reactions in bench-scale Al reduction cells and to determine the bath compositions that optimize corrosion resistance and anode lifetimes.

SUMMARY

Research conducted in FY 1986 suggested that all-metal electrodes should be used in electrochemical studies with molten Na_3AlF_6. Thus, Cu metal was used in the experiments carried out in FY 1987. Results from FY 1987 studies suggest that a series of reactions occurs when Cu metal is immersed in molten Na_3AlF_6 and polarized anodically to give 1 A/cm^2. This reaction sequence was studied, in part, using ac impedance which suggests that, when Cu metal is immersed in molten Na_3AlF_6, the following reaction occurs in the absence of an applied potential:

$$Cu + F^- = CuF + e^- \qquad (1)$$

Although no CuF could be detected in the reaction products, the ac impedance data supported a reaction of this type. Under the test conditions the reaction was found to be controlled by mass transport. The absence of CuF was explained by its instability which has been observed by other workers, including Whiting, Mamantov, and Young (1973).

In the presence of dissolved Al_2O_3, Cu_2O is formed, possibly as a result of the following rapid reaction:

$$2CuF + O^{2-} \rightarrow Cu_2O + 2F^- \qquad (2)$$

This reaction is supported by the large amounts of Cu_2O on Cu electrodes observed with scanning electron microscopy/energy dispersive x-ray spectroscopy (SEM/EDS) and x-ray diffraction analysis (XRD).

Cyclic voltammetry studies suggest that, upon anodic polarization to about 2.1 V relative to a Al/Al_2O_3 couple, the Cu^+-containing Cu_2O converts to a species containing Cu^{2+}, probably CuO or CuF_2:

$$Cu_2O + O^{2-} \rightarrow 2CuO + 2e^- \quad (3)$$

This reaction and the cyclic voltammetry data used to support it were discussed in Hart et al. (1987).

Since species containing Cu^{2+}, notably CuO and CuF_2, were not present in significant quantity in reaction products, as measured by SEM/EDS and XRD, it was proposed that they decomposed. A possible decomposition reaction is the following:

$$2CuO \rightarrow 2Cu + O_2 \quad (4)$$

or, in the presence of Al_2O_3,

$$4CuO + 2Al_2O_3 \rightarrow 4CuAlO_2 + O_2 \quad (5)$$

These reactions are supported by the discovery of both Cu and $CuAlO_2$ in the reaction products in post-test analyses. Also, pure CuO is known to decompose at about 1026°C, not far above the operating temperatures employed in this work. Whiting, Mamantov, and Young (1973) also reported on the instability of CuF_2 in fluoride melts.

The results discussed above indicate the following:

1. Copper is reactive in molten Na_3AlF_6 when polarized anodically.
2. The reaction products of Cu oxidation are poorly defined since in situ techniques like laser Raman spectroscopy do not yet have acceptable sensitivity and products were not observed in post-test analyses. All of the available data suggest the reaction products contain Cu^{2+}, which decomposes prior to post-test analyses.

3. Contrary to proposals by Alcoa, $CuAlO_2$ (copper aluminate) is not a passivating reaction product. It appears to form as a result of the decomposition of the primary Cu^{2+}-containing reaction products.

Concerning the implications for the candidate cermet inert anode materials, this work suggests that:

1. Further work should be conducted to determine the properties of the reaction products on Cu in pure metal and cermet electrodes during polarization at 1 A/cm^2. This may be accomplished using ac impedance techniques or fast linear sweep voltammetry.

2. Since anode surface area was suspected of playing an important role in determining the anode/melt reactions, the size and distribution of the metallic phase in the cermet anode may impact its corrosion resistance. Further work is suggested in this area as well.

3. Copper aluminate was found to be "non-passivating." In the absence of a true passivating phase, there exists the possibility that Cu reacts completely in the surface regions of the cermet anode so that, during operation, primarily spinel/oxide is in contact with the molten electrolyte. This possibility should be investigated further to determine by what mechanism Cu is depleted and how the corrosion process is eventually controlled.

TECHNICAL PROGRESS

Several types of experiments were conducted during FY 1987. These included cyclic voltammetry studies of oxide layers on Cu anodes; ac impedance studies of Cu-Na_3AlF_6 reactions; electrochemical studies of Cu-Ni alloys; in situ laser Raman spectroscopy studies of electrolysis in Al_2O_3-saturated molten Na_3AlF_6; and preliminary experiments of other evaluation methods.

Cyclic Voltammetry Studies

Cyclic voltammetry studies of Cu corrosion were conducted. Studies were done using a new, quick-insertion electrode design. Other tests were run using an electrode assembly with fewer Al_2O_3 components to help determine the "anode effect."

Copper Corrosion

Research in FY 1986 showed that copper oxide layers formed on Cu metal used as an anode in molten Na_3AlF_6. In FY 1987, studies were directed toward determining the effects of cell operating parameters on the morphology and composition of these oxide layers. Initial studies were conducted to serve as a baseline for this future work. Specifically, Cu metal specimens were subjected to conditions similar to those to be used in electrolysis studies but in the absence of applied potential. The oxide layers generated on the samples were then analyzed. As expected, significant Cu oxides, presumably mostly Cu_2O, formed on the specimens. However, the amount of oxide was strongly dependent on how long the sample was held in the vapor above the melt before it was immersed. This finding was surprising since the cell was purged with inert gas and that off-gassing was facilitated by application of a partial vacuum. Apparently, some of the Cu oxides observed in these and previous tests were formed prior to immersion in the molten Na_3AlF_6. The formation of oxide layers prior to the Cu being immersed in Na_3AlF_6 was a possibility discussed in previous interpretations of Cu corrosion data. As a result, a "quick insertion" method was developed in which the Cu anode was placed more rapidly into the molten bath, thus minimizing the quantity of air-formed products.

Nevertheless, the fact that significant amounts of Cu oxides were still observed after prolonged exposure to molten Na_3AlF_6 suggests that the oxides are somewhat stable in the molten bath and that their chemistry is important in the reactions at Cu anodes, as suggested in previous interpretations.

New Electrode Design and Operation

Cyclic voltammetry studies were performed on a Cu metal anode in molten Na_3AlF_6 saturated with Al_2O_3 at 1000°C, at a 1.1 bath ratio. This experiment differed from previous experiments by employing "quick-insertion" of the Cu metal anode into the molten bath to minimize oxidation of the anode. Earlier experiments suffered from an uncertainty in the source of the oxidation products, i.e., whether they were generated in the molten Na_3AlF_6 or in air prior to electrolysis.

The results from this experiment were similar to those reported previously. In particular, an oxidation peak was observed in the forward anodic traces at a potential of about 2.1 V in addition to at least one reduction peak in the reverse traces. Significant amounts of Cu_2O were also found on the anode in post-test analyses.

An Al_2O_3 sheath, which was used to control the exposed surface area of the Cu anode, fractured during the later "quick-insertion" electrochemical tests, despite efforts to reduce the amount of thermal shock during introduction of the electrode. The fracturing resulted in significantly increased uncertainty in the exposed surface areas and current densities during these tests. Subsequently, a boron nitride (BN) jacket was used in place of Al_2O_3 to control the exposed surface area of the anode. The BN was found to be acceptable as a sheathing material in experiments performed on the Cu metal anode in molten Na_3AlF_6 at subsaturation concentrations of Al_2O_3, as discussed below.

Experiments as a Function of Al_2O_3 Concentration

An electrode assembly was developed for tests of the candidate inert anodes using molten Na_3AlF_6 with low Al_2O_3 concentrations. These experiments were important in ascertaining the so-called "anode effect" for the materials under study. The new assembly incorporated as few Al_2O_3 components as possible to reduce the amount of Al_2O_3 dissolved into the molten bath during the experiment and improve the durability of the electrode assembly itself. The assembly included a graphite container, which also functioned as the cathode, and an insertable anode with BN sheath. The anode was inserted into the molten bath just prior to obtaining polarization data. The only Al_2O_3-containing component was the reference electrode whose dissolution can be controlled by limiting the time that it is exposed to the molten bath.

Cyclic polarization curves were obtained for Cu metal electrodes in molten Na_3AlF_6 at 1000°C containing 12, 9, 6, and 3 wt% initial dissolved Al_2O_3. Surprisingly, these traces were all very similar and exhibited two distinct oxidation waves at 1.9 V and 2.6 V and a single reduction wave at 2.3 V. An example of the anodic branch of one of these curves is curve (a) in Figure 19. Apparently Al_2O_3 concentration had no significant effect on the voltammetry data under these conditions.

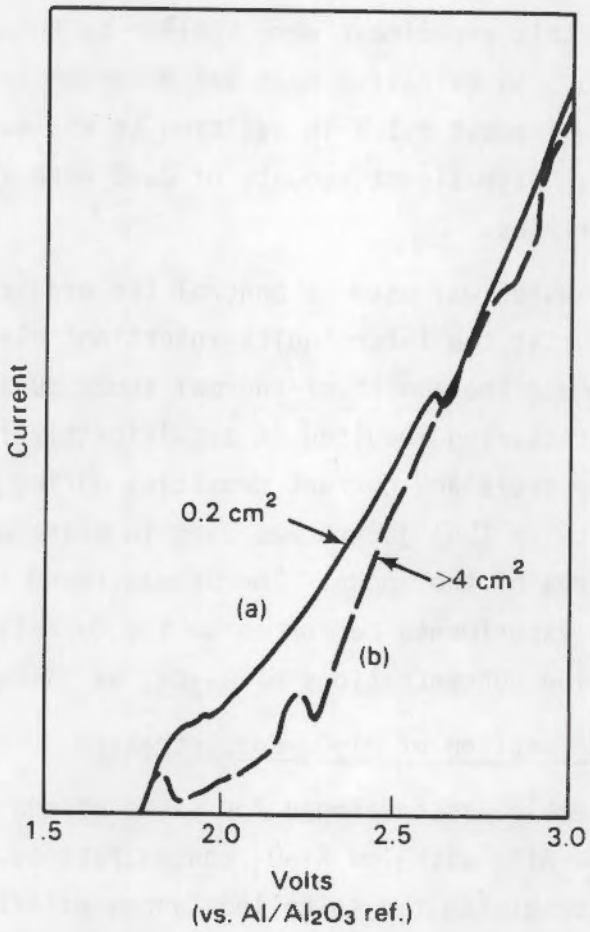

FIGURE 19. Cyclic Polarization Curve for Cu Metal Electrode in Molten Na_3AlF_6 at 1000°C

Since these curves were somewhat different from those obtained for Cu metal in previous studies (Hart et al. 1987), which showed a relatively strong oxidation peak at almost 2.1 V, numerous experiments were performed to determine what might be causing this difference. Quite unexpectedly, anode surface area was found to have an effect on the position and perhaps identity of the cyclic voltammetry peaks. As shown in Figure 1, a surface area larger than 4 cm^2 gave peaks similar to those reported in the FY 1986 studies, whereas a specimen with 0.2 cm^2 surface area gave rise to the 1.9 V and 2.6 V peaks reported above.

The most likely explanation is that, with smaller electrodes, the effects of electrode-design irregularities would be more significant. For example, all of the electrodes exhibited a certain amount of electrolyte leakage into the

gap between the metal and the ceramic sheath. This leakage contributed some uncertainty to quantities such as exposed surface area, which would have an effect on the voltammetry data. Since the relative effects are correspondingly larger for smaller surface-area specimens, some differences between different area electrodes might be expected. Clearly, additional experiments are required to clarify these results.

Studies Using ac Impedance

Studies of the Cu-Na_3AlF_6 reaction were performed using ac impedance techniques. The results of these studies support the cyclic voltammetry work and indicate that Cu reacts with Na_3AlF_6 to form CuF. With Al_2O_3 dissolved in the Na_3AlF_6, CuF in turn reacts with the dissolved oxide or an oxyfluoride to form Cu_2O under open circuit conditions and CuO when the Cu electrode is anodically polarized.

Experiments were performed using the cell shown in Figure 20. The BN-sheathed Cu anode was quickly inserted into the molten bath through the Al_2O_3 sheath just prior to making the ac impedance measurements. This was done to minimize pre-oxidation of the Cu. The Al/Al_2O_3 reference electrode remained in the bath only long enough to obtain ac impedance data for minimizing dissolution of Al_2O_3.

The electrolyte, designated GM#4,[(a)] was formulated from natural Greenland cryolite (Na_3AlF_6) and AlF_3 (prepared by dehydration of $Al_2F_6 \cdot xH_2O$ powder) to give a bath ratio (weight ratio of NaF to AlF_3) equal to 1.1. The bath also contained CaF_2 at 4 wt% concentration. For experiments using Al_2O_3-containing electrolyte, reagent-grade Al_2O_3 was added to the GM#4 composition. The powder starting materials were mixed and then melted at 1273 K in a tube furnace under a N_2 atmosphere prior to inserting the electrodes.

Experiments were performed using a PAR Model 368 ac impedance system. In the impedance tests, signals in the range of 1.1 to 6300S-1 with amplitudes between 5 and 10 mV (about the open circuit potential) were applied to the Cu specimen.

(a) This composition was chosen because of its similarity to the molten electrolyte used in the industrial production of Al.

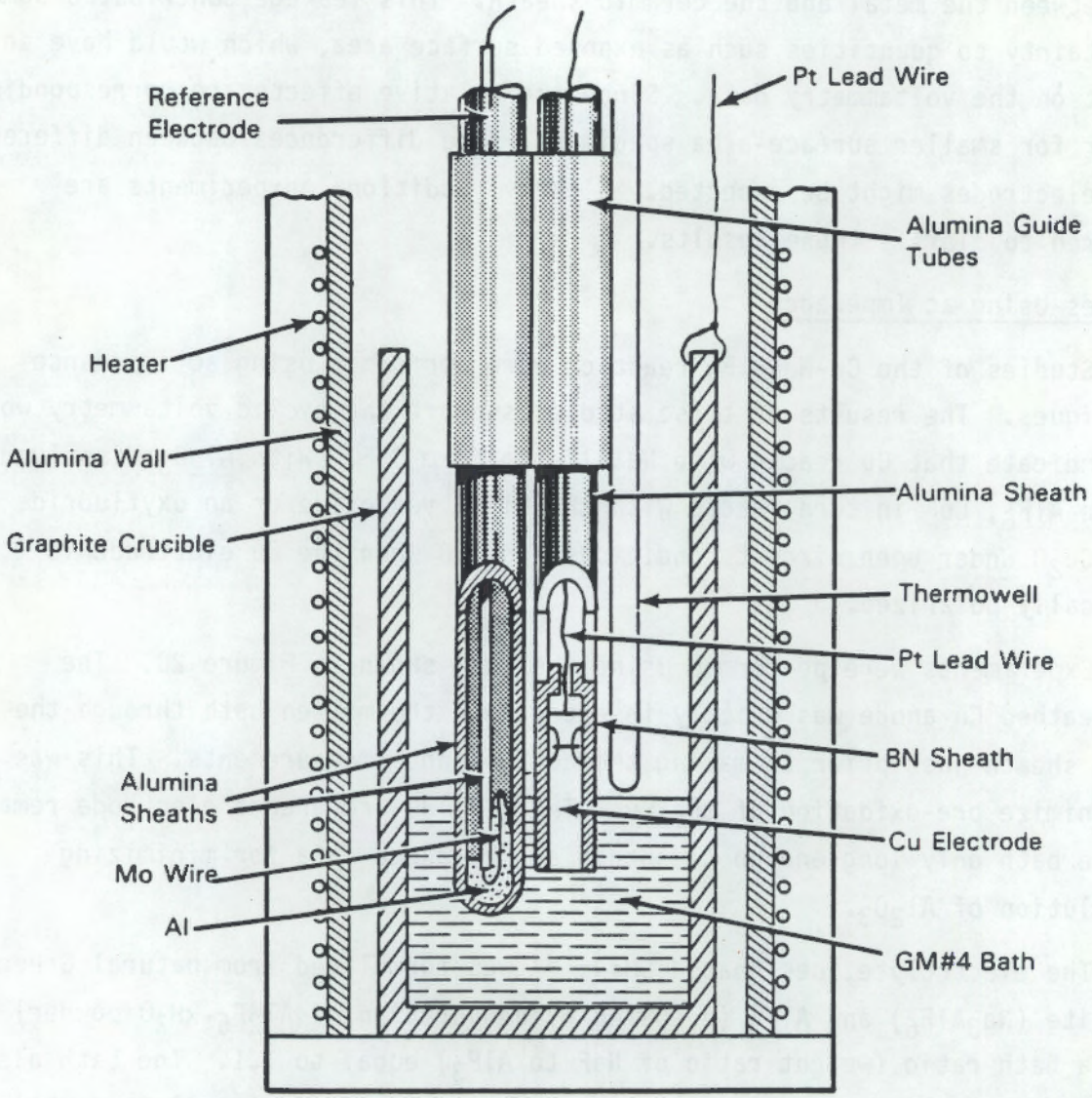

FIGURE 20. Electrochemical Cell for ac Impedance Studies

Results from the ac impedance measurements in Na_3AlF_6 at 1273 K are summarized in a Nyquist plot (Figure 21), where Z' and Z" are the real and imaginary components of the complex impedance. The slope of the straight line is 0.91 ±0.05. Plots of the impedance versus the negative square root of the angular frequency ($\omega^{-1/2}$) are also linear (Figure 22), indicating that the rate-limiting step is diffusion rather than charge transfer.

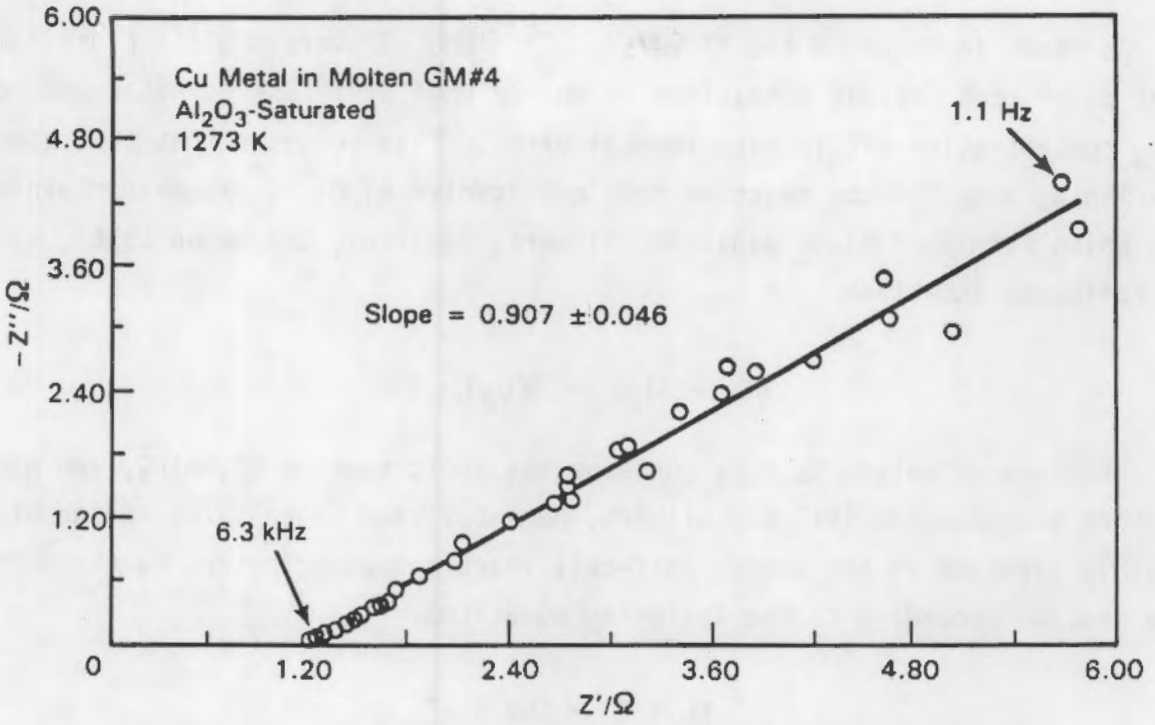

FIGURE 21. Nyquist Plot for Cu Metal in Al_2O_3-Saturated Molten GM#4 at 1273 K

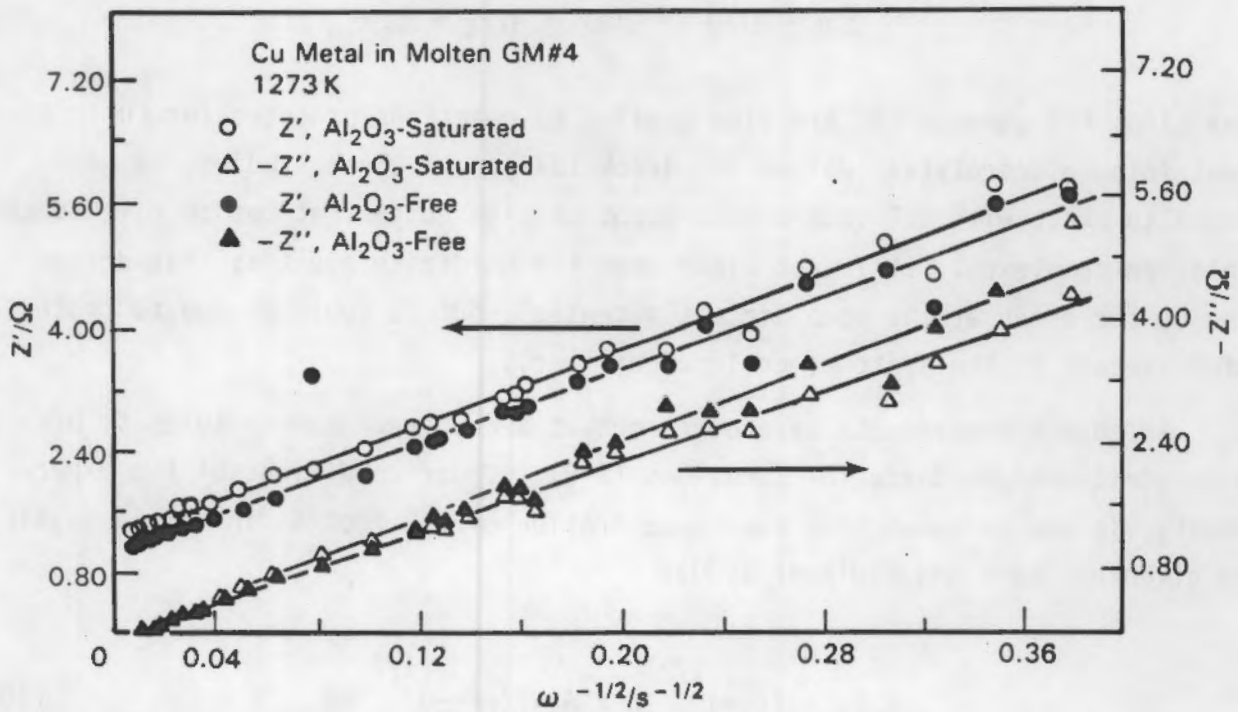

FIGURE 22. Impedance Versus Frequency Plots for Cu Metal in Al_2O_3-Saturated and Al_2O_3-Free Molten GM#4 at 1273 K

As shown in Figure 4 the Z' versus $\omega^{-1/2}$ and -Z" versus $\omega^{-1/2}$ plots for Cu metal under open circuit conditions in molten GM#4 at 1273 K do not depend on Al_2O_3 concentration within experimental error. This suggests that the rate-determining step for the reaction does not involve Al_2O_3 or oxygen-containing ions which form upon Al_2O_3 addition (Gilbert, Mamantov, and Begun 1976), as in the following equation:

$$6Cu + Al_2O_3 = 3Cu_2O + 2Al \quad (6)$$

The structure of molten Na_3AlF_6 contains the ionic species F^-, AlF_4^-, and AlF_6^{3-} (Gilbert and Mamantov 1975 and Gilbert, Mamantov, and Begun 1976), which are probably involved in the anodic half-cell reactions contributing to the corrosion process according to the following equations:

$$Cu + F^- = CuF + e^- \quad (7)$$

$$Cu + AlF_4^- = CuF + AlF_3 + e^- \quad (8)$$

$$2Cu + AlF_6^{4-} = 2CuF + AlF_4^- + 2e^- \quad (9)$$

Reactions (7) through (9) are also similar to reactions proposed for Cu in Cl-containing electrolytes (Walton and Brook 1977). In those studies, Cu was found to react with Cl^- ions when present at high concentrations to give copper chloride complexes. It is not clear what the oxidizing agent is that drives the Cu corrosion at the open circuit potential, but it could be due to traces of O present in the system (mentioned earlier).

Impedance experiments were performed at a number of temperatures to provide additional evidence for Equations (7-9). Under conditions of the experiments, it can be shown that the concentration of CuF from Cu in molten Na_3AlF_6 is given by (Bard and Faulkner 1980):

$$C_{CuF} = \left(\left(\frac{RT}{2}\right)^{1/2} n^2F^2A\right)\cdot\left(\left(\frac{1}{D_{CuF}}\right)^{1/2} \sigma\right) \quad (10)$$

where R = the gas constant
T = the absolute temperature
n = the number of electrons transferred in the reaction
F = the Faraday constant
A = the electrode surface area
D = the diffusion coefficient
σ = the Warburg coefficient.

Based on measurements of diffusion coefficients for similar fluoride species (Grjotheim et al. 1977), D_{CuF} is approximately 10^{-5} cm^2/s. Moreover, since the diffusion coefficient has a relatively low activation energy (Choudray 1973), the variation of D_{CuF} over this temperature range can be neglected. Taking n = 1 per mole of CuF formed according to Reaction (7), and A = 0.196 cm^2, Equation (11) reduces to:

$$C_{CuF} = 1.02 \times 10^{-6} \left(\frac{T}{\sigma}\right). \qquad (11)$$

The ac impedance data were collected for Cu metal in molten GM#4 containing 6 wt% Al_2O_3 at 1243, 1253, and 1263 K. The Z' versus $\omega^{-1/2}$ plots are shown in Figure 23 along with the data obtained for Al_2O_3-saturated GM#4 at 1273 K. Warburg coefficients obtained from the slopes of these curves are given in Table 2, together with values for C_{CuF} calculated using Equation (12).

The data in Table 2 show that the calculated concentration of CuF in the diffusion layer increases with temperature up to 1273 K. If the following reaction is operating at near equilibrium:

$$F^- + Cu^0 + (\text{oxidizing agent}) = CuF + (\text{reducing agent})^- \qquad (12)$$

and this temperature dependence of the CuF concentration arises from the shift in equilibrium at reaction (12), the standard enthalpy change can be obtained from the Gibbs-Helmholtz equation:

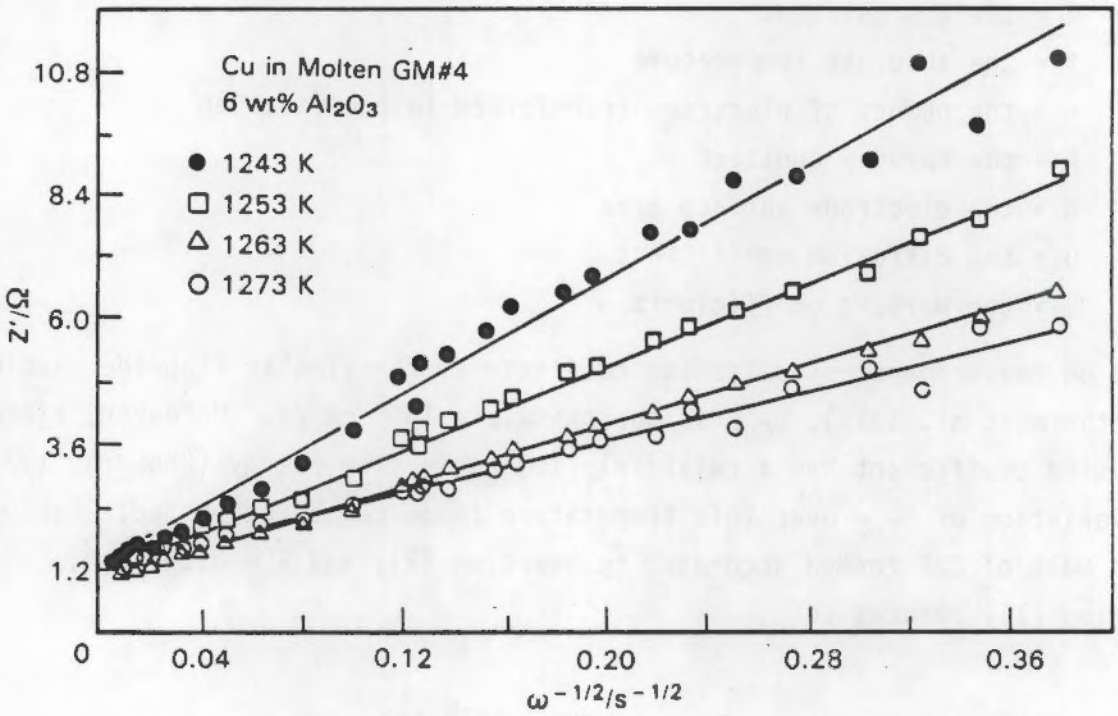

FIGURE 23. Plots of Z' Versus Frequency at Various Temperatures for Cu Metal in Molten GM#4 Containing 6 wt% Al_2O_3

TABLE 2. Warburg Coefficients and CuF Concentrations (Calculated Using Equation 12) for Cu Metal in Molten Na_3AlF_6 Containing 6 wt% Al_2O_3

T, K	σ, ohms·$s^{1/2}$	C_{CuF}, mol/cm^3
1243	27.1 ± 1.2(a)	4.67 (±0.21) x 10^{-5}
1253	19.7 ± 0.6	6.49 (±0.20) x 10^{-5}
1263	14.4 ± 0.2	8.96 (±0.11) x 10^{-5}
1273(b)	11.9 ± 0.5	1.08 (±0.44) x 10^{-4}
1283	13.2 ± 0.1	9.89 (±0.03) x 10^{-5}

(a) 95% confidence limit.
(b) Al_2O_3-saturated molten Na_3AlF_6.

$$\frac{\partial \log K_a}{(1/T)} = - \frac{\Delta H^o}{2.303\ R} \qquad (13)$$

where K is the equilibrium constant, based on 1 mol of CuF:

$$K = \frac{(CuF)(\text{reducing agent})}{(F^-)(\text{oxidizing agent})} \qquad (14)$$

If the concentration of the fluoride ion, oxidizing agent, and reducing agent don't change very much with temperature, then Equation (13) reduces to the following:

$$\frac{\partial \log C_{CuF}a}{(1/T)} = - \frac{\Delta H^o}{2.303\ R} \qquad (15)$$

where ΔH^o is the standard enthalpy change for the reaction over the temperature range studied. According to Equation (15), a plot of log C_{CuF} versus 1/T should be linear with a slope equal to $-\Delta H^o/2.303$ R, provided ΔH^o is constant over the temperature range.

Figure 24 shows the plot of log C_{CuF} versus 1/T for the data given in Table 2. The plot is linear between 1243 and 1273 K, but shows significant deviation from linearity above 1273 K. The linear least-squares fit to the data between 1243 and 1273 K gives a slope of -1.96 (±0.46) x 10^4 K (90% confidence). The ΔH^o calculated from this slope is 372 ±89 kJ/mol CuF (90% confidence). This value compares well with the standard enthalpy of formation at 1300 K, 324.8 kJ/mol for CuF. Above 1273 K, secondary reactions involving Cu or CuF may take place or the parameters assumed to be constant with temperature may change. These factors probably result in the deviation from linearity for the higher-temperature data in Figure 24.

Other reactions may also be important in Al_2O_3-containing melts. In Al_2O_3-containing molten Na_3AlF_6, CuF formed by the reactions of Cu metal and fluoride species may subsequently react according to the following equation:

$$6CuF + Al_2O_3 = 3Cu_2O + 2AlF_3. \qquad (16)$$

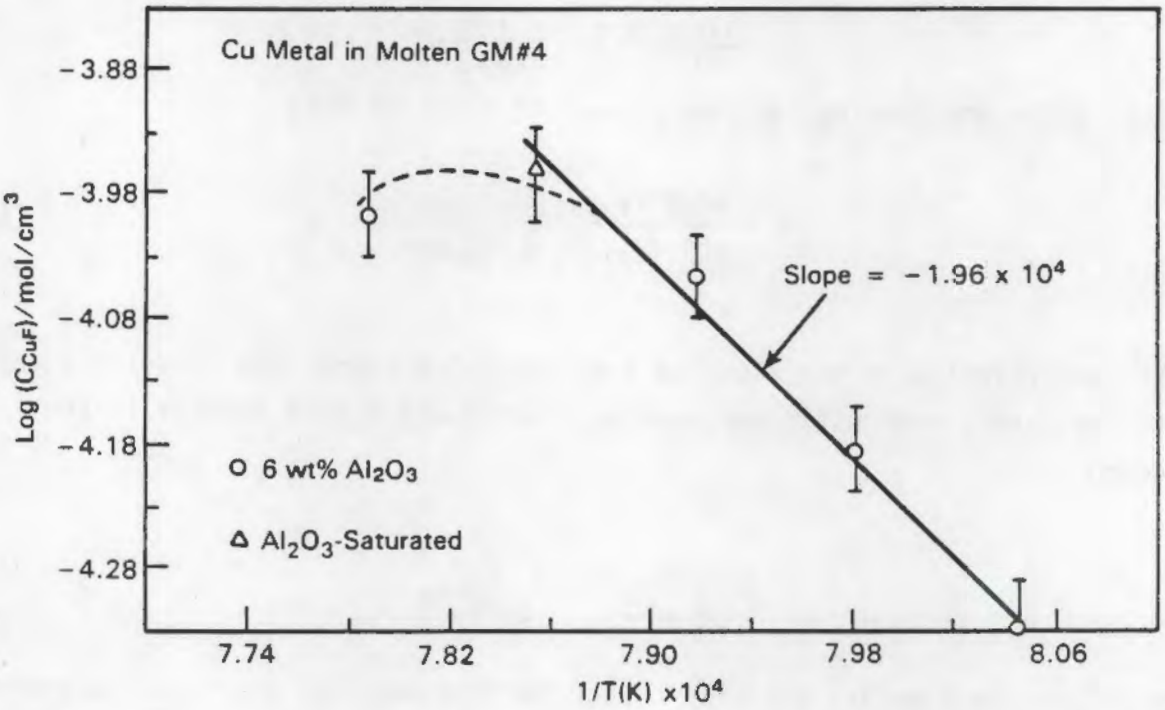

FIGURE 24. Plot of Log C_{CuF} Versus 1/T. C_{CuF} is the concentration of CuF in mol/cm^3 calculated from the ac impedance data using Equation (12).

Reaction (16) has a negative standard free energy change at 1300 K equal to -104.6 kJ/mol CuF. This suggests that any CuF formed probably reacts to form soluble and/or insoluble oxides in Al_2O_3-containing melts. Reaction (16) is supported by the results of cyclic voltammetry (coupled with post-test materials characterization) on Cu metal anodes in Al_2O_3-saturated molten Na_3AlF_6 (Belyaev and Studentsov 1936). In this work it was found that the conversion of Cu_2O to CuO and/or copper aluminates is an important reaction for Cu metal electrodes during anodic polarization. For this reaction to occur, Cu_2O must already be present, suggesting that the oxide or its solution counterpart forms under open circuit conditions.

Cu-Ni Alloy Studies

Electrochemical studies were carried out on alloys of Cu and Ni to determine the beneficial effect on the corrosion of the metallic phase in cermet anodes. Studies of aqueous systems indicated that there was a beneficial effect on metallic corrosion by alloying the Cu with Ni (North and Pryor

1970). In those studies, it was observed that the Cu-Ni alloys formed a protective layer of Cu_2O with a defect structure. Therefore, it seemed possible that such a beneficial effect might be observed in the molten Na_3AlF_6 system.

Potentiodynamic anodic and cyclic polarization techniques were used in conjunction with the Cu-Ni alloy anodes. The alloys that were used were 100-0, 90-10, 80-20, 70-30, and 0-100 ratios of Cu to Ni. The same cell and bath that were used for the ac impedance studies described above were used for these studies. All of the experiments were carried out at Al_2O_3 saturation and 1273 K.

The results of this investigation indicated that there was no beneficial effect of adding Ni to the Cu. Both open circuit and anodically polarized Cu-Ni anodes corroded faster in Na_3AlF_6 than did pure Cu. These studies were not pursued beyond these initial investigations.

In Situ Laser Raman Spectroscopy

In FY 1986, laser Raman spectroscopy was used to study in situ the electrolysis of Al_2O_3-saturated molten Na_3AlF_6. Unfortunately, the technique was not sensitive enough to determine electrolysis mechanisms at cermet anodes. In FY 1987 the approach was used to study the corrosion of Cu metal anodes in molten Na_3AlF_6. Copper metal was studied because it was considered to be the most likely "part" of the cermet anode to undergo oxidation and subsequent dissolution during anodic polarization. This assumption was based on recent cyclic voltammetry work which showed evidence for Cu_2O transformations. If successful, laser Raman spectroscopy could be used to facilitate the identification of these transformations.

Raman spectra were generated using a Spex Model 1403 Raman spectrometer with a Tracor Northern TN-6133 diode array detector and a TN-1710A multichannel analyzer. Using this apparatus about 2 spectra per minute could be collected with 4 cm^{-1} spectral resolution. The speed of the diode array detector was advantageous since the spectroscopic cells used in this work degraded optically with time during the experiment, thus limiting the time available to collect the Raman data to about 2 h. Other important conditions for the Raman

experiments included the use of the 488.0-nm line of a Spectra Physics Ar^+ laser for excitation and the employment of slit widths of 400 cm^{-1}. A Solarton Model 1186 electrochemical interface was used for control of the anode current.

A forward laser scattering geometry was employed, similar to that employed in FY 1986. The laser Raman spectroscopy cell is shown in Figure 25. The optical quality cell was made from a sapphire tube, 3-in. long with 0.5-in. OD (Saphikon of Milford, New Hampshire). This material exhibited the least corrosion in molten Na_3AlF_6. The forward scattering geometry provided the added bonuses of better power throughput of the scattered light to the Raman spectrometer and easier adjustment of the anode during an experiment. The furnace designed and built for these forward scattering experiments is also shown in Figure 7. It consisted of a heated quartz tube with three orthogonally positioned windows. The center window functioned as an observation port.

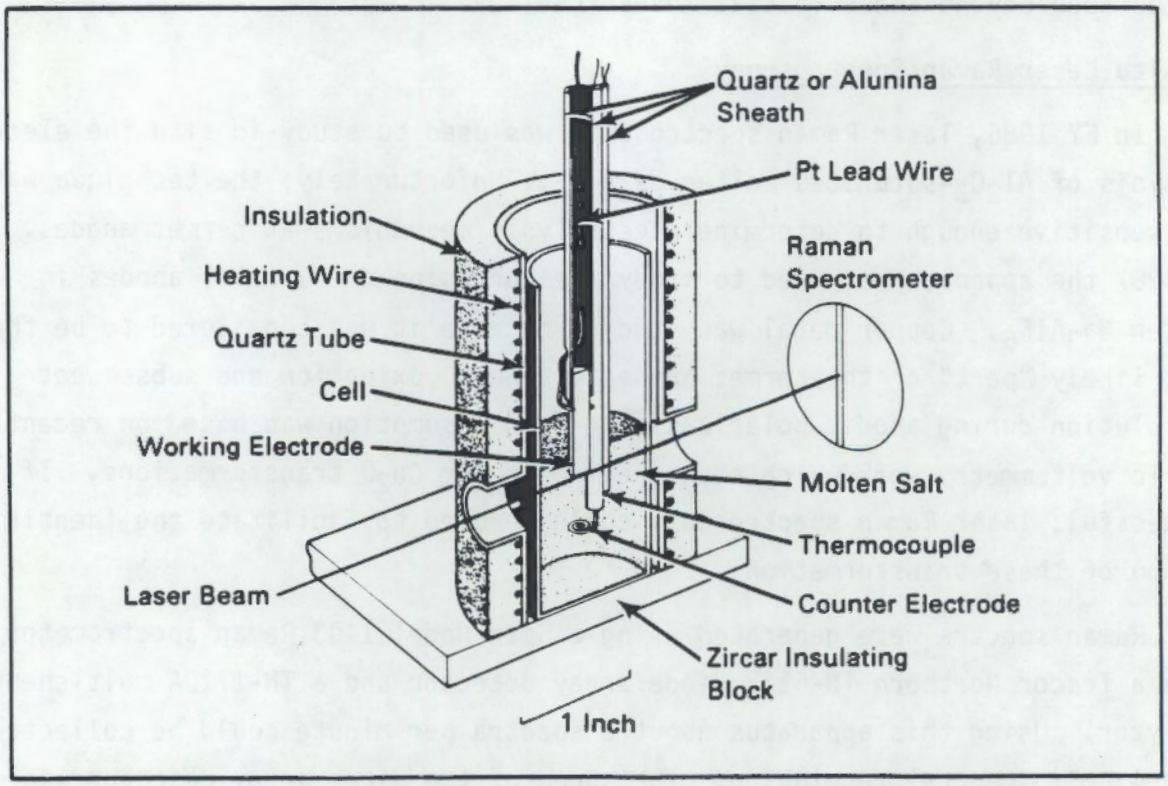

FIGURE 25. In Situ Laser Raman Spectroscopy Cell Employing Forward Scattering Geometry

The electrode assembly used in these in situ laser Raman spectroscopy studies consisted of the following: 1) a Cu anode sheathed in Al_2O_3 with about 0.08 cm^2 of surface area exposed to the molten Na_3AlF_6, 2) a cathode made of W wire partially sheathed in Al_2O_3 with its lower section exposed and coiled about 1 cm below the anode, and 3) a Pt thermocouple. In the experiment, about 4 g of Al_2O_3-saturated Na_3AlF_6 with a bath ratio of 1.1 were added to the sapphire cell and heated to 980°C. The observation port was used to visually ascertain that the bath was molten. The electrode assembly was then lowered into the melt and the laser beam focused to a point directly below the anode interface. The anode position was also adjusted to optimize scattering conditions. Raman spectra of the molten Na_3AlF_6 were collected with no potential applied to the cell and then with potential applied. All the while, the cell was monitored visually to ensure that it was operating without any problems.

In situ laser Raman spectroscopy was performed during the electrolysis of Al_2O_3 in molten Na_3AlF_6 at 980°C. The bath had a ratio of 1.1 and was saturated with Al_2O_3. Spectra were obtained during electrochemical polarization at 0.1 and 1.0 A/cm^2.

As shown in Figure 26, Raman spectra obtained in this study contained the two principal bands for molten Na_3AlF_6 at about 532 and 615 cm^{-1} assigned to AlF_6^{3-} and AlF_4^- vibration, respectively. An unassigned band was observed at 404 cm^{-1}.

No significant change in the Raman spectrum of the molten Na_3AlF_6 near the Cu metal anode occurred at a current density of 1 A/cm^2 (Figure 26). The Al-F octahedral and tetrahedral species do not appear to be affected by the electrolysis process. The same may not be the case for the Al-O-F moieties; however, their very weak spectral features were obscured by the Al-F vibrations and were not observed in this study. No new spectral features were observed during electrolysis, suggesting that the technique was not sufficiently sensitive to the Cu corrosion products. Because of this lack of sensitivity, further laser Raman studies were discontinued in favor of the electrochemical studies reported previously.

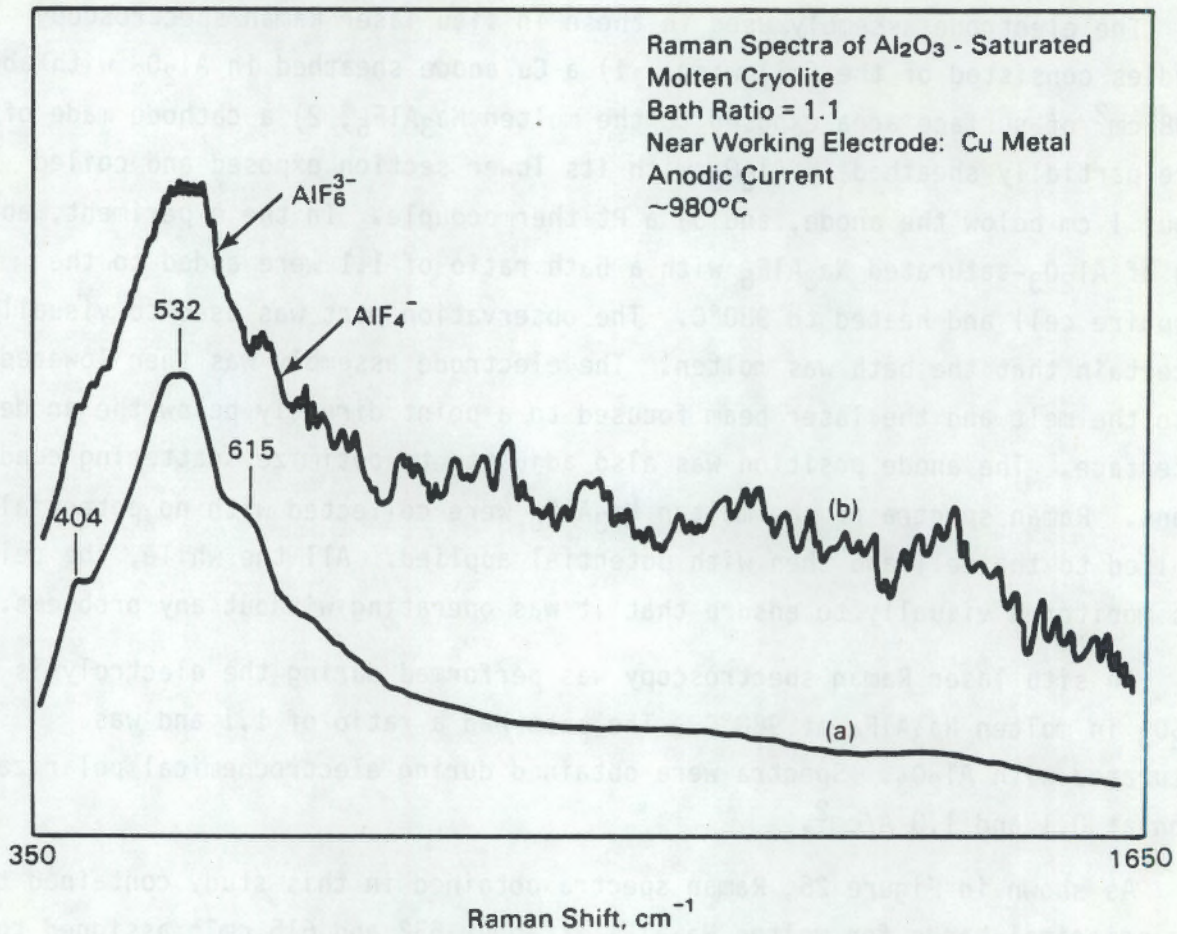

FIGURE 26. Raman Spectra of Al_2O_3-Saturated Molten Na_3AlF_6 Near the NiO-$NiFe_2O_4$-Cu Cermet Anode During the Passage of (a) 0 Current and (b) 1 A/cm^2

Other Materials Evaluation Areas

Preliminary experiments were performed to determine promising areas for future materials evaluation studies. One set of experiments involved studying Al cathode electrochemistry as a method for evaluating NiO-$NiFe_2O_4$-Cu cermet anode wear. The basic idea is that the electrochemical potential of an Al cathode will change if the composition of the Al changes. It has been proposed that cermet anode wear may be controlled by the transport of dissolution products, such as Ni, Fe, and Cu, into the molten Al cathode. Since these species should affect the electrochemical potential of the Al cathode, it may be possible to use this potential as an indicator of the amount of species

transport into the Al cathode. Bath composition, temperature, and other conditions could then be changed to minimize mass transport.

Experiments were performed using a bench-scale Al reduction cell with a Pt anode, an Al cathode, and an Al reference electrode with the same design as the cathode. The cell was operated at 1 A/cm^2 for a short period of time and then turned off. The electrochemical potential of the cathode, with respect to the reference which was zero before electrolysis, was found to have dropped to less than -300 mV after electrolysis. This non-zero potential was interpreted to indicate that a significant quantity of Na^0 metal had formed at the cathode. Careful studies of the Al cathode potential as a function of Ni, Fe, and Cu concentration in the molten electrolyte may provide the data necessary to "calibrate" the cathode potential with respect to these components. Such a calibration curve could then be used to evaluate anode wear during testing of the cermet anodes in experimental Hall-Heroult cells.

CONCLUSIONS

From the work performed during FY 1987, it appears that the corrosion processes that occur at a Cu anode are diffusion limited under open circuit conditions. Copper metal reacts with fluoride species in the molten Na_3AlF_6 to form CuF. When Al_2O_3 is added to the Na_3AlF_6, the process remains diffusive but the species changes from CuF to Cu_2O by reaction of the CuF with oxide or oxyfluoride species. Under an applied potential, Cu_2O reacts to form CuO or Cu aluminates.

Laser Raman experiments were found to be too insensitive to be of use in determining the changes in bath chemistry near the anode under electrolysis conditions. Spectra were obtained for molten Na_3AlF_6, but no changes were observed when the cell was polarized to 1 A/cm^2.

The addition of Ni to the Cu metal anodes did not enhance the durability of the anode in molten Na_3AlF_6 as was observed in aqueous systems. This effect appears to be due to the different nature of the oxide layer that is formed in the two systems.

Work on this task ended at the end of FY 1987. No future work is planned.

REFERENCES

Bard , A. J., and L. R. Faulkner. 1980. Electrochemical Methods. John Wiley & Sons, Inc., New York.

Belyaev, A. I., and Y. E. Studentsov. 1936. Legkie Metally 3:15.

Choudray, G. 1973. J. Electrochem. Soc. 120:381.

Gilbert, B., and G. Mamantov. 1975. J. Chem. Phys. 62:850.

Gilbert, B., G. Mamantov, and G. M. Begun. 1976. Inorg. Nucl. Chem. Letters 12:415.

Grjotheim, K., C. Krohn, M. Malinovsky, K. Matiasovsky, and J. Thonstad. 1977. Aluminum Electrolysis, Aluminum-Verlag, Düsseldorf.

Hart, P. E., et al. 1987. Fiscal Year 1986 Annual Report. PNL-6247, Pacific Northwest Laboratory, Richland, Washington.

North, R. F. and M. J. Pryor. 1970. "The Influence of Corrosion Product Structure." Corrosion Sci. 10:297-311.

Walton, M. E., and P. A. Brook. 1977. Corrosion Sci. 17:593.

Whiting, F. L., G. Mamantov, and J. P. Young. 1973. "Electrochemical Generation and Spectrophotometric Study of Solute Species in Molten Fluoride Media." J. Inorg. Nucl. Chem. 35(5):155.

4.0 STABLE CATHODE STUDIES

C. H. Schilling

The objective of the Stable Cathode Studies task is to evaluate materials and feasible attachment methods for retrofitting existing commercial Hall-Heroult cells with TiB_2-based cathodes. Research is focused on retrofit applications that specifically entail use of inert anodes.

SUMMARY

In FY 1987, electrolysis tests and non-polarized immersion tests in molten Al were used to analyze the wear behavior of prime candidate cathode materials and attachment designs which had been selected based on a literature review (Schilling, Hagen, and Hart 1987) and previous research at PNL (Hart et al. 1987). Based on all experiments to date, there are two feasible retrofit methods for scale-up: 1) replaceable cathodes which rest, unattached, on carbonaceous cell bottoms, and 2) replaceable fixtures which use ceramic spacers to attach the anodes to the cathodes and align the anode-cathode spacing. Cathode materials with acceptable corrosion resistance include TiB_2-graphite (TiB_2-G) composites, TiB_2-AlN composites, and high-purity TiB_2 sintered from plasma-process powders. Key results of the task for FY 1987 are summarized below:

- The majority of the experiments involved electrolysis testing of replaceable TiB_2-G Type B composite (TiB_2-G) cathodes supplied by the Great Lakes Research Corporation. Electrolysis tests were performed in the laboratory with cermet anodes for time durations of up to 90 h. Based on optical ceramography, most of the cathodes exhibited acceptable performance with no evidence of TiB_2 grain spalling or intergranular penetration by Al. One test showed TiB_2 fragments suspended in Al, which may possibly be attributed to chemical attack from Al_2O_3-supersaturated bath.
- High-resolution optical ceramography and elemental mapping showed molten Al replacing the graphite phase contained within the TiB_2 pores at the surfaces of a TiB_2-graphite cathode. Beneath this

layer, the TiB_2 pores exhibited a reaction layer that contained Na and F but was depleted of Al and C. Sodium and Al_4C_3 transport processes within the reaction layer may be enhancing the wear resistance and useful life of these materials. These results are summarized in a poster, which will be published in the American Ceramic Society Bulletin.

- Four types of TiB_2-based materials were evaluated by non-polarized immersion at 970°C in molten Al without Na_3AlF_6 under an Ar atmosphere. In the tests, which lasted up to 20 wk, Alcoa high-purity TiB_2 and TiB_2-AlN composites exhibited superior resistance to chemical attack, with no evidence of fragmentation or intergranular penetration by Al. Composites of chemical-vapor-infiltrated TiB_2 on SiC fiber mesh exhibited mixed results: the coatings were resistant to chemical attack, but the fibers reacted with molten Al during the first 4 weeks of exposure. Composites of TiB_2-G exhibited damage that may be related to expansion stresses exerted on the TiB_2 pore walls as a result of Al_4C_3 formation. It is hypothesized that such stresses are not expected to damage TiB_2-G materials during electrolysis because of subsurface chemical reactions resulting in the rapid removal of Al_4C_3 from TiB_2 pores.
- Alcoa high-purity TiB_2 was evaluated as a replaceable cathode in a 140-h small-scale electrolysis test. Optical ceramography analysis indicated acceptable performance by the cathode with no evidence of microcracking or penetration by Al.
- A small-scale electrolysis test of a replaceable anode/cathode fixture, which used a BN spacer to mechanically align the anode-cathode spacing, was performed. The anode material performed satisfactorily during 7 h of electrolysis testing, although the spacer was chemically attacked at surfaces exposed to the anode/cathode spacing. Evaluation of wear-resistant spacer materials is recommended.
- A TiB_2-based paint coating on graphite was evaluated during short-term exposure to molten Al under non-polarized conditions. The coating was extensively attacked as a result of reactions between the Al

and a SiO_2-based component of the paint coating, and Al_4C_3 formation from reactions between graphite and elemental Al.

- Preliminary experiments were performed to evaluate in situ formation of TiB_2 coatings that may be self-healing in an operating Hall-Heroult cell. Aluminum-Ti reactions resulted in extensive degradation of Ti during non-polarized exposure of Ti to B-saturated molten Al. Evaluation of alternative coating methods, such as electrodeposition and diffusion saturation using molten salts, is recommended.
- Sintering studies were performed to evaluate whether TiB_2 cathodes may be fabricated with powder prepared by a low-temperature precursor process; the TiB_2 powder was supplied by J. J. Ritter at the National Bureau of Standards. Samples could not be pressureless sintered to reasonable densities for cathode evaluation studies. Additional research is needed to enhance densification kinetics using smaller-sized particulates, applied pressure, and/or sintering additives.

TECHNICAL PROGRESS

Several laboratory experiments were conducted in support of the Stable Cathode Studies task in FY 1987. These included electrolysis tests of replaceable TiB_2-G Type B cathodes, non-polarized immersion tests of four TiB_2-based materials in Al, a 140-h electrolysis test of high-purity TiB_2 used as a replaceable cathode, and an electrolysis test of a replaceable anode-cathode fixture that used a ceramic spacer to attach the anode to the cathode and align anode-cathode spacing. Preliminary experiments were also performed to evaluate 1) wear resistance of a TiB_2-based paint coating on graphite, 2) in situ formation of TiB_2 coatings that may be self-healing in an operating Hall-Heroult cell, and 3) fabrication of TiB_2 cathodes by sintering TiB_2 powder that has been prepared by a low-temperature precursor process. Key results of all experiments are briefly summarized below; detailed discussions of these experiments are reported by Schilling (1988) and Schilling and Graff (1988).

Electrolysis Tests of TiB_2-G Replaceable Cathodes

The TiB_2-G composites[a] were evaluated as replaceable cathodes in electrolysis tests of up to 95-h duration in cells using cermet anodes. Replaceable cathodes, originally proposed by Goodnow and Payne (1982), are advantageous for retrofit applications because the TiB_2-based articles rest, unattached, on carbonaceous cell bottoms and may be removed from the cells without shutdown or major reconstruction. In nearly all of the electrolysis tests, the TiB_2-G replaceable cathodes exhibited acceptable performance with no indication of physical damage based on results from optical ceramography analysis. However, one test showed TiB_2 fragments that were suspended in Al. The wear behavior of another TiB_2-G cathode was evaluated using high-resolution optical ceramography and elemental mapping. Aluminum was found to replace the graphite contained within the TiB_2 pores at the surfaces of the sample. Beneath this layer, the TiB_2 pores exhibited a reaction layer that was concentrated with Na and F and depleted of Al and C. Chemical reactions occurring in this layer may control the overall wear resistance and useful life of these materials.

A total of four electrolysis tests of up to 95-h duration were performed in the small-scale cell, and seven tests of up to 20-h duration were performed in the laboratory-scale cell.[b] Complete details for each experiment are reported in Schilling (1988). In each of the small-scale cells, a TiB_2-G plate was loosely set into a slotted cavity in the prebaked C cell bottom, and in each of the laboratory-scale cells, a TiB_2-G disc was set in place on the graphite cell bottom.[c] All tests were started by heating the cell to 970°C with a layer of Al on top of the TiB_2-G; this procedure was used to alleviate chemical attack of the TiB_2-G by contact with the Na_3AlF_6 bath (Hart et al. 1987). Nominal bath compositions having bath ratios between 1.08 and 1.15 were

---

(a) TiB_2-graphite type B composites supplied by L. Joo' of Great Lakes Research Corporation, Elizabethton, Tennessee.

(b) Small-scale cells were operated at 1 to 5 amperes (A). Laboratory-scale cells were operated at 10 to 25 A.

(c) Each small-scale cell had a TiB_2-G rectangular parallelepiped measuring 7.6 mm tall by 14 mm wide by 25 mm long. Each laboratory-scale cell had a TiB_2-G disc that was 67 mm diameter by 9 mm thick, except for one experiment which used a larger disc of 94 mm diameter x 9 mm thick.

used. All experiments were performed with cermet anodes in conjunction with the anode evaluation task; anode-cathode spacings were made large enough (>1.9 cm) to alleviate anode degradation caused by contact with molten Al.

Optical ceramography revealed four key features typical of all TiB_2-G cathodes evaluated in the small-scale cell (see Figures 27 and 28): 1) wetting of the exterior surfaces by Al, 2) no evidence of Al contamination caused by fragmentation of the TiB_2 matrix, 3) an Al penetration layer filling the TiB_2 pores directly beneath the exterior surfaces of the TiB_2G, and 4) a reaction layer in the TiB_2 pores directly beneath the Al penetration layer. The elemental mapping feature of the scanning electron microscope (SEM) was used to describe the nature of the reaction layer. The thicknesses of the Al penetration layers were measured from micrographs of the polished samples and were found to reach a maximum thickness of 250 to 275 μm after 95 h of electrolysis (Figure 29).

The TiB_2-G discs were removed intact from the laboratory-scale cells with no visual evidence of physical damage; however, optical ceramography performed on one sample revealed TiB_2 fragments suspended in the Al (Figure 30). The exact cause of the TiB_2 fragmentation has not been positively established, although a previous report (Hart et al. 1987) suggests that Na_3AlF_6 bath attack may be responsible. The layer of bath instead of Al directly above the top surface of the TiB_2-G in Figure 30 may have resulted from sedimentation of undissolved Al_2O_3 after electrolysis started. Manual stirring indicated that Al_2O_3 supersaturation occurred near the end of the test. The relative bouyancies of the phases present suggest that undissolved Al_2O_3 may have displaced the Al pad that was originally present above the TiB_2-G when the cell was heated.

The remaining tests in the laboratory-scale cells were performed without supersaturating the bath with Al_2O_3. The top surfaces of the TiB_2-G cathodes appeared to be in direct contact with Al (not Na_3AlF_6 bath) based on visual observations of the uncut samples dismantled from the cells. However, optical ceramography was not performed on these samples to confirm the absence of TiB_2 fragmentation.

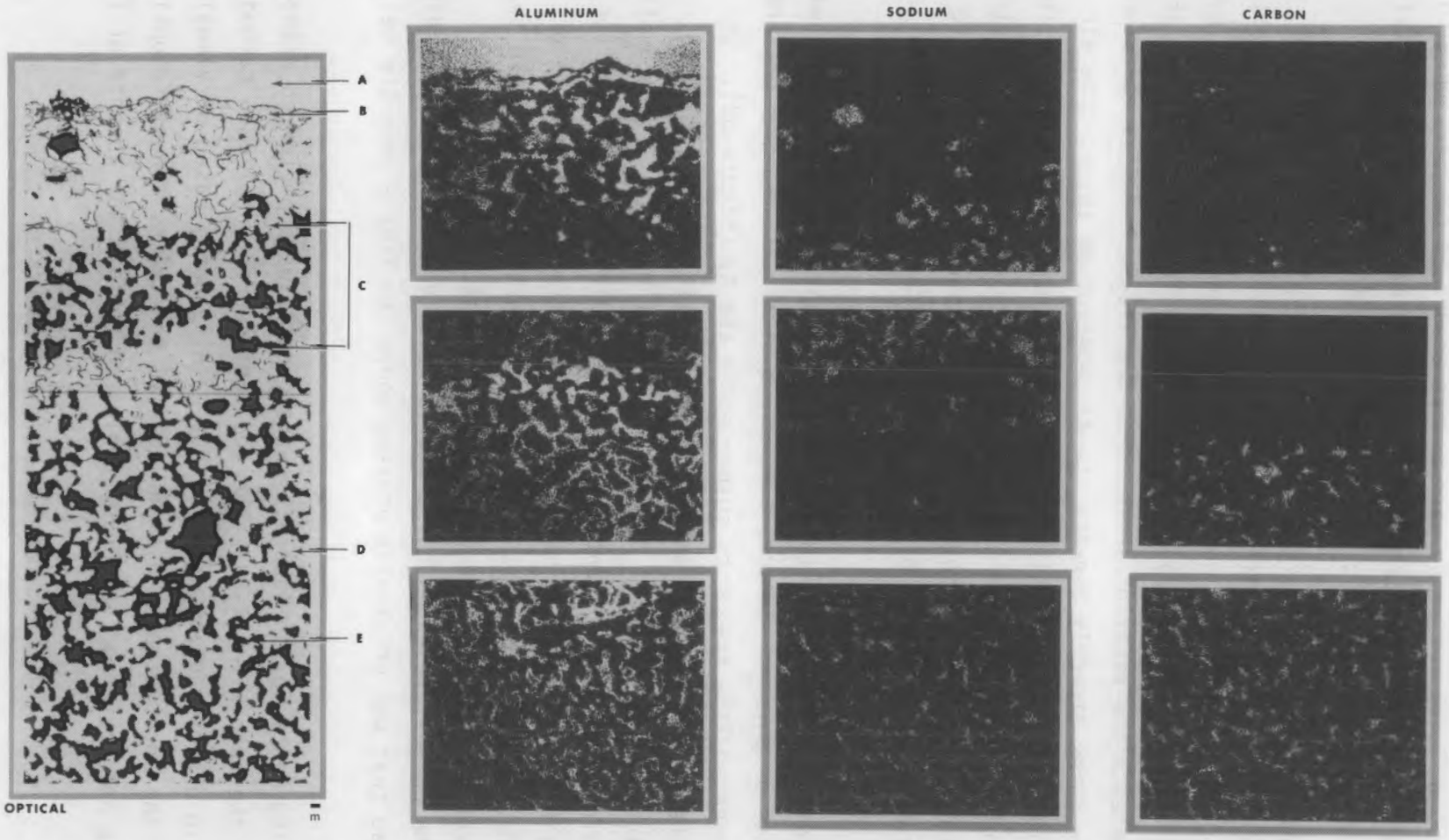

FIGURE 27. Elemental Map of TiB_2-G Replaceable Cathode After 24 h of Electrolysis in Small-Scale Cell: Vertical Section Beneath Anode-Facing Edge A = Al Coating; B = Anode-Facing Edge; C = Reaction Zone; D = TiB_2; E = Graphite

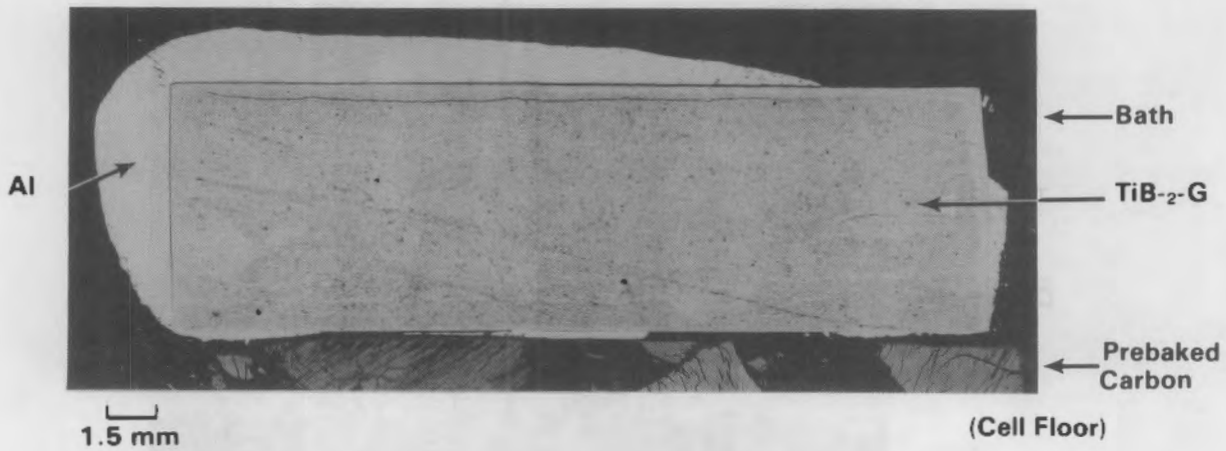

FIGURE 28. Microstructure of TiB_2-G Replaceable Cathode After 95 h of Electrolysis in Small-Scale Cell. All samples evaluated in the small-scale cell show typical features: Al wetting the surfaces and no visible evidence of physical damage. Cracks in the material existed in as-received samples and appear to have no effect on wear resistance.

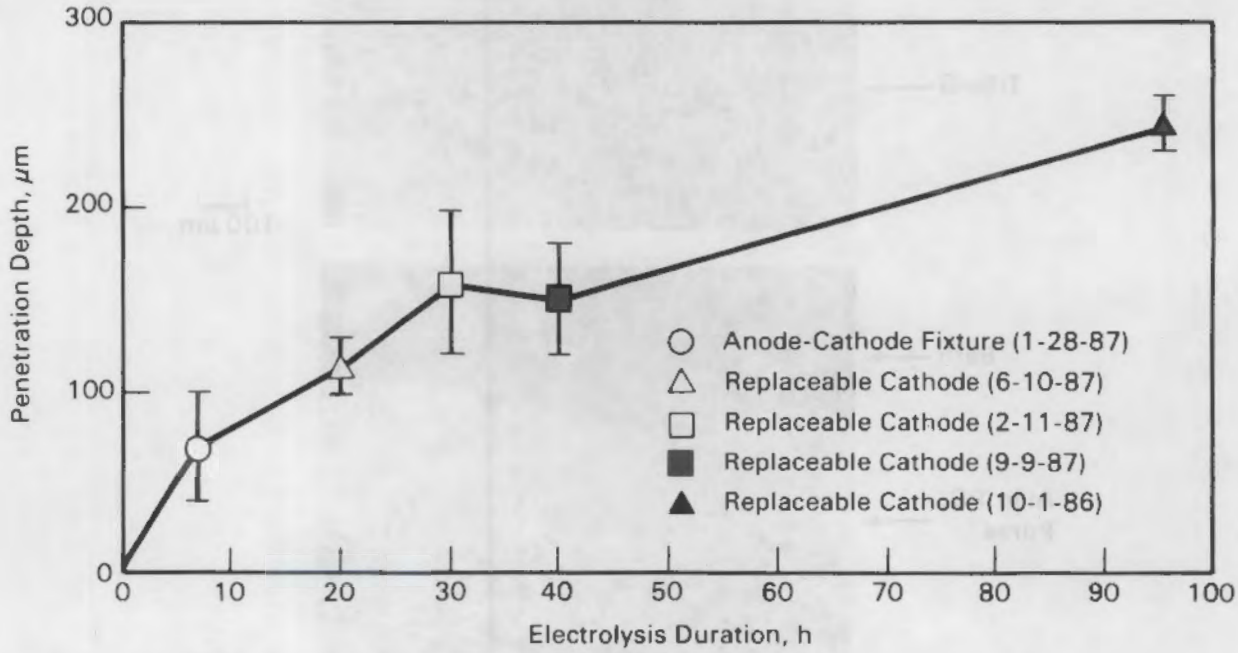

FIGURE 29. Thickness of Al Penetration Layer in TiB_2-G Replaceable Cathodes as a Function of Electrolysis Time. The penetration rate decreases with electrolysis time.

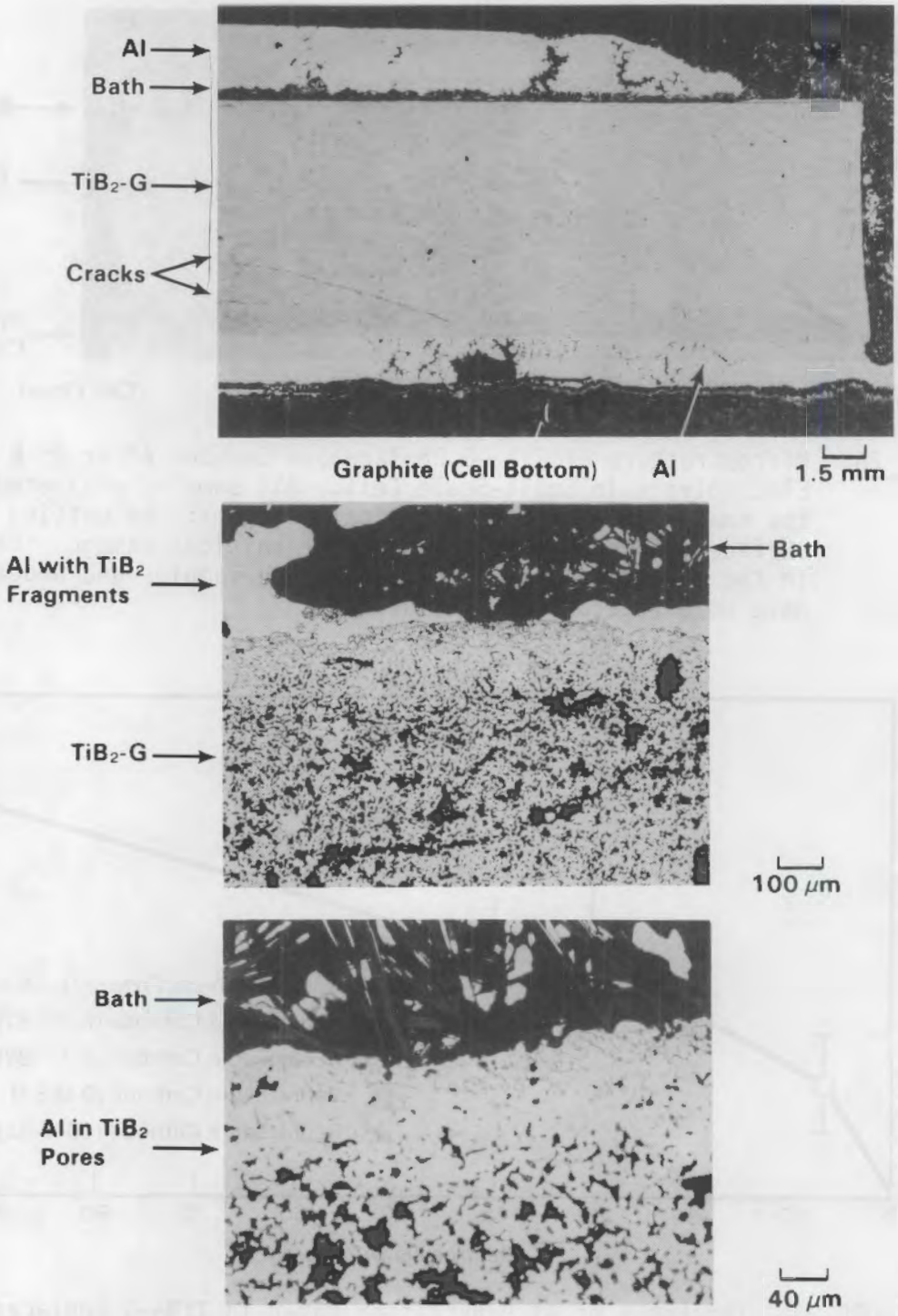

FIGURE 30. Microstructure of TiB_2-G Replaceable Cathode After 20 h of Electrolysis in Laboratory-Scale Cell. The top surface (center and below) of the TiB_2-G is coated with Na_3AlF_6 bath. Cracks are related to materials processing, as they also appear in the as-received samples.

The microstructural behavior of a TiB_2-G cathode, like the one shown in Figure 1, was further evaluated using optical ceramography and elemental mapping by x-ray spectroscopy. Important features of the cathode, which was electrolysis tested for 24 h in the small-scale cell, include the following: 1) no evidence of TiB_2 microcracking, fragmentation, or intergranular penetration by Al, 2) depletion of the graphite phase within the TiB_2 pores to a depth of 200 to 250 μm beneath the surface of the cathode, 3) a molten Al penetration layer that fills the TiB_2 pores up to a depth of 50 to 80 μm beneath the exterior surface of the cathode, 4) a Na- and F-rich layer depleted in C and Al directly beneath the molten Al penetration layer, and 5) the presence of Na and F throughout the TiB_2 pores in the remainder of the sample. Although the F map is not shown in Figure 1, the map appeared nearly identical to the Na map. The presence of Na and F within TiB_2 pores in the bulk of the sample suggests the possibility of a polishing artifact, and/or that Na and F may have indeed migrated to the interior of the composite during electrolysis. Such migration is possible, considering Na intercalation through graphite and bath penetration through the open pores of the TiB_2-G.[a]

The elemental map raises important concerns regarding the basic chemical reactions and transport processes that may be affecting the wear resistance of TiB_2-G cathode materials. Although these materials are reported to exhibit minimal deterioration in 6-month electrolysis tests (Tucker et al. 1986; Tabereaux 1987), the properties of the primary constituents (TiB_2 and graphite) suggest the possibility that surface reactions in the TiB_2-G may be controlling cathode lifes. Specifically, it may be suggested that fragmentation of the brittle TiB_2 is possible as a result of expansion stresses exerted on the TiB_2 pore walls. These expansion stresses may originate from volumetric expansion of the graphite as a result of Na intercalation and salt crystallization,[b] and the volume expansion associated with the formation of Al_4C_3 from

---

(a) TiB_2-G exhibits 25 vol% porosity based on Tabereaux (1987).
(b) Waddington 1963; Sorlie and Oye 1984a and 1984b; Panebianco and Bacchiega 1966; Dell 1967 and 1985; Dewing 1963 and 1974.

graphite.[a] Chemical reactions and transport processes occurring in the Na-rich layer may also have controlling effects on the wear resistance of these cathodes, as the structure of this layer may affect the following: 1) the rate of Na intercalation into the graphite and consequently the graphite expansion rate beneath this layer, 2) the rate of Al_4C_3 formation and subsequent dissolution into the Al pad, and 3) the rate of bath penetration into the open porosity of the TiB_2-G. Additional research with these materials is needed to evaluate chemical reactions and transport processes that are associated with the Na-rich layer and may be controlling the wear behavior and useful life of these materials. Additional data pertaining to reactions in this layer are shown below by comparing the microstructure behavior of TiB_2-G before and after non-polarized exposure to molten Al.

Immersion Tests in Molten Al

The microstructural behavior of four types of TiB_2-based materials was evaluated using immersion tests in molten Al. The samples were submerged in Al with no Na_3AlF_6 present at 970°C under an Ar atmosphere for variable time durations of up to 20 weeks. The test samples included Alcoa-supplied high-purity TiB_2,[b] PNL-fabricated TiB_2-AlN composites, composites of chemical-vapor-infiltrated TiB_2 on ceramic fiber mesh,[c] and TiB_2-graphite type B composites supplied by Great Lakes. Each sample was contained in an Al_2O_3 crucible; heating and cooling rates were approximately 3°C per minute. Complete details of these experiments are reported by Schilling and Graff (1988). Key results from this study were that high-purity TiB_2[b] and TiB_2-AlN composites exhibited superior resistance to chemical attack, with no evidence of fragmentation or intergranular penetration by Al.

(a) Based on the 4 Al + 3C → Al_4C_3 reaction, 3.8 cm^3 of Al_4C_3 is formed from 1 cm^3 of graphite (Weast, Astle, and Beyer 1985) (Schilling and Graff 1988).

(b) R. R. Baumgartner of Alcoa Laboratories supplied a TiB_2 plate that was sintered from high-purity powders produced by the halide plasma reduction process (Hoejke 1981; Baumgartner 1984a and 1984b; Baumgartner and Steiger 1984).

(c) Samples were supplied by T. Besmann of Oak Ridge National Laboratory. The chemical-vapor-infiltration process is described by Caputo and Lackey (1984) and Stinton et al. (1986). Samples contained Nicalon SiC-based fibers produced by Nippon Carbon Co., Tokyo, Japan.

Samples of SiC fiber mesh coated by chemical-vapor-infiltrated TiB_2[a] exhibited mixed results during the immersion tests. The TiB_2 coatings were resistant to chemical attack, but the fibers reacted with molten Al during the first 4 weeks of exposure. Additional research is needed to evaluate more wear-resistant fibers (such as Al_2O_3) for these composites, as the processing of fiber mesh structures has two potential advantages over traditional powder sintering methods of processing TiB_2 cathodes: 1) a significantly greater variety of shapes can be processed, and 2) smaller amounts of relatively high-cost TiB_2 (with thin-coated structures) may be used.

The fourth TiB_2-type material to be immersion tested, the Great Lakes TiB_2-G composites, were extensively attacked within 8 h of exposure. Typical features of attack included intergranular Al penetration of the TiB_2 and Al_4C_3 formation as a result of a direct reaction between the Al and graphite (Figure 31). After immersion in molten Al, x-ray diffraction was performed on cut surfaces of a specimen, and the results suggest that graphite is consumed by the formation of Al_4C_3 (Schilling and Graff 1988). Anoxic conditions during the immersion tests are not expected to result in a mechanism for rapid, steady removal of Al_4C_3 from the TiB_2 pores.[b] Therefore, it may be suggested that stresses are exerted on the TiB_2 pore walls as a result of the 3.8:1 volume expansion of Al_4C_3 relative to graphite (Weast, Astle, and Beyer 1985; Schilling and Graff 1988). It is hypothesized that this process may fracture the brittle TiB_2 matrix, subsequently exposing Al to deeper regions of the composite and allowing the attack process to proceed inward from the exterior surfaces. Supporting this hypothesis, molar volume calculations and solubility calculations suggest that if all of the C present formed Al_4C_3, the saturation solubility of dissolved Al_4C_3 in Al would be exceeded by several times during the immersion tests (Schilling and Graff 1988). As a result, dissolution rates

---

(a) Samples were supplied by T. Besmann of Oak Ridge National Laboratory. The chemical-vapor-infiltration process is described by Caputo and Lackey (1984) and Stinton et al. (1986). Samples contained Nicalon SiC-based fibers produced by Nippon Carbon Co., Tokyo, Japan.

(b) Several authors report that oxidizing atmospheres enhance transport of Al_4C_3 from molten Al into the atmosphere: Hollingshead and Brown 1981; Takemoto et al. 1963; Dorward 1973a and 1973b; Grjotheim, Naeumann, and Oye 1977.

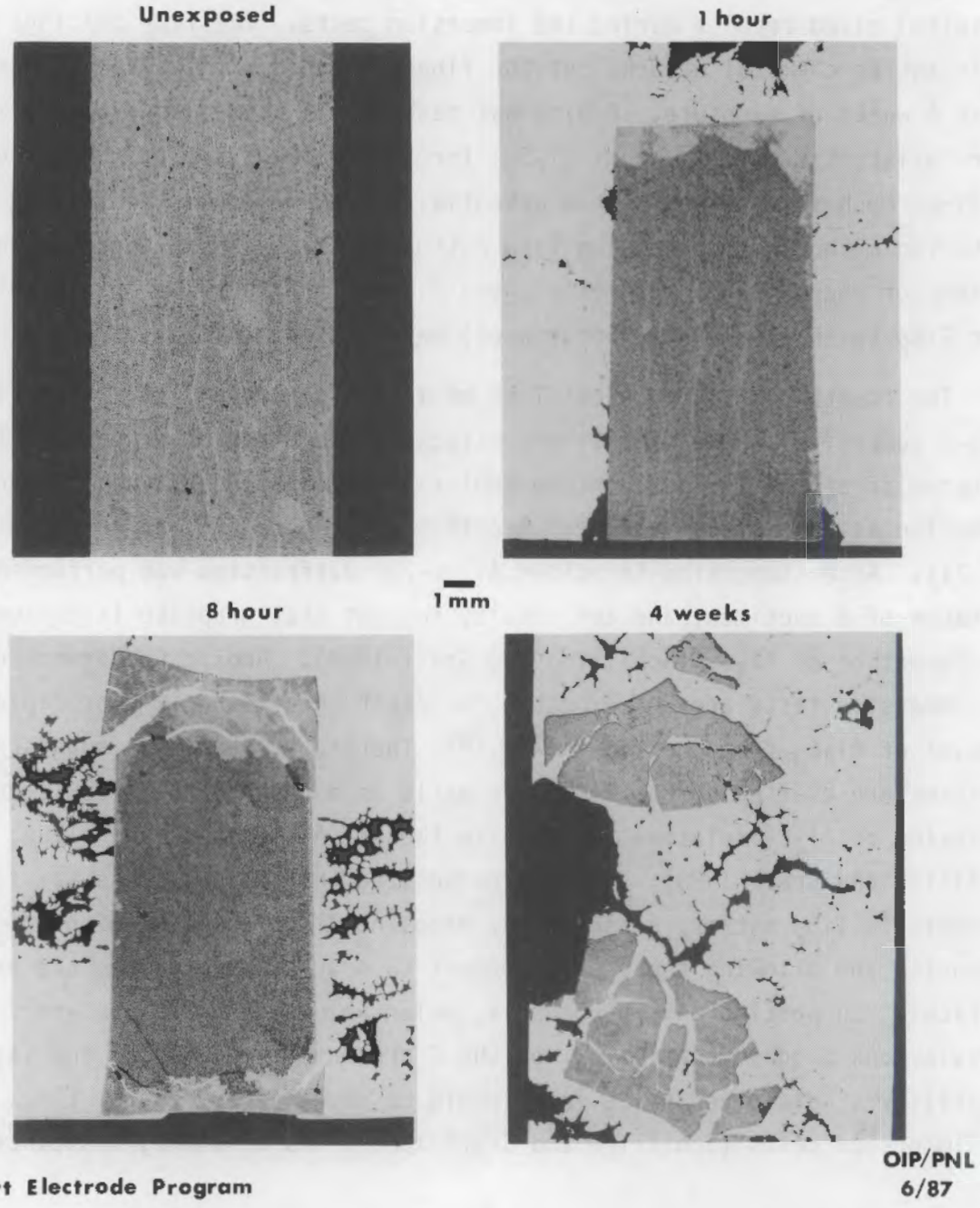

FIGURE 31. Polished Surfaces of TiB_2-G as a Function of Time Immersed in Al. Surface penetration by Al occurs during early stages of attack. Eventual disruption by intergranular penetration of TiB_2 may be attributed to expansion stresses exerted on TiB_2 pore walls as a result of Al_4C_3 formation.

would approach zero as the saturation solubility is reached, and Al_4C_3 crystals would accumulate without dissolving inside the TiB_2 pores.

This form of attack may never occur in a TiB_2-G cathode, because the literature suggests that commercial cell conditions favor the rapid removal of Al_4C_3 from Al-graphite interfaces and into the Al. It is possible that this process prevents disruption of the TiB_2 matrix during electrolysis because of the rapid removal of Al_4C_3 from the Al-filled TiB_2 pores. In support of this argument, several authors report that Al in Hall-Heroult cells typically contains Al_4C_3 at concentrations of 10 to 25 ppm, which are well below the saturation solubility of approximately 360 ppm at 960°C (Hollingshead and Brown 1981; Takemoto et al. 1963; Dorward 1973a and 1973b; Grjotheim, Naeumann, and Oye 1977). As a result, Al_4C_3 formed at Al/graphite interfaces is expected to dissolve into the metal pad during electrolysis; the Al_4C_3 subsequently diffuses through the Al and Na_3AlF_6 and is removed from the cell by reacting with CO_2 or O_2 at the anode (Hollingshead and Brown 1981; Takemoto et al. 1963; Dorward 1973a and 1973b; Grjotheim, Naeumann, and Oye 1977). Transport of Al_4C_3 may be by a similar mechanism during electrolysis with cermet anodes. In addition, the existance of a Na-rich layer observed within the TiB_2-G cathode in Figure 27 may affect the rate of Al_4C_3 formation and subsequent dissolution into the Al pad.

High-Purity TiB_2 in 140-Hour Electrolysis Test

Alcoa high-purity polycrystalline TiB_2 was evaluated as a replaceable cathode in a 140-h electrolysis test in the small-scale cell. The TiB_2 was supplied by H. R. Baumgartner of Alcoa Laboratories in the form of a plate that was sintered from high-purity powders produced by the halide plasma reduction process (Hoejke 1981; Baumgartner 1984a and 1984b; Baumgartner and Steiger 1984). The as-received TiB_2 was cut into a rectangular parallelepiped (32 x 20 x 6.6 mm) and loosely set on edge inside a slot cut into the graphite cell bottom. Electrolysis was performed at 970°C with a bath composition of 79.6 wt% Na_3AlF_6-13.5 wt% AlF_3-8 wt% Al_2O_3 (bath ratio = 1.08). The cermet

anode was $NiO-NiFe_2O_4$-X.[a] The TiB_2 tile fell out of its retaining slot as a result of manual probing during the test. Electrolysis was terminated after 140 hs when it was discovered that the Na_3AlF_6 bath had successivily penetrated through the Al_2O_3, graphite, and Inconel® walls of the cell; this penetration was observed at the level of the bath/air interface.

Optical ceramography on the TiB_2 cathode (Figure 32) showed no evidence of microcracking, spalling of TiB_2 grains, or any apparent penetration by Na_3AlF_6 bath or Al. A layer of Al was observed coating portions of the exterior surfaces of the TiB_2 tile. This film contained a second phase that possibly resulted from the Fe contamination after the Fe-based sidewall of the cell was penetrated by Na_3AlF_6 bath during electrolysis. Further analysis was not performed to identify this phase nor were attempts made to analyze the TiB_2 at higher magnification.

Replaceable Anode-Cathode Fixture

A small-scale electrolysis test of a replaceable anode-cathode fixture was performed. A BN spacer was used to attach the anode to the cathode and mechanically align the anode-cathode spacing (Figure 33). This design concept, originally proposed by Jarrett and Hornack (1985), was evaluated because it has unique advantages: 1) anodes and cathodes are contained in removable fixtures, which may be easily retrofitted to existing commercial cells, 2) anode-cathode spacings are precisely aligned because the anode and cathode surfaces are separated by ceramic spacers and the cathodes do not physically contact cell bottoms, which are dimensionally unstable, and 3) the replaceable fixtures can accommodate bipolar electrodes, which are revolutionary design candidates for advanced, energy-saving cells.

The replaceable cathode fixture was constructed using a TiB_2-G cathode, a $NiO-NiFe_2O_4$-17 wt% Cu anode brazed to a Ni rod current lead, and a BN sleeve attached to both electrodes which fixes the anode/cathode spacing at 1.3 cm (Figure 33). Electrolysis was performed at 970°C in the small-scale cell using

(a) X refers to a metal phase of proprietary composition.
® Inconel is a trademark of Huntington Alloys (INCO Alloys International) Huntington, West Virginia.

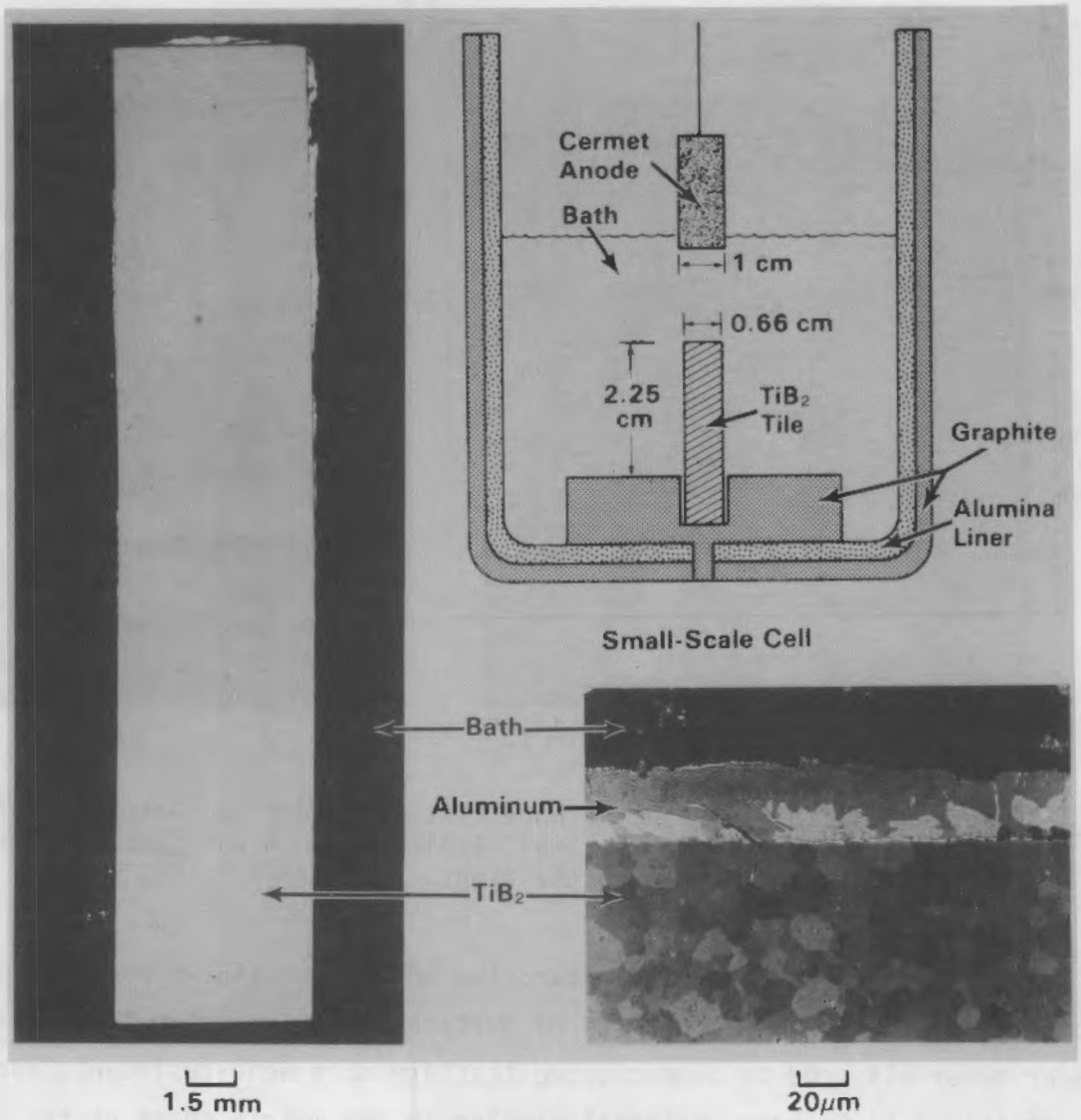

FIGURE 32. Microstructure of Alcoa High-Purity TiB_2 Cathode After 140 Hours Electrolysis in Small-Scale Cell. The TiB_2 shows no evidence of microcracking, spalling, or penetration by Al or bath.

a bath composition of 79.6 wt% Na_3AlF_6-13.5 wt% AlF_3-8 wt% Al_2O_3 (bath ratio = 1.08). Current densities for the anode and cathode were approximately 1 A/cm^2. The cell operated for 7 h at a total voltage drop of 3.4 volts. The assembled fixture was subsequently sectioned with a diamond saw and polished for optical ceramography. Complete details are reported by Schilling (1988).

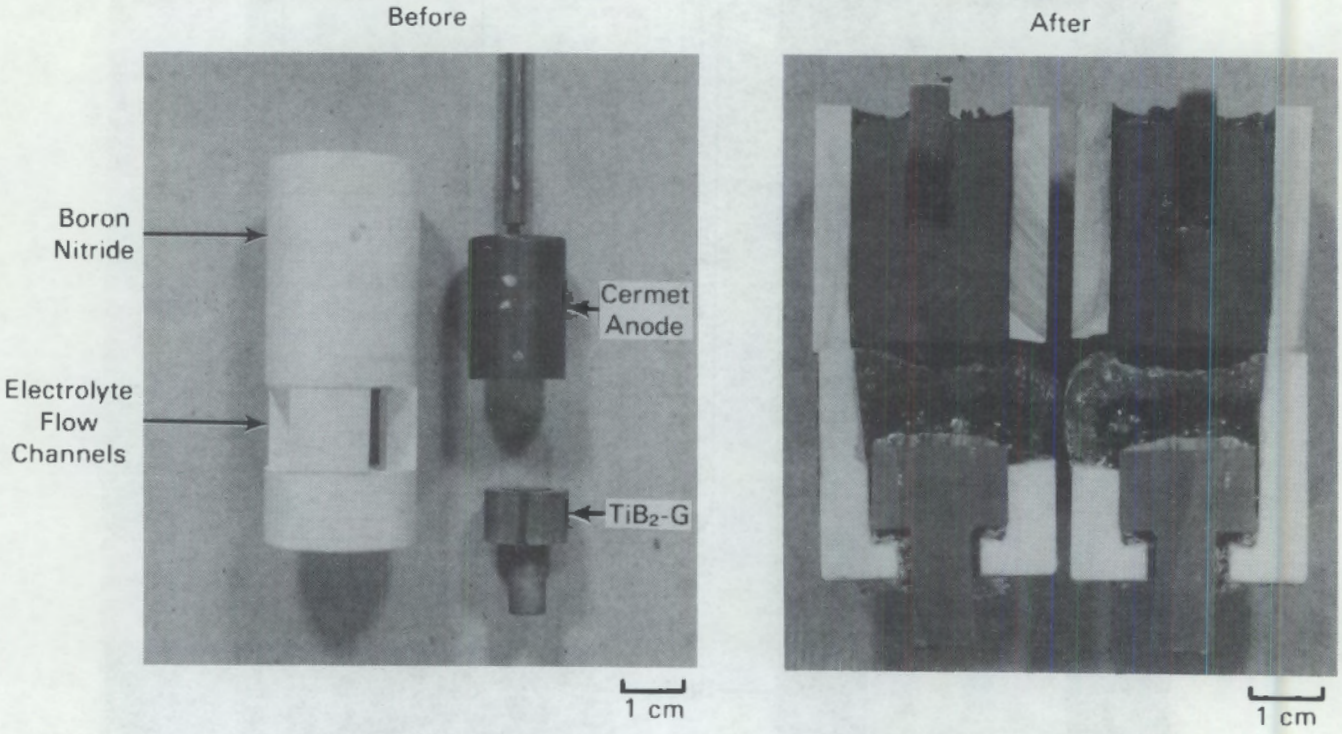

FIGURE 33. Replaceable Anode Cathode Fixture Before and After 7 h of Electrolysis in the Small-Scale Cell. A cut section of the fixture is shown on the right.

The anode exhibited minimal wear; the BN and the TiB_2-G remained intact, but both materials showed features of surface attack. Alternative ceramic spacer materials need to be evaluated that are more wear-resistant, such as AlN or possibly a Ni-Fe-based material similar to the matrix phase of the cermet anodes.

Optical ceramography indicated a thin layer of Al coating the exterior surfaces of the TiB_2-G; surface attack was visible in the form of microcracks in the TiB_2-G and spalled TiB_2 grains that were entrained in the Al and Na_3AlF_6 bath. Previous experiments suggest that the fragmentation of the TiB_2 was caused by chemical attack by the Na_3AlF_6 bath; this phenomenon may be avoided if the TiB_2-G is coated with a protective layer of Al prior to exposure to molten Na_3AlF_6 (Hart et al. 1987).

The cell used in the above tests operated at approximately 50% current efficiency, based on the weighed amount of Al produced during electrolysis. It

is possible that the low efficiency was caused in part by gas bubble resistance in the anode-cathode spacing and Na intercalation into the graphite floor of the cell. Minimized bubble resistance, through improved circulation of electrolyte, is necessary for large-scale fixtures operating at anode/cathode spacings of less than 1 to 2 cm. It is recommended that improved mechanical designs be evaluated, such as those using grooves in the bottom surfaces of the anodes to assist the removal of gas bubbles from the anode-cathode spacing.

TiB_2-Based Paint Coating

The performance of a TiB_2-based paint coating[(a)] on graphite was evaluated during short-term exposure to molten Al under non-polarized conditions. Paint coatings were analyzed because they provide a relatively inexpensive approach to producing elaborate shapes with a thin coating of TiB_2-based material. The coated samples were extensively attacked after immersion in molten Al. Ceramography results indicate that this attack may result from molten Al penetration through preexisting cracks in the coating, causing chemical attack of the graphite. In addition, chemical attack may be caused by reactions between elemental Al and SiO_2, a primary constituent of the coating (Brondyke 1953; Standage and Gani 1967). Complete details of these tests are reported by Schilling (1988). We recommend that future research focus on developing coating procedures that are less susceptible to producing cracks and causing unwanted chemical reactions in molten Al.

In-Situ TiB_2 Coating Study

Preliminary experiments were performed to evaluate in situ formation of TiB_2 coatings that may be self-healing in a Hall-Heroult cell. Synthesis of TiB_2 coatings was attempted by soaking Ti in B-saturated molten Al. Aluminum-Ti reactions resulted in extensive degradation of the Ti. Microchemical analysis of reaction products was not performed, although the Al-Ti phase diagram suggests the formation of phase separation from Al-Ti compound formations. The TiB_2 is also expected to be present in the reaction layer around the sample that was exposed to the 10% B solution, based on the negative Gibbs free energy

(a) Aremco Products, Inc., Ossining, New York; Graphi-Coat 623.

of the Ti + 2B = TiB_2 reaction (Zavitsanos and Morris 1983). Additional details of these experiments are reported by Schilling (1988).

Although this preliminary procedure was unsuccessful, further evaluation is recommended as 1) there are significant economic advantages to self-healing TiB_2 cathodes in a Hall-Heroult cell, and 2) reports in the open literature suggest possible avenues for producing self-healing coatings by electrodeposition and diffusion saturation using molten salts.[a]

TiB_2 Sintering Studies

A set of brief experiments was performed to evaluate the feasibility of fabricating TiB_2 cathodes by sintering powders prepared by the low-temperature synthesis of a TiB_2 precursor (Ritter 1987). The TiB_2 powder was supplied by J. J. Ritter, the inventor of the process, at the National Bureau of Standards. The goal of this study was to prepare cathodes for electrolysis testing. Unfortunately, cathode test samples could not be produced because of insufficient densification during sintering. It is recommended that processing modifications be attempted to improve sinterability. Such modifications might entail the use of smaller average particle sizes, higher sintering temperatures, and/or applied pressure during sintering. This powder-making process may have economic advantages over traditional powder processing and sintering methods if fabrication costs are reduced and the powders show acceptable wear resistance in a Hall-Heroult cell. A larger development program is needed to evaluate these and other types of TiB_2 powders as they become available.

FUTURE DIRECTIONS

Of the six methods of Al cell retrofitting investigated during the work performed in FY 1987, two approaches are recommended. It appears that these two methods can yield practical, near-term retrofit of existing Hall-Heroult cells using drained cathodes, cermet anodes, and reduced anode-cathode spacing. They are 1) use of replaceable cathodes that rest, unattached, on C cell bottoms, and 2) use of replaceable anode-cathode fixtures that have ceramic

(a) Sane, Wheeler, and Kuivila 1983 and 1985; Singhal 1978; Epik 1977; and Samsonov and Epik 1966.

spacers to align anode-cathode spacing. Both approaches require the use of wear-resistant cathode materials such as TiB_2-G, TiB_2-AlN, and high-purity TiB_2.

The replaceable cathode is the more conservative approach, since it requires only minimal alterations to the structure and operation of existing Hall-Heroult cells and also enables retrieval and replacement of the TiB_2-based parts. However, a long-term drawback to the replaceable cathode approach is that the anode-cathode spacings may become misaligned as a result of dimensional instabilities in the C cell bottom caused by Na intercalation and salt crystallization. Reduced anode-cathode spacings, with cermet anodes and drained TiB_2-based cathodes, must be precisely aligned to improve power efficiency and reduce electrode wear.

The replaceable anode-cathode fixture appears to overcome the problem of dimensional stability; however, the main difficulty is that of spacer materials wear. If wear-resistant spacer materials can be found, breakthroughs in monopolar- and bipolar electrode designs may be possible and may entail minimum alteration to existing Hall-Heroult cells. Prime candidate spacer materials for evaluation include AlN and possibly a Ni-Fe-based phase similar to the cermet anode matrix.

To reach the long-range program objective of retrofitting commercial cells with drained TiB_2-based cathodes, an integrated cell design must be developed incorporating the TiB_2 cathodes with cermet anodes and reduced anode-cathode spacing. It is recommended that near-term research focus on developing a basis for designing TiB_2-based cathode which can be retrofitted into a 5- to 10-kA pilot cell using cermet anodes. Replaceable TiB_2-G cathodes, such as those being developed by Reynolds Corporation and Great Lakes Research Corporation (Tucker et al. 1986; Tabereaux 1987), are recommended for conservative cell designs that will enable near-term evaluation of cathode wear behavior and expected energy efficiency for larger-scale cells. Specifically, it is recommended that cathode research activities be pursued in two areas: 1) assembling a team of experts to evaluate design parameters pertaining to heat balance, cell magnetohydrodynamics, cell operations and related control systems, electrode wear processes, and the physical geometries of electrodes and electrode

attachments, and 2) performing laboratory-scale electrolysis tests in support of the pilot cell design; the latter experiments are mainly for evaluation of anode-cathode geometries, electrode holder systems, gas bubble release, and cathode wear processes at reduced anode-cathode spacing.

Although not within the scope of the FY 1988 Inert Electrodes Program, processing of TiB_2-based cathode materials needs to be evaluated with the goal of reducing fabrication costs and improving wear behavior, mechanical properties, thermal shock resistance, and shape fabricability. For example, TiB_2-AlN cathodes are reported to exhibit wear resistance; however, these materials are traditionally fabricated into simple shapes using costly hot pressing procedures. Use of injection molding or slip casting--methods which may produce acceptably dense parts--might reduce costs and make more complex shapes available. In addition, three promising avenues are recommended for developing inexpensive cathode fixtures having complex shapes while conserving the amount of TiB_2 required: 1) evaluation of TiB_2-based paint coatings which consist of inexpensive TiB_2 powder suspended in a durable matrix phase, 2) evaluation of ceramic fiber weave structures that are coated with TiB_2, and 3) evaluation of diffusion saturation or electrodeposition methods to enable self-healing TiB_2 coatings in an operating Hall-Heroult cell.

REFERENCES

Baumgartner, H. R. 1984a. "Mechanical Properties of Densely Sintered High-Purity Titanium diborides in Molten Al Environments." J. Amer. Ceram. Soc. 67(7):490-497.

Baumgartner, H. R. 1984b. "Subcritical Crack Velocities in Titanium Diboride Under Simulated Hall-Heroult Cell Conditions." Amer. Ceram. Soc. Bull. 63:1172.

Baumgartner, H. R., and R. A. Steiger. 1984. "Sintering and Properties of Titanium Diboride Made From Powder Synthesized in a Plasma-Arc Heater." J. Amer. Ceram. Soc. 67(3):207-212.

Brondyke, K. J. 1953. "Effect of Molten Al on Alumina-Silica Refractories." J. Amer. Ceram. Soc. 36(5):171-174.

Caputo, A. J., and W. J. Lackey. 1984. "Fabrication of Fiber-Reinforced Ceramic Compositions by Chemical Vapor Infiltration," Ceramic Engineering and Science Proceedings 5(7-8):654-667, American Ceramic Society, Columbis, Ohio.

Dell, M. B. 1967. "Potlining Failures in Al Electrolysis Cells," J. Metals, March 1967, pp. 14-17.

Dell, M. B. 1985. "Potlining Failure Modes," Light Metals 1985, H. D. Bohner, editor, American Institute of Mining and Metallurgical Engineers, New York, pp. 957-966.

Dewing, E. W. 1963. "The Reaction of Sodium with Nongraphitic Carbon: Reactions Occurring in the Linings of Al Reduction Cells," Transactions of the Metallurgical Society of AIME, December, 227:1328-1334.

Dewing, C. B. 1974. "The Chemistry of the Alumina Reduction Cell," Can. Met. Quart. 13:607-618.

Dorward, R. C. 1973a. "Al Carbide Formation and Removal During Electrolytic Reduction and Hot Metal Processing Operations," Light Metals 1973, American Institute of Mining and Metallurgical Engineers, New York, pp. 105-118.

Dorward, R. C. 1973b. "Al Carbide Contamination of Molten Al," Aluminium 49:686-688.

Epik, A. P. 1977. "Boride Coatings," Boron and Refractory Borides, ed. V. I. Matkovich, Springer-Verlag pp. 597-612.

Goodnow, W. H., and J. R. Payne. 1982. "Al Reduction Cell Electrode." U.S. Patent 4,349,427.

Grjotheim, K., R. Naeumann, and H. A. Oye. 1977. "Formation of Al Carbide in the Presence of Cryolite Melts," Light Metals 1977, American Institute of Mining and Metallurgical Engineers, New York, pp. 233-242.

Hart, P. E., B. B. Brenden, N. C. Davis, O. H. Koski, S. C. Marschman, K. H. Pool, C. H. Schilling, C. F. Windisch, and B. J. Wrona. 1987. Inert Anode/Cathode Program Fiscal Year 1986 Annual Report, PNL-6247, Pacific Northwest Laboratory Report, Richland,Washington.

Hoejke, H. H. "Submicron Titanium Boride Powder and Method for Preparing Same." U.S. Patent 4,282,195. 1981.

Hollingshead, E. A., and J. A. Brown. 1981. "Rate of Solution of Carbon in Molten Al Under a Cryolite Melt," Light Metals 1981, American Institute of Mining and Metallurgical Engineers, New York, pp. 625-634.

Jarrett, N., and T. R. Hornack. 1985. "Support Member and Electrolytic Method." U.S. Patent 4,504,366.

Panebianceo, B., and R. Bacchiega. 1966. "Deformation Phenomena in the Bottoms of Electrolytic Reduction Cells for Production of Al," Alluminio 35(3):69-78.

Ritter, J. J. 1987. "A Low-Temperature Chemical Process for Precursors to Boride and Carbide Ceramic Powders," Advances in Ceramics Volume 21: Ceramic Powder Science, editors G. L. Messing, K. S. Mazdiyasni, J. W. McCauley, and R. A. Haber, American Ceramic Society Inc., Westerville, Ohio, pp. 21-31.

Samsonov, G. V., and E. P. Epik. 1966. "Part 1e. Coatings of High Temperature Materials: Boride Coatings," Coatings of High Temperature Materials, ed. H. H. Hausner, Plenum Press, New York, pp. 7-34.

Sane, A. Y., D. J. Wheeler, and C. S. Kuivila. 1983. "Al Wettable Materials." European Patent Application EP 94353 A2.

Sane, A. Y., D. J. Wheeler, and C. S. Kuivila. 1985. "Al Wettable Materials for Al Production." U.S. Patent 4,560,448.

Schilling, C. H. 1988. Laboratory Testing of TiB_2-Based Cathodes for Electrolytic Production of Al. PNL-6594, Pacific Northwest Laboratory, Richland, Washington.

Schilling, C. H., and G. L. Graff. 1988. Immersion Tests of TiB_2-Based Materials for Al Processing Applications. PNL-6593, Pacific Northwest Laboratory, Richland, Washington.

Schilling, C. H., D. I. Hagen, and P. E. Hart. 1987. Stable Attachment of TiB_2-Based Cathodes for the Al Industry: Review and Recommendation. PNL-6144, Pacific Northwest Laboratory, Richland, Washington.

Singhal, S. C. 1978. "An Erosion Resistant Coating for Titanium and Its Alloys," Thin Solid Films 53(3):375.

Sorlie, M., and H. A. Oye. 1984a. "Chemical Resistance of Cathode Carbon Materials During Electrolysis," Light Metals 1984, American Institute of Mining and Metallurgical Engineers, New York, pp. 1059-1071.

Sorlie, M. and H. A. Oye. 1984b. "Deterioration of Carbon Linings in Al Reduction Cells, Part II - Chemical and Physical Characterization of Cathode Carbons," Metallwissenschaft und Technik 38:109-115.

Standage, A. E., and M. S. Gani. 1967. "Reaction Between Vitreous Silica and Molten Al," J. Amer. Ceram. Soc. 50:(2)101-105.

Stinton, D. P., A. J. Caputo, R. A. Lowden, and T. M. Besmann. 1986. "Improved Fiber-Reinforced SiC Composites Fabricated by Chemical Vapor Infiltration," Ceramic Engineering and Science Proceedings, July-August, American Ceramic Society, Columbus Ohio, pp. 983-989.

Tabereaux, A. T. 1987. "Stable TiB_2-Graphite Cathodes for Al Production," Cathode Workshop Proceedings, Light Metals Production Research Group, February 27-28, Carnegie-Mellon University.

Takemoto, M., T. Yashimoto, K. Oida, and L. Yanagida. 1963. "Effect of Holding on Some Properties of Metal Tapped from Electrolytic Cells," in Extractive Metallurgy of Aluminum, Volume 2, G. Gerard, editor, Wiley Interscience, New York, pp. 297-311.

Tucker, K. W., J. R. Shaner, J. T. Gee, and L. A. Joo'. 1986. "TiB_2-Graphite Cathodes in Al Reduction Cells," Extended Abstracts: Electrochemical Society Fall 1986 Meeting, San Diego, California.

Waddington, J. 1963. "Processes Occurring in the Carbon Lining of an Aluminum Reduction Cell," Extractive Metallurgy of Aluminum, Volume 2, G. Gerard, editor, Wiley Interscience, New York, pp. 435-452.

Weast, R. C., Astle, M. J., and Beyer, W. H.. 1985. CRC Handbook of Chemistry and Physics Sixty-Sixth Edition, CRC Press, Boca Raton, Florida, p. B-68, p. B-84.

Zavitsanos, P., and J. R. Morris, Jr. 1983. "Synthesis of Titanium Diboride by a Self-Propagating Reaction," Ceramic Engineering and Science, Vol. 4, No. 7-8. Proceedings of the Amer. Ceramic Society, July to August.

5.0 SENSOR DEVELOPMENT

O. H. Koski and B. B. Brenden

The objective of the Sensor Development Task is to develop sensors to control the bath chemistry of Hall-Heroult cells being operated with stable anodes and cathodes.

SUMMARY

Activities for the Sensor Development task during FY 1986 and 1987 included the determination of bath ratio and Al_2O_3 concentration through bath vapor spectral analysis; development of contact and noncontact methods for determining the liquidus temperature of the Na_3AlF_6 bath used in Hall-Heroult cells; and Al_2O_3 determination from analysis of process-generated electrical signals (work done in conjunction with Professor C. Nikias of Northeastern University).

Highlights of these activities include the following:

- Electrical models from digital signal analysis of cell process signals prove that a passivation film can form on the anodes during cell operation, prolonging anode lives. The signal analysis suggests that the bath does not need to be maintained at Al_2O_3 saturation to maintain this protective film, that stochastic processes may be the dominant mode of anode degradation and that, if a passivation film remains intact, metal anodes can be considered.
- A portable contact method for determining liquidus temperature by detecting the "thermal arrest" in the cooling curve of bath temperatures from bath withdrawn from an operating cell was successfully demonstrated at the Kaiser aluminum plant in Spokane, Washington.
- A method for determining liquidus temperature without touching the corrosive Na_3AlF_6, by use of a laser reflectance method, was laboratory-tested and determined unsuitable because it could not be used to determine Al_2O_3 concentrations in excess of 6 wt%.

- Bath vapor spectral analysis results were not promising and that effort was discontinued due to low probability of success.

TECHNICAL PROGRESS

The three major thrusts of the task for FY 1987 were 1) bath vapor spectral analysis, 2) liquidus temperature determination, and 3) Al_2O_3 determination. The work done in these three areas is described in the following sections.

Bath Vapor Spectral Analysis

The theory behind this analysis is that the bath ratio and Al_2O_3 concentration of the Na_3AlF_6 bath can be inferred from monitoring the effect of NaF vapor on vapor-deposited $NaAlF_4$ films.

The basis for the study is derived from the fact that the major constituent of the vapor above the Na_3AlF_6 bath is $NaAlF_4$. The minor vapor pressure of NaF was assumed likely to change the optical properties of $NaAlF_4$ vapors which were collected as a film on quartz plates held above the bath. If this assumption were substantiated, then it would be possible to monitor the activity of NaF in the bath and, by inference, the bath ratio and Al_2O_3 concentration.

Initial experimentation appeared promising; reflectance data on vapor-deposited films on a quartz substrate correlated well with bath ratio. Alumina (Al_2O_3) concentrations (of 0, 5, 10, and 15 wt%) at various bath ratios (1.1, 1.2, and 1.3) were used to determine basic reflectance information. The results, however, suggested that a bias might have been introduced by the sampling method. Additional tests with samples collected at a higher temperature resulted in lack of variation of reflectance with bath ratios from 1.0 to 1.4.

The electrical conductivity of vapor-deposited films derived from bath ratios of 1.1, 1.2, and 1.3 was studied as a function of temperature as supportive evidence regarding vapor composition changes with bath ratio. The energy of activation for the conduction process did not appear to be influenced by bath ratio.

This study, though not conclusive, was not supportive of continued efforts in bath vapor spectral analysis. Thus, this analysis was discontinued because of the low probability of success.

Liquidus Temperature Measurement

The liquidus temperature is the maximum temperature at which both solid and liquid phases are present in the Na_3AlF_6 bath. This temperature is strongly affected by both the concentration of Al_2O_3 and the ratio of NaF to AlF_3 (bath ratio or Na_3AlF_6 ratio) in the bath. Since the bath ratio is relatively constant, the determination of a liquidus temperature would, in effect, be a determination of Al_2O_3 concentration.

Two types of methods for determining liquidus temperature have been evaluated at PNL: noncontact and contact. Three noncontact methods were investigated in FY 1986 (Hart et al. 1987). Laboratory tests of the laser reflectance noncontacting method were conducted in FY 1987. A contact method of liquidus determination, known as the thermal arrest method, has been developed and successfully demonstrated in FY 1987. Both types of methods for determining liquidus temperature are described below.

Noncontact Liquidus Temperature Determination: Laser Reflectance

The measurement of liquidus temperature by laser reflectance refers to the use of a combined laser, pyrometer, and radiometer to determine liquidus temperature by detecting solids on the bath surface through diffuse reflectance. The laser directs a narrow spectra of light down at the surface of the bath. When solids have formed on the surface (which can be induced by blowing a cold gas stream across the bath surface), the light reflects off the surface, is detected by the radiometer, and signals the pyrometer to acquire a temperature. The maximum temperature at which the bath turns from a liquid to a solid is the liquidus temperature.

Laboratory tests of the laser reflectance system showed that the method produces uncertain results in measuring the Al_2O_3 content in Na_3AlF_6 with an Al_2O_3 concentration in excess of 6 wt%. Because the measurement of Al_2O_3 to saturation in excess of 6 wt% was needed, the method was judged unsuitable and further development was not pursued.

Contact Liquidus Temperature Determination: Thermal Arrest

A less expensive, but more accurate and portable contact method for determining liquidus temperature, known as the thermal arrest method, was developed for in-plant demonstration.

Phase boundaries in phase diagrams result from the thermodynamic law known as the Gibbs Phase Rule. This rule can be used to determine the number of degrees of freedom in a system. Cooling of a melt of a certain composition results in the precipitation of solid phases, the heat of fusion of which causes a change in the rate of cooling. At a eutectic, there are no degrees of freedom and hence the temperature of the system is fixed until all of the liquid has solidified. This inflection, or thermal arrest, is the liquidus temperature.

This information was used to devise a portable contact system for determining liquidus temperature. Further laboratory tests proved this method of solids detection to be more accurate than the noncontact devices tested; furthermore, it uses less expensive, though limited-life sampling parts.

The portable thermal arrest system consists of an HP-3421 data acquisition system, an HP-71B hand-held computer, a type K thermocouple, and a graphite dip cup (see Figure 34). A sample of molten bath is withdrawn, temperatures are measured with the thermocouple, and the temperature-versus-time is digitally stored in the hand-held computer.

A program was developed for the HP-71B that analyzes the cooling curve to identify three distinct regions, differentiated by their slopes. These three regions are the initial cooling period with the fastest cooling rate, the thermal arrest period with the slowest cooling rate, and the final period with a cooling rate of intermediate magnitude. The computer is programmed to calculate the slope (S) of the cooling curve and the rate of change of the slope (H). The temperature at which thermal arrest occurs is determined by finding the maximum value of H/S since a maximum value of H occurs in the region where the slope S is at a minimum. The resultant inflection point in the cooling curve as the system cools through the liquidus temperature is reported, as is the process temperature. Furthermore, by selecting the appropriate bath ratio, a wt% Al_2O_3 is also reported.

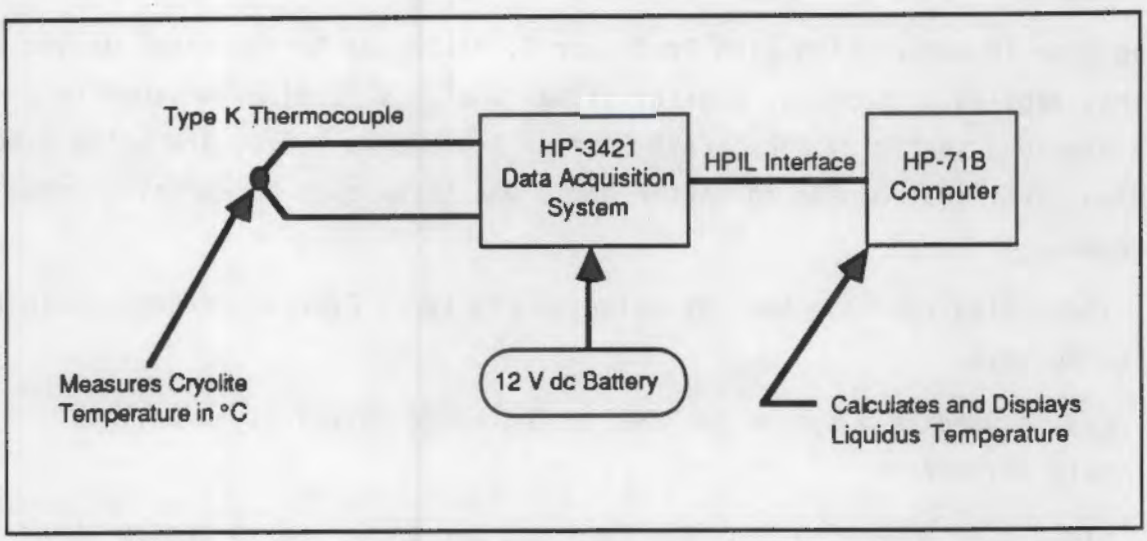

FIGURE 34. Portable Contact System for Measuring the Liquidus Temperature of Na_3AlF_6

Laboratory tests of this system using a bath ratio of 1.1 with 6, 7, 8, 9, and 10 wt% Al_2O_3 indicate that, if the bath ratio is known, the repeatability for the determination of Al_2O_3 content is better than ±0.15 wt%. As an example, a set of five measurements with a mean value of 8.24% had a standard deviation of 0.14%.

This system was successfully demonstrated under industrial conditions at the Kaiser/Mead plant in Spokane, Washington, in September 1987.

Alumina Determination from Process Generated Signals

The acoustic signals generated by the anode during gas evolution are projected to be associated with the Al_2O_3 concentration.[a] Also, information from the gas-wetted portion of the anode is likely to be reflected in capacitance values determined by cell voltage/current signatures. Thus, a combination of acoustic and electronic measurements can be useful for process control.

Since March 1987, efforts have been directed toward analyzing these process-generated signals from Hall-Heroult cells to define the effect of operating and chemical parameters on measurable electronic values. This work is

(a) Personal communication with Gary Tarcy, Alcoa Aluminum Company, 1986.

being done in cooperation with Professor C. Nikias of Northeastern University, who has applied a number of digital signal analysis (DSA) algorithms to process data provided to him by PNL. Fast Fourier transforms (FFTs) are being used to develop electrical models to better apply DSA techniques in defining anode processes.

These findings have been of value to the Inert Electrodes Program in the following ways:

- can be used as a system for evaluating anode materials as well as bath parameters
- prove that a passivation film forms on the anode and is central to achieving long anode life
- suggest that operating the baths at Al_2O_3 saturation is not required to achieve longevity (The basis for our instrumentation development criteria may require redefinition.)
- suggest that stochastic processes may be the dominant mode of anode degradation
- suggest that, if passivation films are intact, metal anodes may be considered.

The analysis of signals generated by the electrolytic process is attractive in that no additional structures are exposed to the highly corrosive bath. Furthermore, the signatures in the frequency or time domain may well be used to indicate the value of such diverse process measurements as

- Al_2O_3 concentration in the electrolyte
- conductivity of the electrolyte
- dispersed gas content of the electrolyte
- corrosion rate of the anode
- hydrodynamics of the molten Al cathode
- catalysis and rate signatures for aluminum oxyfluoride absorption, electron transfer, and gas evolution.

The experimental design, shown in Figure 35, was intended to accentuate the anode and indicate the effects of process variables on anode properties. It was assumed that low frequencies would define anode properties and higher frequencies bath properties. At the anode, the electrochemical system was operated under current density values which covered the range of current density values at which aluminum plants operate. In addition, a superimposed white noise made possible the measurement of anode parameters under actual process operating conditions using FFT techniques. The techniques used in the laboratory are not usable in the actual plant but will allow the interpretation of DSA which will use actual plant values.

Preliminary data composed of current, voltage, and acoustic signals were collected during a typical 20-h anode materials test. These data were analyzed by Professor C. Nikias. The purpose of the exercise was to establish that the data collection and analytical programs were functioning.

The analysis of Hall-Heroult cell electronic attributes has shown that the dominant characteristic of the Hall-Heroult cell under typical operating conditions are resistive, with no significant imaginary component to cell impedance to 5 kHz. (See Figure 36.) Because the ratio of cathode surface area to anode surface area in the test apparatus is about 300 to 1, the cathode resistance is

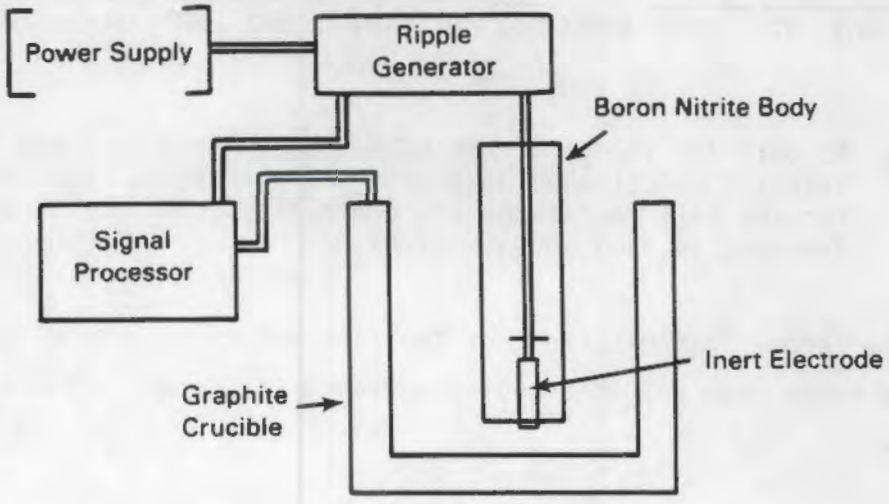

FIGURE 35. Inert Anode FFT Apparatus

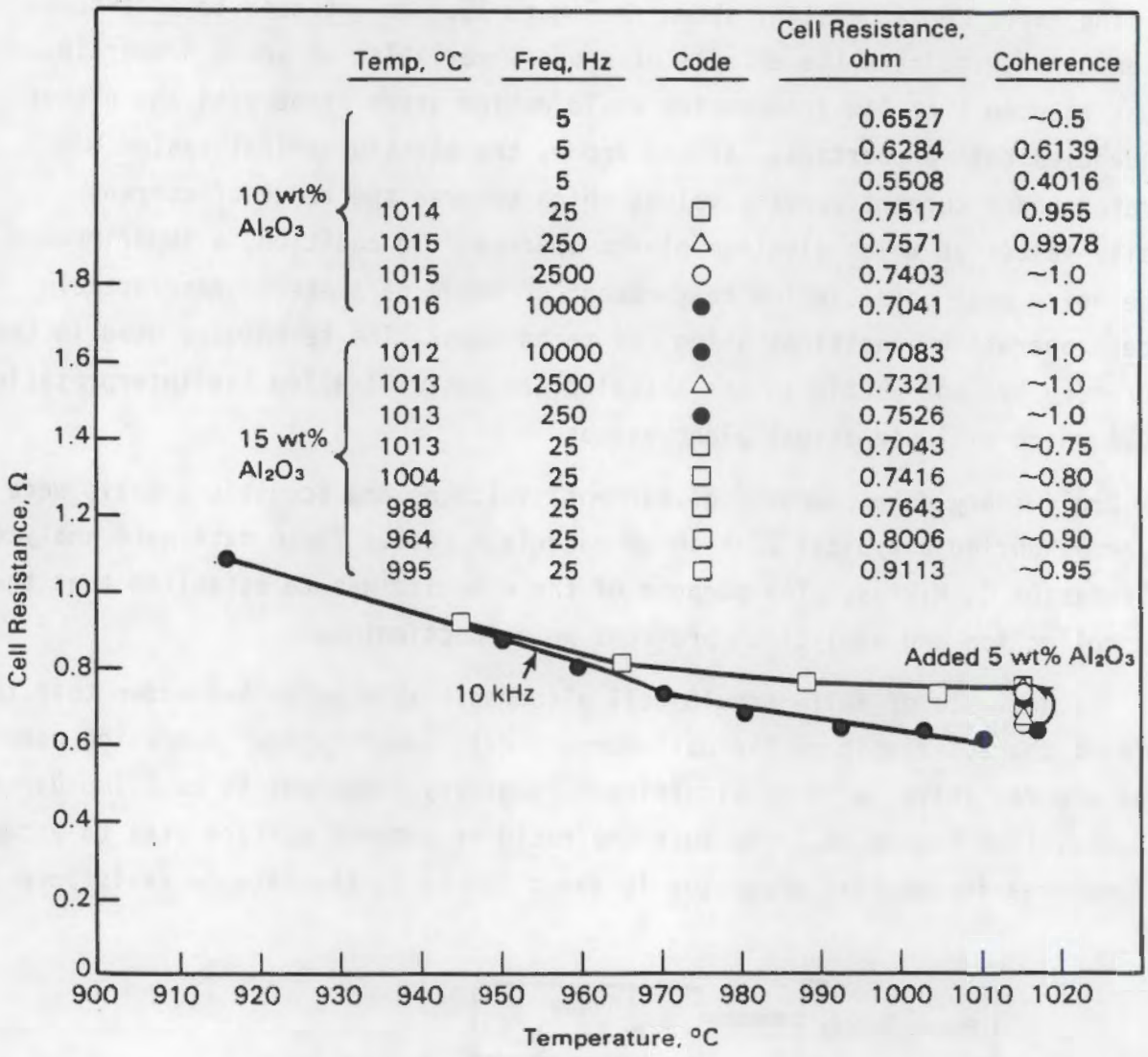

FIGURE 36. AC Cell Resistance of the 5324/17% Cu Anode Computed from the Transfer Function Using the Signal Processor. The table shows ferrite cell resistance and coherence at various temperatures, frequencies, and amounts of Al_2O_3.

assumed to be zero. The resistance of the electrolyte is predominantly determined by the anode area and is computable from a knowledge of the bath composition.

The above considerations allow that an IR[(a)]-free cell potential can be computed. Assuming that the large cathode is stable in time, then the observed cell potential minus the IR drop should provide a measure of the anode potential dynamics as a function of current densities. (See Figure 37, plot of E_p.)

Since the circuit impedance for the test apparatus is the sum of the electrolyte resistance and any anode film resistance, the anode resistance can be resolved by subtracting away the known electrolyte resistance. The circuit resistance is determined from 16 averaged FFTs performed under the test conditions. The frequency at which the resistance is measured has been shown to be unimportant. Nominally, the value is taken at 50 Hz. A plot of the resistance (real) and the imaginary components of the circuit transfer function are made for the frequency range 0 to 100 Hz, also based on an average of 16 FFTs. This procedure ensures that the real part is not a function of frequency and that the imaginary part is inconsequential, as stipulated above. See Table 3 for resistances of the electrodes illustrated in Figure 38. Note that a negative resistance is computed for the Mo electrode. Also note that the electrode potential is lower than C, indicating rapid corrosion. The invar, NiO-$NiFe_2O_4$-Cu-Ni, and Ni electrodes have a potential above the C, which indicates possible operation as O_2-producing electrodes.

The plots of cell voltage and electrode potential with respect to current density illustrated in Figure 39 can be interpreted as follows. The ferrite cermet electrode lies about 0.7 volts above the C anode at 0 current density. Since a C anode is accepted to be 1.6 volts with respect to an Al cathode, the ferrite cermet anode is therefore at 1.6 plus 0.7 or 2.3 volts with respect to an Al cathode. Note that the repeatability of measured points on the plot when derived from ascending or descending current magnitude is better than 10%.

The data do not always imply that the cell voltage at zero current is the theoretical 2.3 volts with respect to the Al cathode. The plot in Figure 40 shows a drooping cell and electrode potential at low current values. This is interpreted as the effects of an anode corrosion process.

(a) Current resistance product.

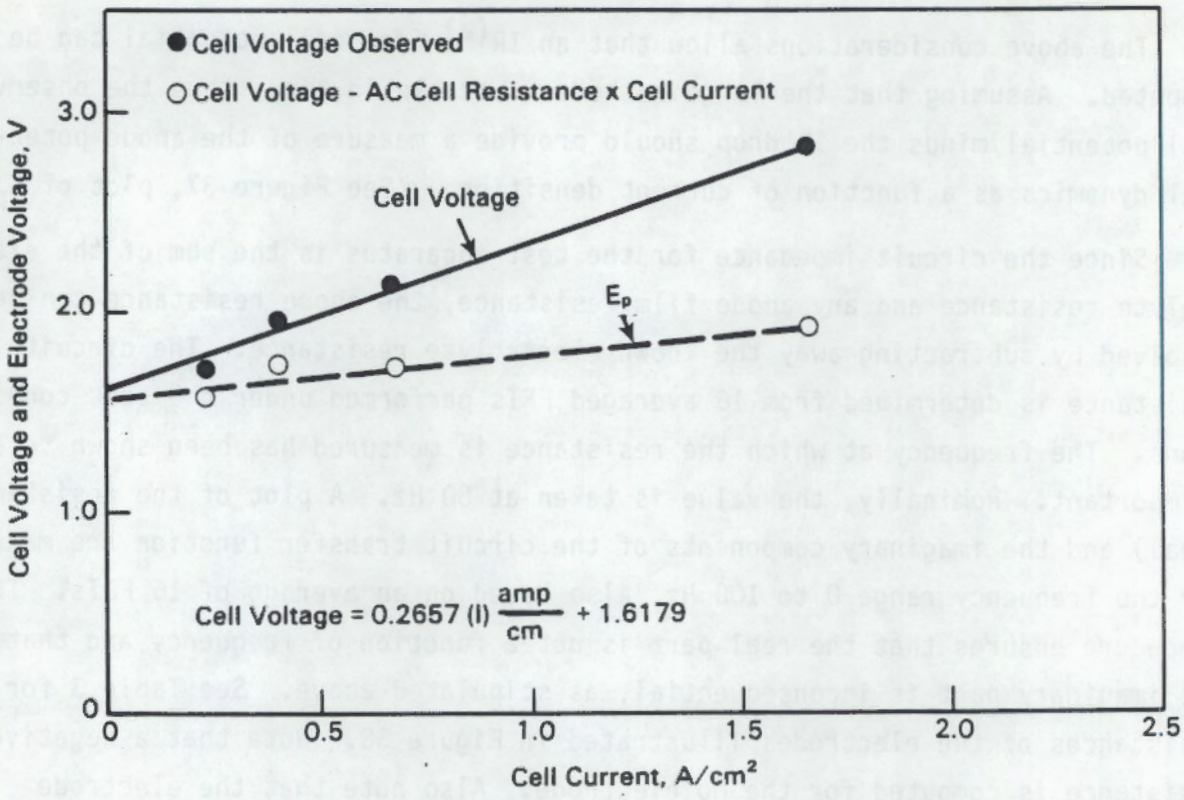

FIGURE 37. Cell Voltage and Electrode Potential Versus Cell Current

As the electrode potential and electrode resistance can be computed, these values may suggest means or techniques for control and measurement. In Figure 41, the electrode resistance is shown as a function of Al_2O_3 content. Figure 42 shows the electrode potential as a function of Al_2O_3 content. The data suggest that the resistance, a measure of the anode's resistance to corrosion, improves in the 0 to 5 wt% Al_2O_3 range and is not greatly affected above this concentration. The electrode potential is markedly lower for a bath ratio of 1.4 at 0 wt% Al_2O_3. It has been observed that the electrode potential at 0 wt% Al_2O_3 may not be repeatable and is cyclic with respect to time and current density. Note the scatter on Figure 43 which covers the electrode potential for current densities from 0 to 2.5 amp/cm^2 at bath ratios of 1.1, 1.2, 1.3, and 1.4. It would appear that the higher bath ratios are more aggressive at low Al_2O_3 content.

TABLE 3. Electrode Resistance Values of Nickel, Molybdenum, Ferrite, Invar, and Carbon Anodes at a Bath Ratio of 1.1 with 15 wt% Al_2O_3

Current Density	Resistance of Electrolyte plus Leads, ohms	Observed Circuit Resistance, ohms	Electrode Resistance[a] ohms
	Ni		
0.4101	0.3214	0.6769	0.3555
2.1027		0.4277	0.1063
1.0338		0.4688	0.1474
	Mo		
0.4601	0.3214	0.2701	-0.0513
1.1292		0.2644	-0.0570
2.086		0.2813	-0.0401
	$NiO-NiFe_2O_4$-Cu-Ni		
2.489	0.3214	1.408	1.0866
1.3006		0.9619	0.6405
0.571		0.7673	0.4459
2.626		1.110	0.7886
	Invar		
0.4124	0.3214	0.4463	0.1249
0.4053		0.4568	0.1354
1.0356		0.3845	0.0631
1.992		0.4375	0.1161
0.4596		0.3853	0.0639
	C		
0.4685	0.3214	0.6799	0.3585
1.1572		0.692	0.3706
2.117		0.7482	0.4268

(a) Electrode resistance = observed circuit resistance - resistance of (electrolyte + leads)

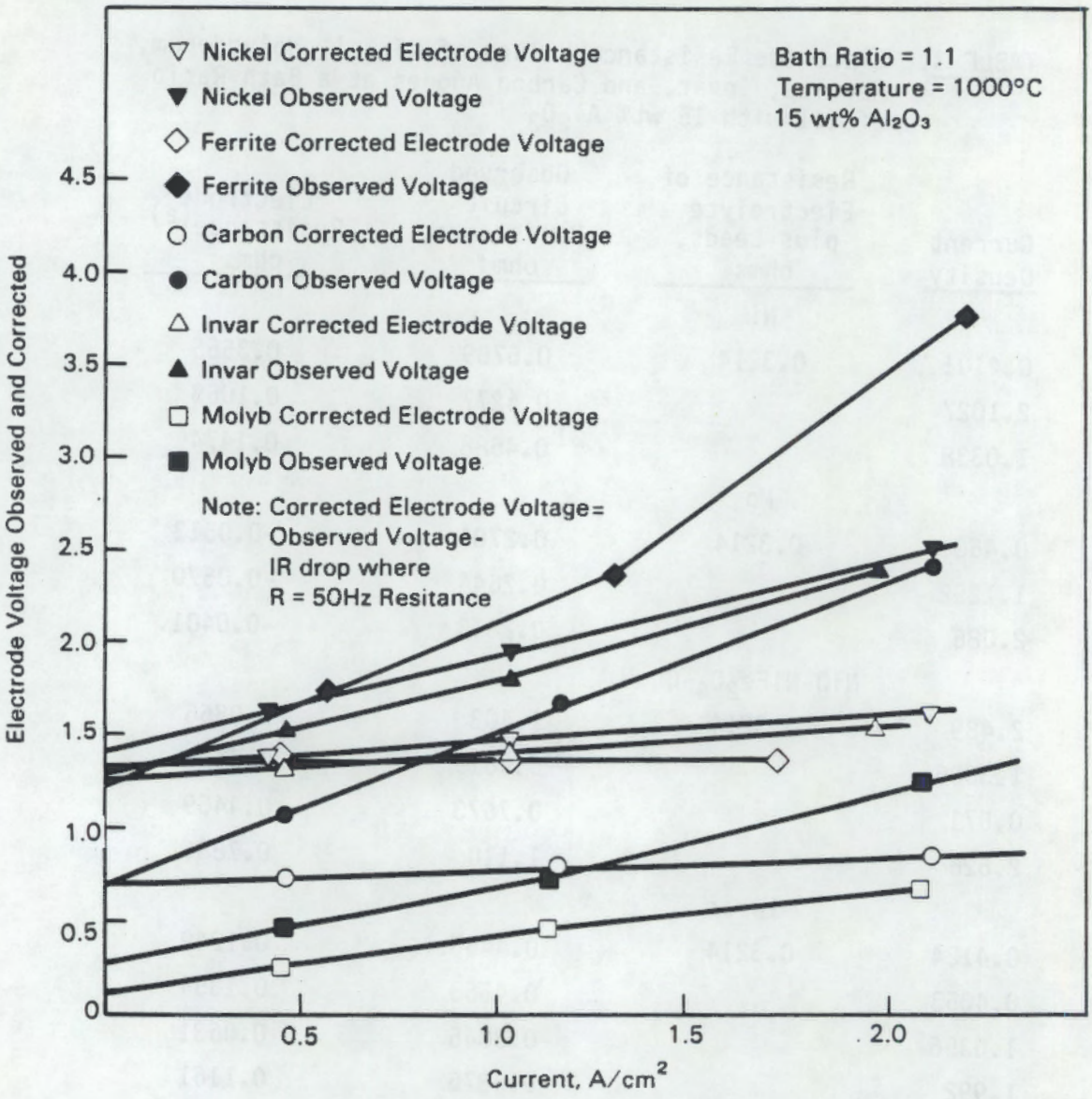

FIGURE 38. Anode Electrical Behavior. Ferrite = $NiO-NiFe_2O_4$-Cu-Ni

Alumina content and electrode potential are presented in a different format in Figure 44. This plot shows that, at the 0 wt% Al_2O_3 level, the electrode potential is clearly low and presumed to be corroding.

The resistance of the anode as a function of Al_2O_3 content and temperature is depicted in Figure 45 at a bath ratio of 1.1. The tests were run by adding successive increments of 5 wt% Al_2O_3 to the bath and heating from about 900 to 1030°C. This procedure was intended to simulate the continuous addition of Al_2O_3 to baths at a variety of temperatures. The salient feature derived from

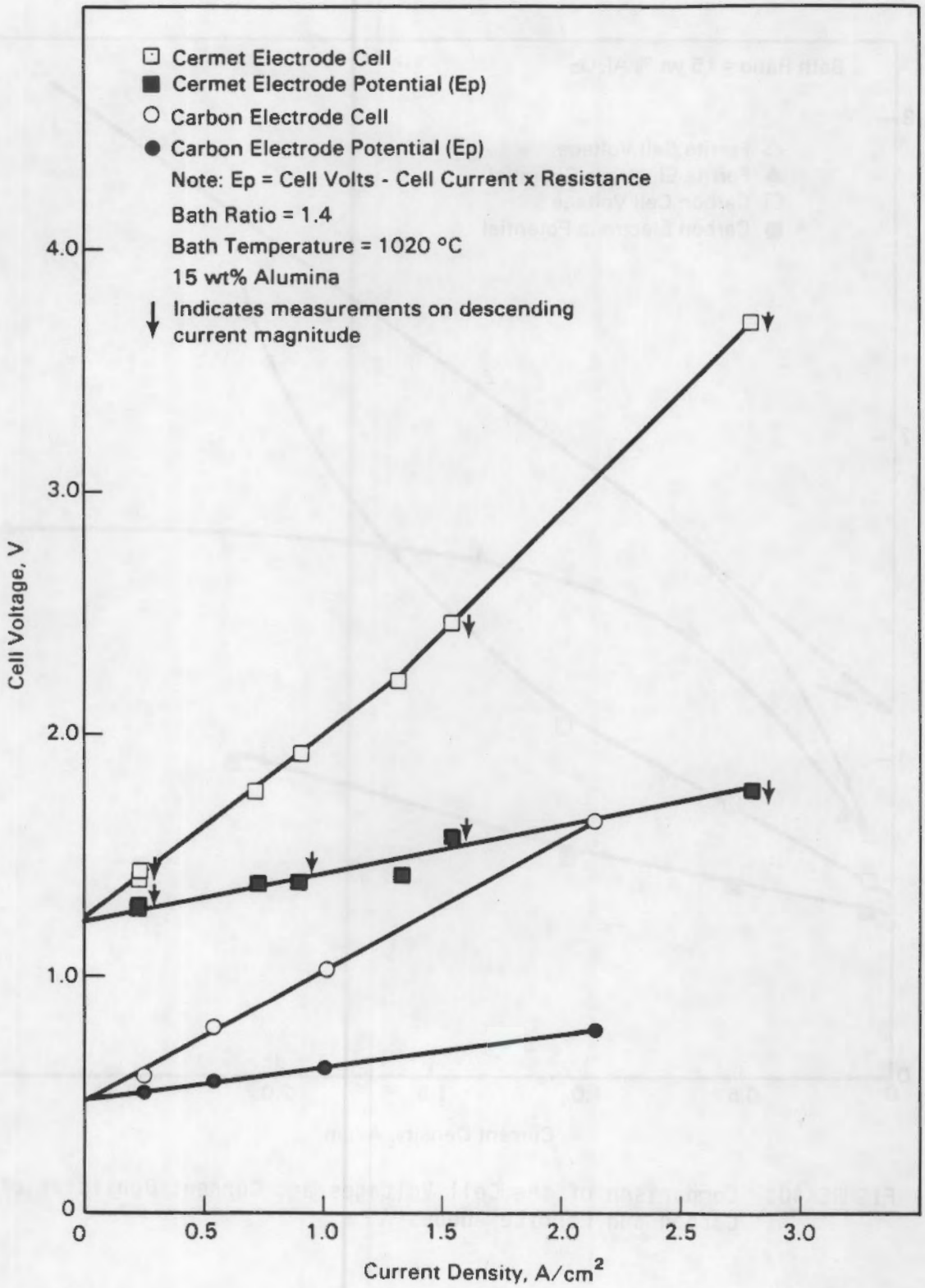

FIGURE 39. Comparison of the Cell Voltage/Electrode Potential (Ep) Versus Current Density for Cermet and Carbon Electrodes

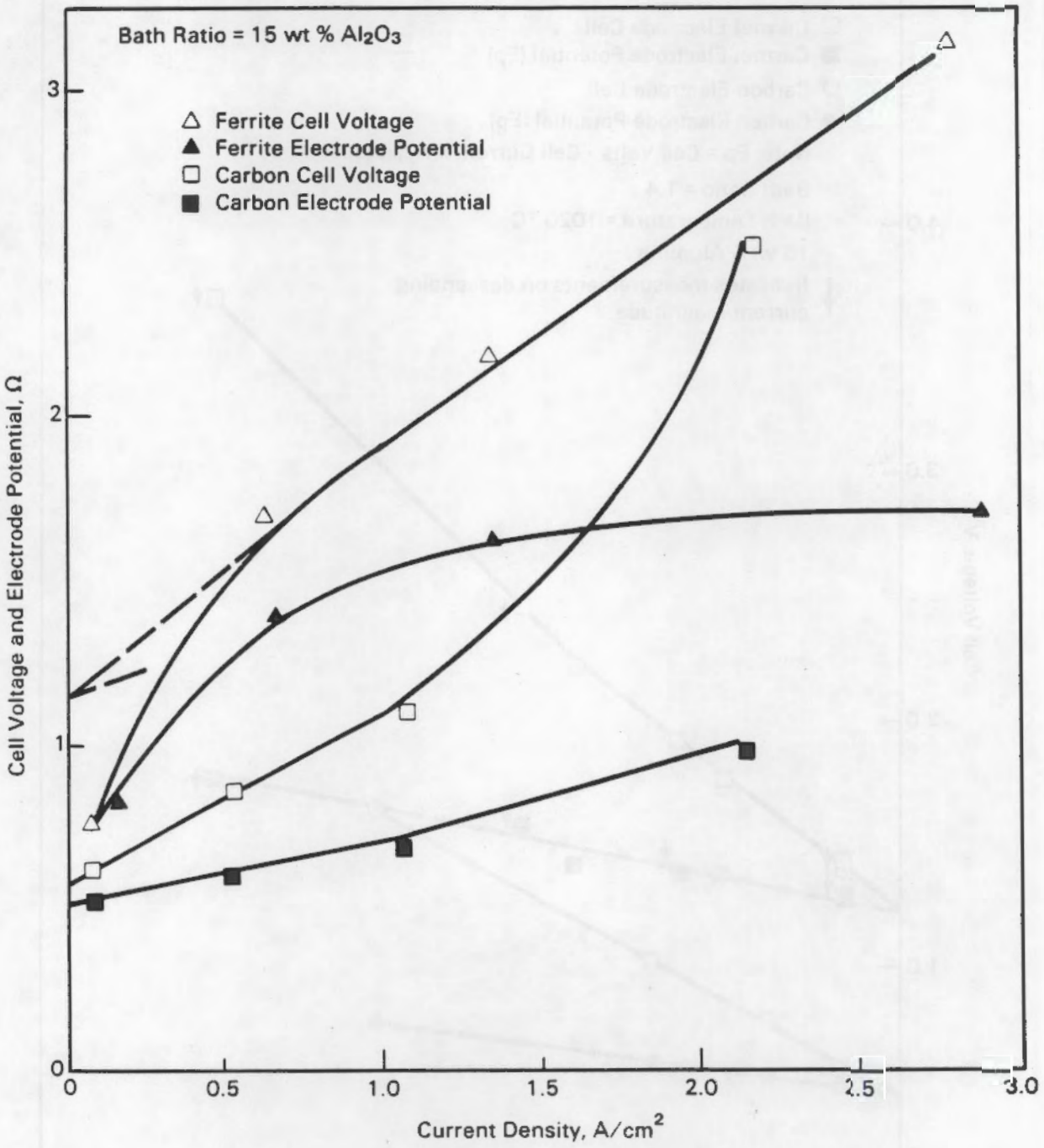

FIGURE 40. Comparison of the Cell Voltages and Current Densities of Carbon and Ferrite Anodes

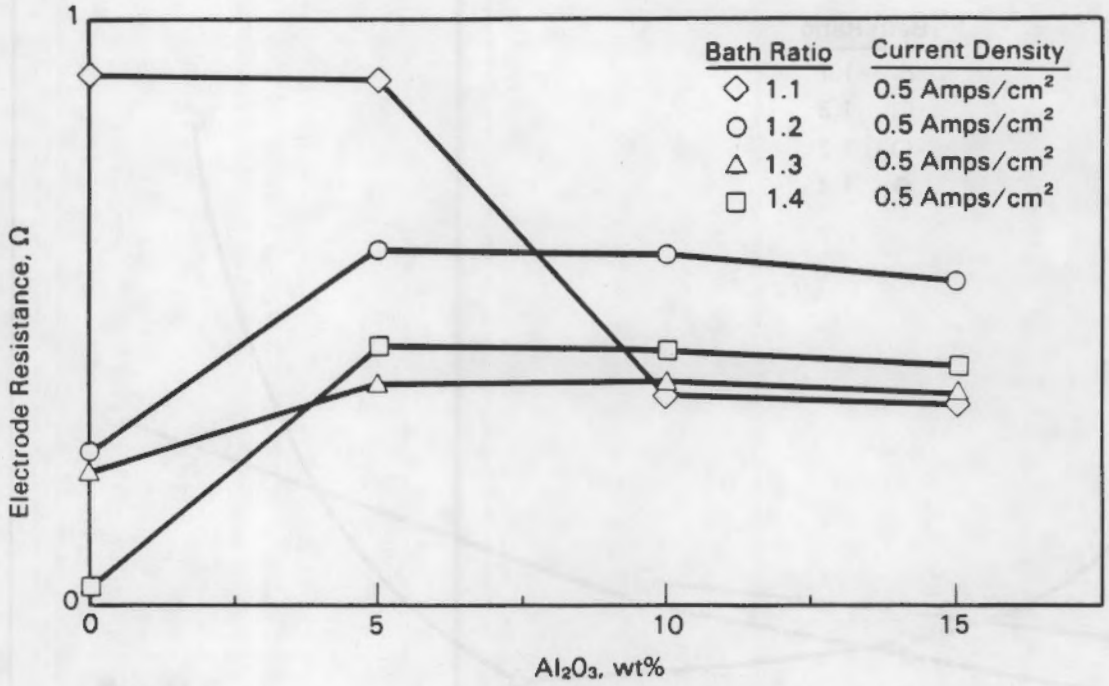

FIGURE 41. Electrode Resistance Versus Al_2O_3 Content

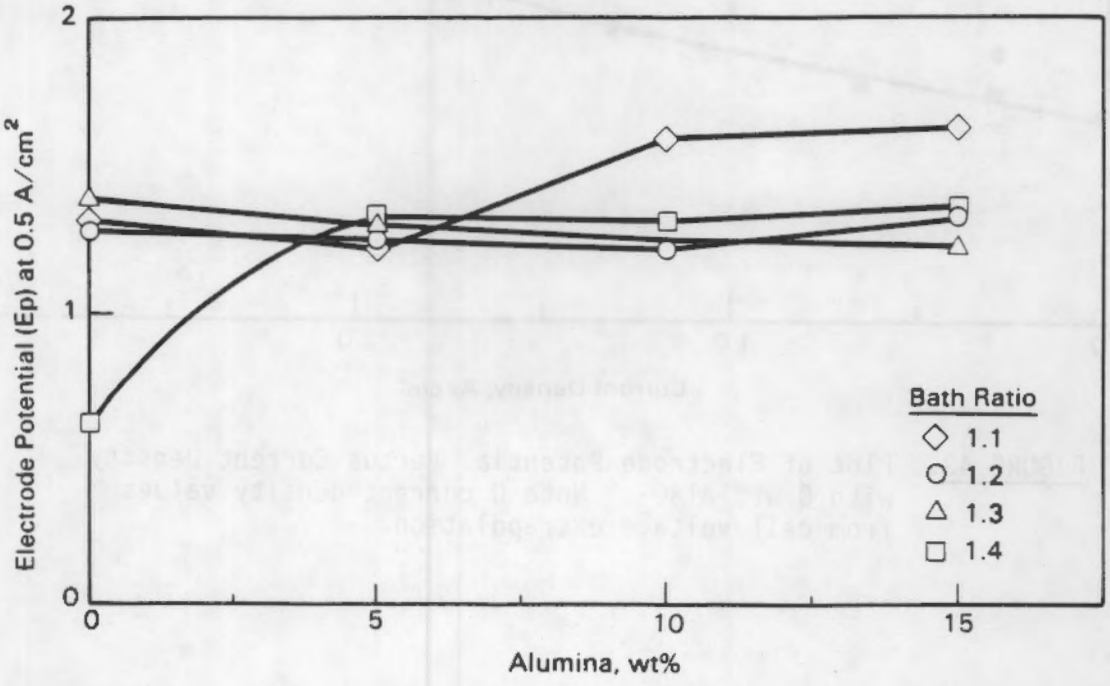

FIGURE 42. Electrode Potential Versus Al_2O_3 Content at 0.5 amps/cm^2

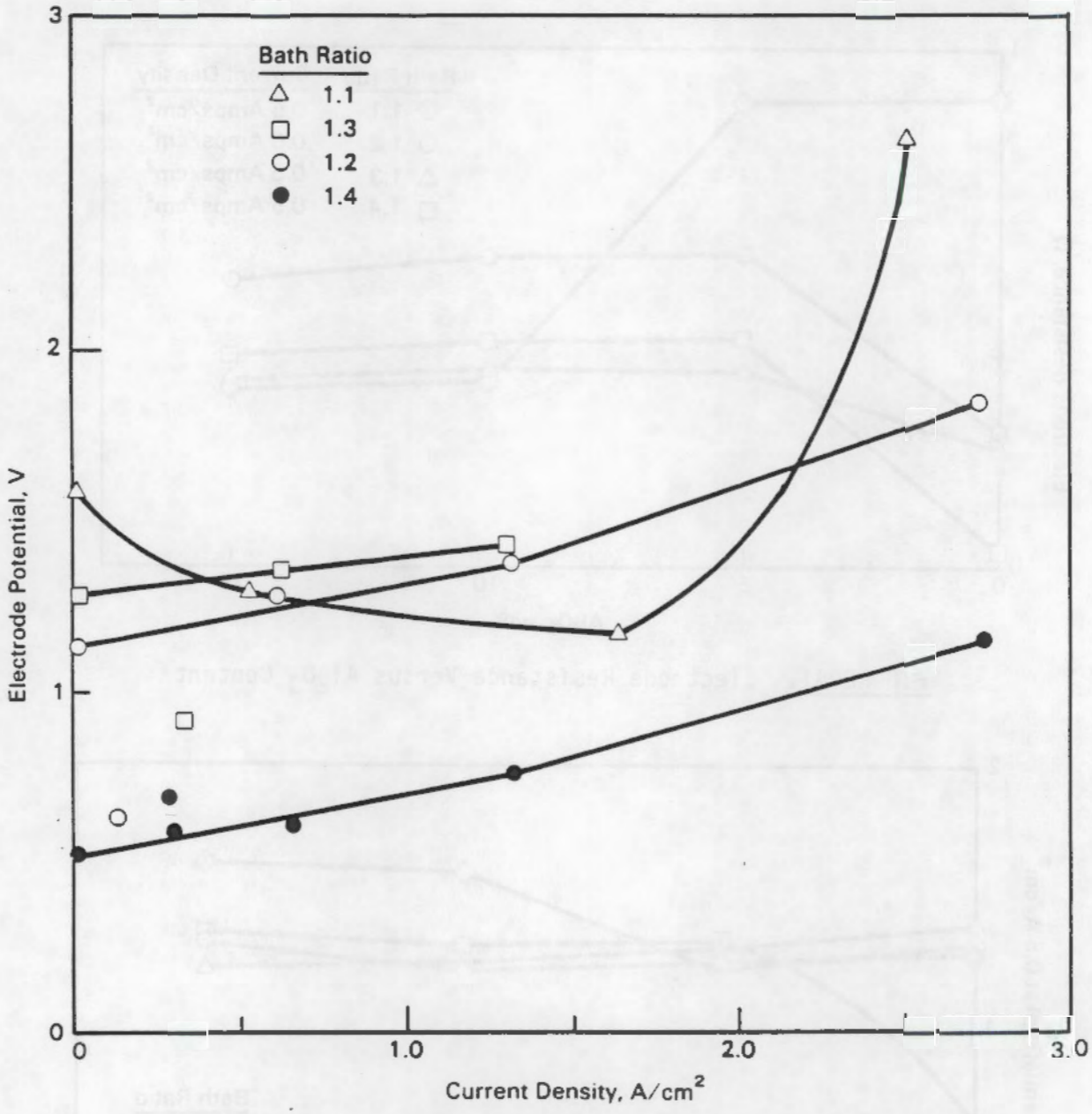

FIGURE 43. Plot of Electrode Potential Versus Current Density with 0 wt% Al_2O_3. Note 0 current density values from cell voltage extrapolation.

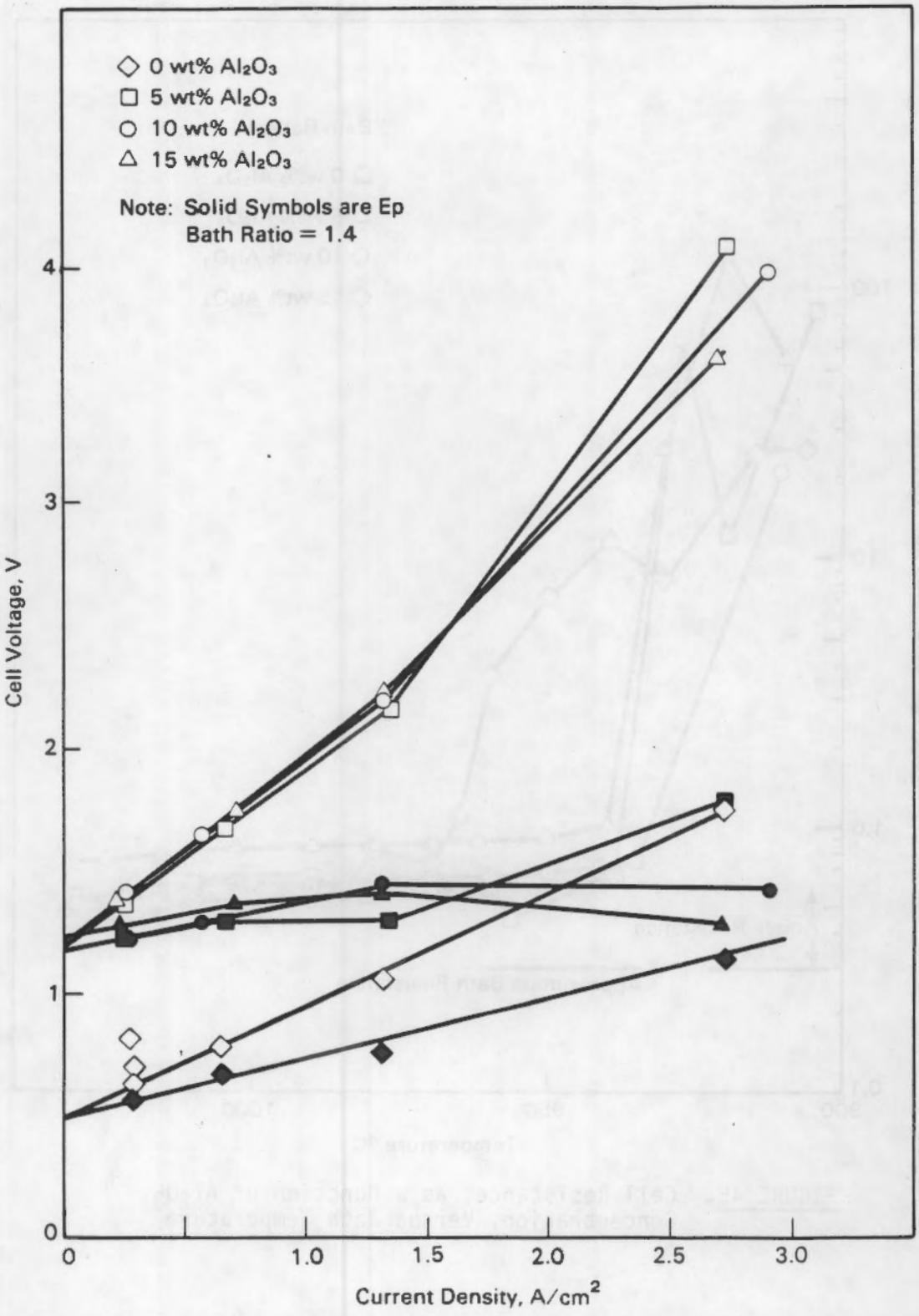

FIGURE 44. Cell Voltage Versus Current Density at Several Al_2O_3 Concentrations

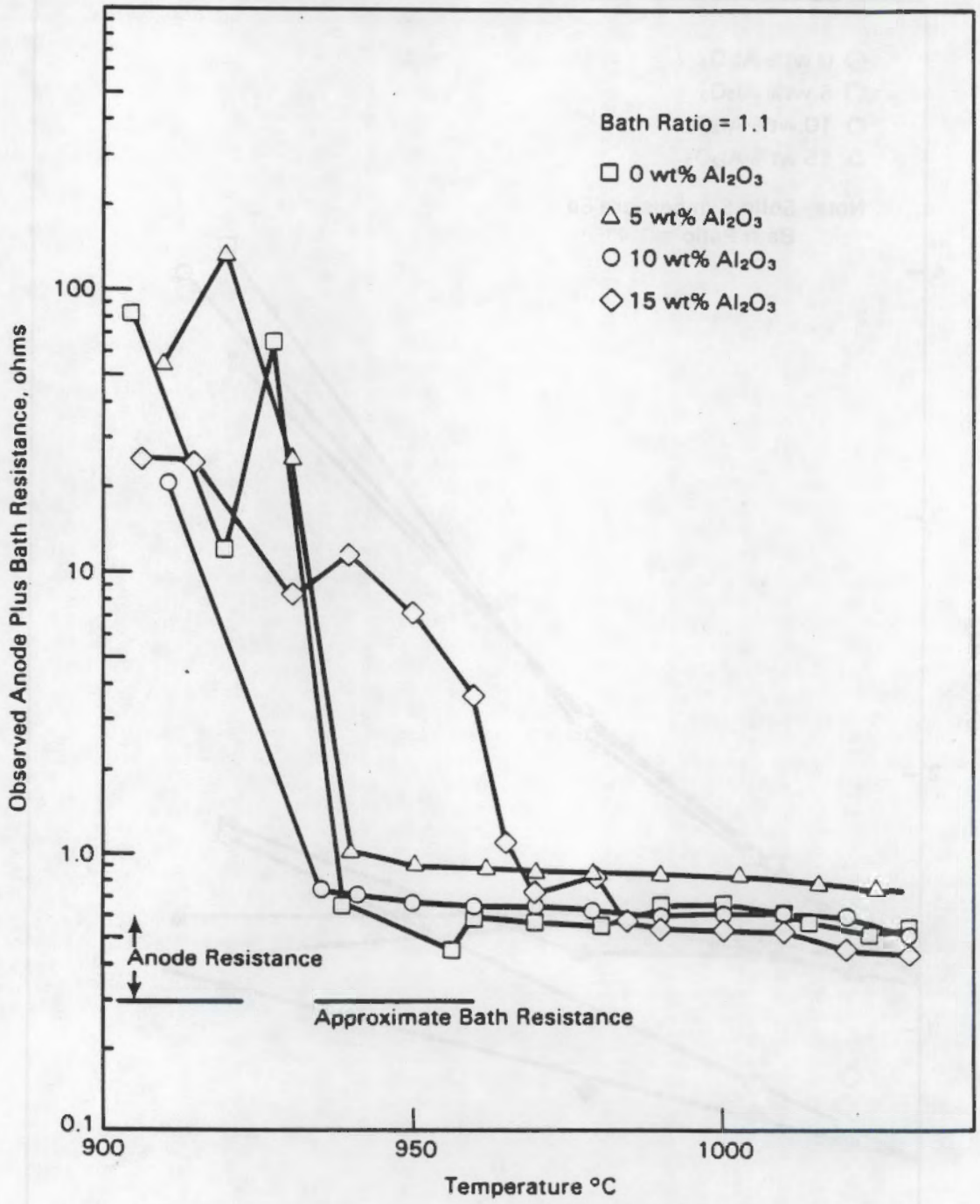

FIGURE 45. Cell Resistance, as a Function of Al_2O_3 Concentration, Versus Bath Temperature

this procedure was that the resistive nature of the anode was cyclic in time, though less so with Al_2O_3 present, and was apparently current-density dependent. This figure suggests that anode operation above 960°C may be necessary to avoid cyclic and destructive anode behavior caused by excessive Al_2O_3 content.

A measurement of coherence was also obtained from the test apparatus. The coherence is a ratio of the square of the cross spectrum divided by a product of the power spectra of the voltage and current measured at the cell. Basically, it is a measure of linear relationship between the voltage and the current.

Several plots are presented to demonstrate the relationships between coherence and current density and Al_2O_3 concentration and cell resistance. The effect of Al_2O_3 concentrations on FFT spectra at low current density is shown in Figure 46. Note that, at low frequencies, a marked increase in resistance occurs for all baths with 5 wt% or more Al_2O_3. Also note the similarity in curves at the various Al_2O_3 concentrations of 5%, 10%, and 15%. In comparison, the resistance at 0 wt% Al_2O_3 drops and levels off.

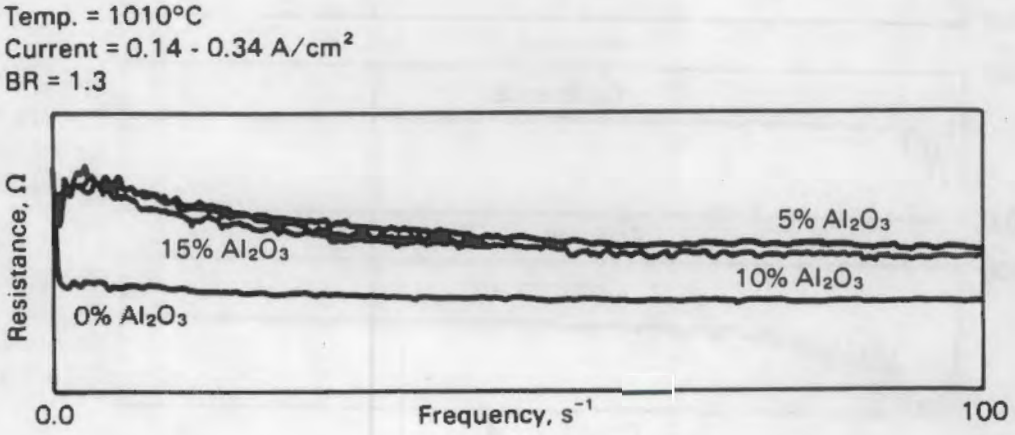

FIGURE 46. Effect of Al_2O_3 on FFT Spectra at Low Current Density

Figure 47 shows the change of coherence with current density. Note the progressively poorer coherence as the current increases from 0.12 amp to 2.12 amp. The coherence levels off again when the current is reduced back to 0.12 amp. Lack of coherence is thought to be associated with stochastic conduction processes in the electrolyte-anode interface film and is likely a measure of an anode degradation phenomenon.

The application of DSA algorithms to laboratory data is scheduled to be delivered to PNL by Professor Nikias concluded December 30, 1987, in a report on the applicability of the various processing techniques to process measurement and control.

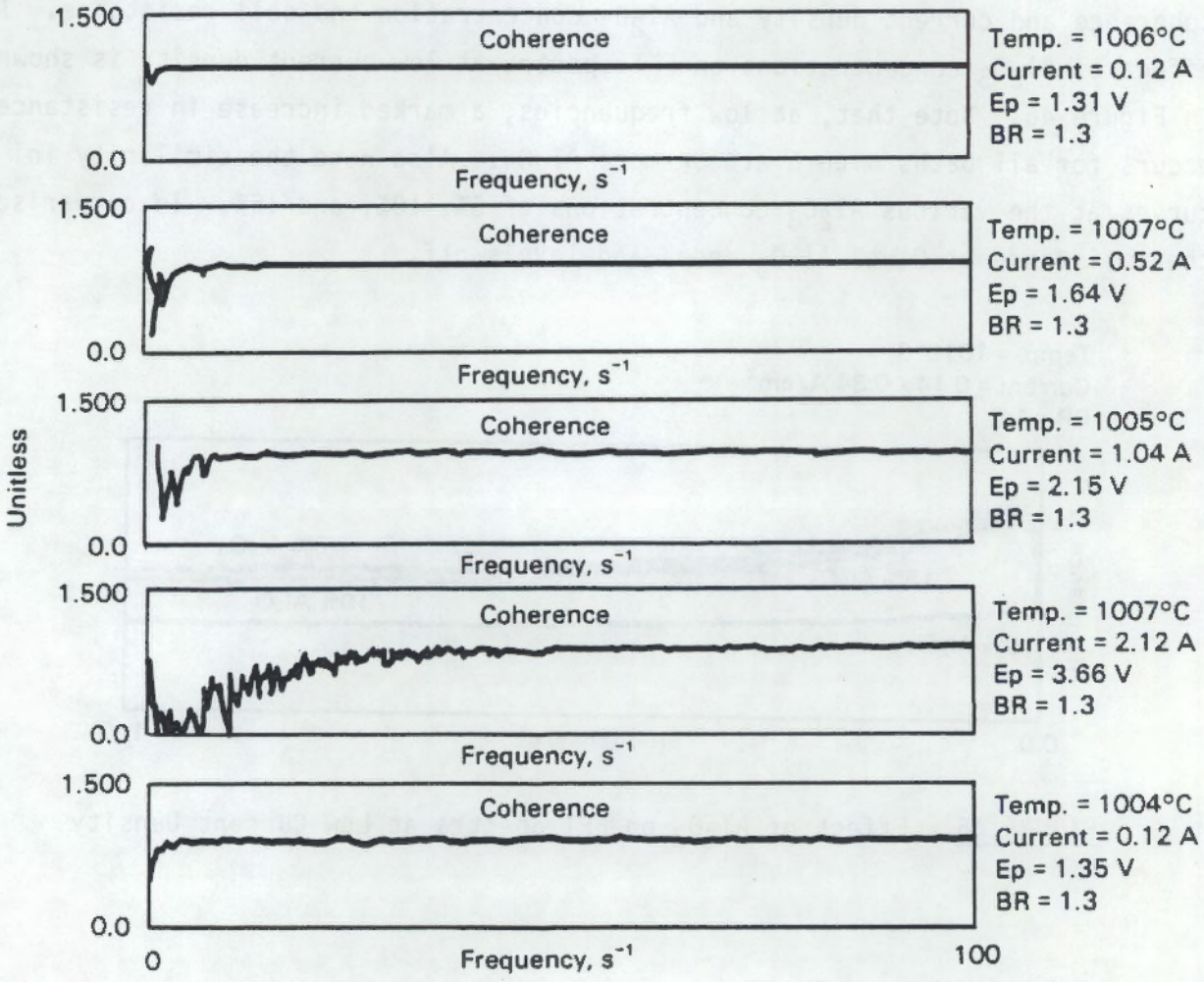

FIGURE 47. Change of Coherence with Increase in Current

FUTURE DIRECTIONS

In FY 1988, efforts will be directed toward three scheduled tasks, as follows:

1. Reference Anode Development--A pilot anode of material electrochemically similar to the reference anode has been shown to provide a suitable reference for controlling a Hall-Heroult cell employing inert anodes. Additional development is required to ensure stability and corrosion resistance. The task will provide support of laboratory anode development and demonstration tests which will also produce performance data on the reference anode and associated control schemes.

2. Pilot Electrode Evaluation--It is projected from previous work on impedance analysis of anode film characteristics that at sufficiently low current densities the capacitive and resistive components of the frequency spectra show a sensitivity to Al_2O_3 content. A pilot electrode operated at sub-electrolysis voltages and analyzed for the capacitive and resistive components should disclose if the use of this technique is applicable to the analysis of bath Al_2O_3 content. This electrode need not be a different structure than the reference anode above.

3. Digital Signal Analysis Control Evaluation--This task is a combination of laboratory tests and data acquisition procedures with on-site analyses and off-site extended analyses conducted by Nikias. Fast Fourier transforms of the test cell current and voltage are coupled with impedance and coherence determinations. Samples of the process-generated signals are also collected and supplied to Professor Nikias for further analysis using a multiplicity of DSA processing algorithms. Correlations of the laboratory test conditions and analyses with the DSA techniques by Nikias are then possible. An iterative process is envisioned where additional tests are suggested by the results of the analyses. However, the use of the DSA technique depends on the results from the FY 1987 work done by Professor Nikias.

REFERENCE

Hart, P. E., et al. 1987. Fiscal Year 1986 Annual Report. PNL-6247, Pacific Northwest Laboratory, Richland, Washington.

DISTRIBUTION

No. of Copies

OFFSITE

M. J. McMonigle
U.S. Department of Energy
Office of Industrial Programs
Forrestal Building
Washington, DC 20585

T. J. Gross
U.S. Department of Energy
Office of Industrial Programs
Forrestal Building
Washington, DC 20585

R. L. Sheneman
U.S. Department of Energy
Office of Industrial Program
Forrestal Building
Washington, DC 20585

10 DOE Office of Scientific and Technical Information

J. V. Anderson
WCVE3
EG&G Idaho, Inc.
Idaho Falls, ID 83415

D. Auburg
Bonneville Power Administration
P.O. Box 3621, PDX 97208
Portland, OR 97208

F. W. Baker
Ceramics Division
Alcoa Laboratories
Alcoa Center, PA 15069

M. Baltzell
Eastalco Aluminum Company
Alumax, Inc.
5601 Manor Woods
Frederick, MD 21701

No. of Copies

J. A. Barclay
U.S. Bureau of Mines
2401 "E" Street N.W.
Washington, DC 20241

W. L. Barham
Kaiser Aluminum and Chemical Corp.
P.O. Box 877
Pleasanton, CA 94566

H. Robert Baumgartner
Ceramics Division
Alcoa Laboratories
Alcoa Center, PA 15069

T. R. Beck
Electrochemical Technology Corp.
1601 Dexter Avenue
Seattle, WA 98109

S. Berwagan
Bonneville Power Administration
P.O. Box 3621 K
Portland, OR 97208

T. M. Besmann
Metals and Ceramics Division
Oak Ridge National Laboratory
P.O. Box X, Bldg. 4515
Oak Ridge, TN 37831-6063

K. A. Blakely
President
Advanced Refractory Technologies, Inc.
699 Hertel Ave.
Buffalo, NY 14207

M. H. Blenk
Du Pont
P.O. Box 787
Niagara Falls, NY 14302

No. of
Copies

L. G. Boxall
Martin Marietta Laboratories
1450 South Rolling
Baltimore, MD 21227

J. Bracher
Kaiser Aluminum and Chemical
Corp.
825 N.E. Multnomah St.,
Suite 960
Portland, OR 97232-2150

R. Bradt
Department of Materials Science
and Engineering
University of Washington FB-10
Seattle, WA 98195

J. J. Brown, Jr.
Materials Engineering
Virginia Polytechnic Institute
Blacksburg, VA 24061

A. Budner
Bonneville Power Administration
P.O. Box 3621--EPC
Portland, OR 97208

A. J. Caputo
Metals and Ceramics Division
Oak Ridge National Laboratory
P.O. Box X
Oak Ridge, TN 37831-6063

N. Clark
Bonneville Power Administration-
Industrial Conservation
P.O. Box 3621
Portland, OR 97208

A. Cooke
Martin Marietta Laboratories
1450 South Rolling
Baltimore, MD 21227

No. of
Copies

J. A. Coppola
Standard Oil Engineered
Materials Company
P.O. Box 156
Niagara Falls, NY 14302

R. Curtis
Materials Development
Corporation
81 Hicks Avenue
Medford, MA 02155

J. V. Day
Mail Drop 2232
Kaiser Aluminum and Chemical
Corp.
300 Lakeside Drive
Oakland, CA 94643

R. Dethlefsen
Maxwell Laboratories
8888 Balboa Ave.
San Diego, CA 92123

D. H. DeYoung
Alcoa Technical Center
Alcoa Center, PA 15069

S. Diamond
Battelle Columbus Laboratories
505 King Avenue
Columbus, OH 43201-2693

C. W. Doerr
The Stackpole Corporation
Cermag Division
201 Stackpole Street
St. Marys, PA 15857

T. Dwonch
Snake River District
BPA
101 W. Poplar
Walla Walla, WA 99362

No. of
Copies

R. C. Dorward
Kaiser Aluminum and Chemical
Corp.
P.O. Box 877
Pleasanton, CA 94566

G. L. Eitel
Stone & Webster Engineering
Corp.
Greenwood Plaza Box 5406
Denver, CO 80217

R. Engdahl
Deposits and Composites, Inc.
318 Victory Drive
Herndon, VA 22070

J. F. Elliott
MIT
Room 4-138
77 Massachusetts Avenue
Cambridge, MA 02139

B. G. Epstein
A. D. Little, Inc.
955 Lenfant Plaza SW 4200
Washington, DC 20024-2119

J. W. Evans
University of California
Dept. of Matl. Sci. and Mineral
Eng.
Berkeley, CA 94720

R. A. Fenimore
ICI Advanced Materials
Rollins Building, Eighth Floor
Wilmington, DE 19897

D. A. Figgins
ARCO Petroleum Products Co.
P.O. Box 61004
Anaheim, CA 92803-6104

P. Foster
Alcoa Laboratories
P.O. Box 772
New Kensington, PA 15068

No. of
Copies

J. Gee
Great Lakes Research Corp.
P.O. Box 1031
Elizabethton, TN 37643

T. Gilligan
Eltech Systems Corp.
625 East Street
Fairport Harbor, OH 44077

W. M. Goldberger
Superior Graphite Co.
120 S. Riverside Plaza
Chicago, IL 60606

J. Goodwell
Center for Metals Production
Mellon Institute
4400 Fifth Avenue
Pittsburgh, PA 15213

J.A.S. Green
Martin Marietta Laboratories
1450 South Rolling
Baltimore, MD 21227

C. Griffin
Ceramatec Inc.
2425 S. 900 West
Salt Lake City, UT 84119

L. I. Grindstaff
Great Lakes Research Corp.
P.O. Box 1031
Elizabethon, TN 37643

J. Haggerty
MIT
Building 12, Room 009
77 Massachusetts Avenue
Cambridge, MA 02139

I. L. Harry
Electric Power Research
Institute
P.O. Box 10412
Palo Alto, CA 94303

No. of
Copies

W. E. Haupin
2820 7th Street Road
Lower Burrell, PA 15068

H. W. Hayden, Jr.
1419 East 21st Street
The Dalles, OR 97058

R. Hill
Union Carbide Corp.
P.O. Box 94637
Cleveland, OH 44101

H. F. Hillegass
Alcoa Wenatchee Works
P.O. Box 221
Wenatchee, WA 98807

D. G. Howitt
College of Engineering
University of California, Davis
Davis, CA 95616

G. R. Hyde
U.S. Bureau of Mines
2401 "E" Street N.W.
Washington, DC 20241

S. C. Jacobs
Primary Processing
Aluminum Company of America
Alcoa Technical Center
Alcoa Center, PA 15069

R. A. James
Kaiser Aluminum and Chemical
Corp.
E2111 Hawthorne Road
Mead, WA 99021

S. H. Jan
Tennessee Valley Authority
1850 Commerce Union Bank Bldg.
Chattanooga, TN 37401

N. Jarrett
149 Jefferson Avenue
New Kensington, PA 15068

No. of
Copies

J. Joesowicz
Material Development Laboratory
Atlantic Richfield
20717 Prairie Street
Chatsworth, CA 91311

A. R. Johnson
Kaiser Aluminum
P.O. Box 877
Pleasanton, CA 94366

J. Johnson
Intalco Aluminum Company
P.O. Box 937
Ferndale, WA 98248

M. H. Johnson
Alcoa Wenatchee Works
P.O. Box 221
Wenatchee, WA 98801

L. Joó
Great Lakes Research Corp.
P.O. Box 1031
Elizabethon, TN 37643

M. Karmous
Oregon State Department of
Energy
625 Marion Street, N.E.
Salem, OR 97310

R. Keller
RD 3
Roundtop Road
Export, PA 15632

C. Anderson
Columbia Aluminum Co.
85 John Day Dam Road
Goldendale, WA 98620

K. Krupinski
Mail Stop 57
U.S. Steel Technical Center
1 Technical Center Drive
Monroeville, PA 15146

No. of
Copies

G. Y. Lai
Cabot Corporation
P.O. Box 9013
Kokomo, IN 46902-9013

J. E. Lane
Ceramic Research and
Development Center
Westinghouse Electric
Corporation
1310 Beulah Road
Pittsburgh, PA 15235

Sai-Kwing Lau
Standard Oil Engineered
Materials Company
Niagara Falls R&D Center
P.O. Box 832
Niagara Falls, NY 14302

J. J. Leddy
Dow Chemical U.S.A.
1776 Building
Midland, MI 48640

W. W. Liang
Gas Research Institute
8600 West Bryn Mawr Avenue
Chicago, IL 60631

W. H. Link
Columbia Aluminum Corp.
85 John Day Dam Road
Goldendale, WA 98620

Steve Loftness
Washington State Energy Office
400 E. Union
Olympia, WA 98504

W. Long
Building B815
Dow Chemical
Freeport, Texas 77541

No. of
Copies

R. A. Lowden
Metals and Ceramics Division
Oak Ridge National Laboratory
P.O. Box X, Bldg. 4515
Oak Ridge, TN 37831-6063

W. N. Maclay
Koppers Company, Inc.
440 College Park Drive
Monroeville, PA 15146

V. H. Markant
Du Pont
P.O. Box 787
Niagara Falls, NY 14302

C. J. McMinn
Extractive Metallurgical
Department
Reynolds Metals Company
P.O. Box 1200
Sheffield, AL 35660

C. H. McMurtry
Standard Oil Engineered
Materials Company
Niagara Falls R&D Center
P.O. Box 832
Niagara Falls, NY 14302

M. A. Mittnick
Avco Specialty Materials
Subsidiary of Textron Inc.
2 Industrial Avenue
Lowell, MA 01851

A. Moussa
A. D. Little, Inc.
20 Acorn Park
Cambridge, MA 02140

B. C. Mutsuddy
Battelle Columbus Division
505 King Avenue
Columbus, OH 43201-2693

No. of
Copies

A. N. Patel
Battelle Columbus Laboratories
505 King Avenue
Columbus, OH 43201-2693

J. R. Payne
Kaiser Aluminum and Chemical
Corp.
P.O. Box 877
Pleasanton, CA 94566

T. Payne
Columbia Falls Aluminum Co.
Columbia Falls, MT

W. Pebley
Oregon Freeze Dry Corp.
525 25th Ave SW
P.O. Box 1048
Albany, OR 97321

K. Peterson
Columbia Aluminum Corp.
85 John Day Dam Road
Goldendale, WA 98620

R. D. Peterson
Reynolds Metals Company
P.O. Box 1200
Sheffield, AL 35660

T. R. Prichett
Kaiser Aluminum and Chemical
Corp.
P.O. Box 877
Pleasanton, CA 94566

W. W. Pritsky
Aluminum Association
900 19th St. N.W.
Washington, DC 20006

S. P. Ray
Alcoa Technical Center
Alcoa Center, PA 15069

No. of
Copies

J. F. Rhodes
Advanced Composite Materials
Corp.
1525 S. Buncombe Rd.
Greer, SC 29651

N. E. Richards
Reduction Laboratory
Reynolds Aluminum Corporation
P.O. Box 1200
Sheffield, AL 35660

J. J. Ritter
Ceramics Division
National Bureau of Standards
Gaithersburg, MD 20899

R. C. Rohwedder
3028 Ohio Street
Longview, WA

J. Rosling
Myers Metals and Minerals
459 Colman Building
Seattle, WA 98104

D. R. Sadoway
MIT
Room 8-109
77 Massachusetts Avenue
Cambridge, MA 02139

W. Scott
Department of Materials Science
& Engineering
Wilcox Hall FB-10
University of Washington
Seattle, WA 98195

D. R. Secrist
Great Lakes Research Corp.
P.O. Box 1031
Elizabethon, TN 37643

A. B. Shah
Noranda Aluminum, Inc.
P.O. Box 70
New Madras, MO 63869

No. of
Copies

N. Shelton
Intalco
1300 S.W. 5th, Suite 3508
Portland, OR 97201

F. W. Spillers
Dow Chemical U.S.A.
B-1210 Building
Freeport, TX 77541

D. V. Stewart
Reynolds Metals Co.
P.O. Box 1200
Sheffield, AL 35660

D. Strahan
Reynolds Metals Company
P.O. Box 27003
Richmond, VA 23261

A. T. Tabereaux
Reynolds Metals Company
P. O. Box 1200
Sheffield, AL 35660

G. P. Tarcy
Aluminum Company of America
Alcoa Technical Center
Alcoa Center, PA 15069

P. Thaure
Primary Planning and Production
Alumax
400 S. El Camino Rd.
San Mateo, CA 94402

W. H. Thielbahr
Conservative Technology
Division
DOE-Idaho Operations Office
785 DOE Place
Idaho Falls, ID 83402

S. Thomson
General Manager
Klickitat PUD
1313 S. Columbus
Goldendale, WA 98620

No. of
Copies

R. Unger
Merner Research
P.O. Box 248
Ridgewood, NJ 07451

A. Vinnard
Bonneville Power Administration
(KWI)
P.O. Box 3621
Portland, OR 97208

T. Von Muller-KWI
Bonneville Power Administration
P.O. Box 3621
Portland, OR 97208

D. H. Weinblatt
AIMCOR
One Parkway North
Deerfield, IL 60015

J. D. Weyand
Alcoa Technical Center
Alcoa Center, PA 15069

B. Wilcox
Northwest Aluminum Co.
3313 W. Second St.
The Dalles, OR 97058

C. B. Wilson
Dow Chemical U.S.A.
Texas Operations
B-101 Building
Freeport, TX 77541

W. Winnard
Battelle Washington Office
2030 "M" Street N.W.
Washington, DC 20036

J. C. Withers
Keramont Research Corporation
4233 S. Fremont Avenue
Tucson, AZ 85714

No. of
Copies

W. A. Zdaniewski
Engelhard Corporation
Menlo Park, CN28
Edison, NJ 08818

FOREIGN

D. Brodie
Comalco Ltd.
55 Collins St.
Melbourne, AUSTRALIA

T. Kjar
Comalco Ltd.
55 Collins St.
Melbourne, AUSTRALIA

E. W. Dewing
Alcan International
P.O. Box 8400
Kingston, Ontario
CANADA K7L 4Z4

T. J. Hudson
Alcan International
2001 rue University
C.P. 6090
Montreal, Quebec
CANADA H3C 3H2

D. N. MacMillan
Alcan International
C.P. 1250
Jonquieve, Quebec
CANADA G7S 4K8

T. Rawlings
Alcan International Limited
Engineering Division
C.P. 6090
Montreal, Quebec
CANADA, H3C 3H2

No. of
Copies

J. H. Reimers
Jan H. Reimers and Associates
Inc.
221 Lakeshore Road East
Oakville, Ontario
CANADA L6J 1H7

A. Oye
Institute of Inorganic
Chemistry
Norwegian Institute of
Technology
University of Trondheim
N-7034 Trondheim-NTH, NORWAY

J. Thonstad
Laboratories of Industrial
Electrochemistry
Norwegian Institute of
Technology
University of Trondheim
N-7034 Trondheim-NTH, NORWAY

K. O. Vee
ASV
Ardal Verk
N-5875 Ardalstargen, NORWAY

ONSITE

DOE Richland Operations Office

E. C. Norman

41 Pacific Northwest Laboratory

K. E. Bailey
B. B. Brenden
M. Clement
N. C. Davis
J. R. Divine
G. J. Exarhos
G. L. Graff
P. E. Hart
D. K. Hilliard
R. H. Jones
G. H. Koski
S. C. Marschman (10)

No. of
Copies

G. L. McVay
N. L. Moore
C. H. Schilling
M. J. Danielson

No. of
Copies

D. M. Strachan (10)
Publishing Coordination
Technical Report Files (5)